Mechanical and chemical compaction of carbonates - An experimental study

(Compaction mécanique et chimique des roches carbonatées)

Delphine Croizé

Dissertation for the degree of Philosophiae Doctor (Ph.D.)

Faculty of Mathematics and Natural Sciences

University of Oslo, Norway

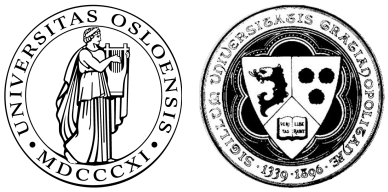

Thèse présentée pour obtenir le titre de Docteur

Spécialité : Science de la Terre et de l'Univers

Université de Grenoble, France

Composition du jury:

Christopher Spiers	Président, rapporteur	Prof., University of Utrecht, Pays-Bas
Ida L. Fabricius	Rapporteur	Dr., Denmark Technical University, Danemark
François Renard	Directeur de thèse	Prof., Université Joseph Fourier, Grenoble
Jens Jahren	Directeur de thèse	Dr., University of Oslo, Norvège

Submitted: June 15, 2010

Defended: September 30, 2010

Summary

Understanding compaction processes in sediments or rocks is important for instance for the characterisation of compaction in sedimentary basins or for sealing of active fault. The aims of the present study are firstly to separate and quantify the relative role of mechanical and chemical compaction in carbonate sediments. Secondly to better understand chemical compaction processes acting on sediments.

The potential for porosity loss by mechanical compaction of platforms carbonate strata was investigated by carrying out K_0 triaxial tests. Eleven samples cemented with low–Mg calcite and five dolomitized samples from the Marion plateau, offshore northeast Australia (ODP (ocean drilling program) Leg194) were uniaxially compacted at effective stresses up to 70 MPa. Early cementation of bioclastic carbonate samples created a stable cemented framework with a high degree of over–consolidation and low compressibility. Water saturation of the samples produces weakening of the mechanical strength and greater scatter in the correlation of P–wave velocity versus porosity. Most of the tested samples were already so strongly cemented at 30–400 meters that further porosity loss during burial up to 4–5 km depth must occur mainly by chemical rather than mechanical processes. To study chemical processes two other types of experiments were carried out.

Pressure solution is the main chemical compaction mechanism affecting sediments during burial, therefore the rate of calcite deformation by pressure solution creep at a single contact was studied. The results enable the identification of the relative importance of pressure solution driven by normal load, and free surface dissolution driven by strain energy. Two different processes occur during pressure solution of calcite crystals at the grain scale. In one case, diffusion of the dissolved solid takes place in the pore fluid present along a rough interface between calcite and the indenter. In the second case, diffusion occurs through cracks that propagate from the contact toward the less stressed part of the crystal. Strain rates are higher for experiments in which crack propagation occurred. Overall it seems strain rates are not really stress dependent but rather dependent on whether crack propagation occurs or not.

Eventually, both mechanical and chemical compaction processes were studied on aggregates of calcite and bioclastic carbonate sands. Experimental compaction showed that compaction of carbonates sands should be modelled as a function of both mechanical and chemical compaction also at relatively shallow depth and low temperature. In all cases, the nature of the fluid, the initial grain packing, and the grain size represent important control parameters of the final strain and the strain rates at a given stress. Samples saturated with non–reactive fluids, *e.g.* air or

decane, show less strain than samples saturated with reactive fluids at the same effective stress since the compaction was only mechanical. During the loading phase, chemical compaction occurs by pressure solution creep which is enhanced by the presence of cracks at the grain–to–grain contacts. This is also supported by the identification of compaction related microstructures in thin–sections. During creep tests, the samples compressibility is controlled by, in order of importance, grain size, stress, and water saturation. Low ultrasonic velocities are especially observed in samples saturated with reactive fluids. Dissolution and transport affecting the grain–to–grain contacts geometry and crack propagation are likely to be the reason for such velocity alteration.

In conclusion, porosity loss in carbonate sediments is mostly due to chemical compaction and very little to mechanical compaction. Chemical compaction processes are pressure solution and pressure solution enhanced by subcritical crack growth. The predominance of one or the other mechanism is to be related to the fluid in presence and to the nature of the grains.

Résumé

La compréhension des mécanismes de compaction des roches et des sédiments est importante dans différents domaine des géosciences en particulier pour caractériser la compaction dans les bassins sédimentaires ou le colmatage dans les failles actives. Les objectifs de cette thèse sont d'une part de séparer et de quantifier le rôle respectif de la compaction mécanique et chimique dans les sédiments carbonatés. D'autre part d'obtenir une meilleure compréhension des procédés aboutissant au fluage des roches sédimentaires carbonatées.

La perte de porosité par compaction mécanique a été étudiée en réalisant des essais triaxiaux K_0 sur des échantillons provenant de plateformes carbonatées. Onze échantillons cimentés par de la calcite faiblement magnésienne et cinq échantillons dolomitisés provenant du Marion Plateau au large de la côte nord-est Australienne (ODP (ocean drilling program) Leg194) ont été compactés de manière uniaxiale à des contraintes effectives allant jusqu'à 70 MPa. La cimentation à faible profondeur à laquelle ces échantillons ont été soumis a créé une structure cimentée stable ayant un fort degré de sur–consolidation et une faible compressibilité. La plupart des échantillons testés étaient tellement cimentés à 30–400 mètres que la perte de porosité à des profondeurs atteignant 4–5 km doit être principalement liée à des procédés chimiques et non à des procédés mécaniques. Pour étudier ces processus chimiques deux autres types d'expériences ont été réalisées.

La dissolution sous contrainte est le principal mécanisme responsable du fluage des roches sédimentaires pendant leur enfouissement. Par conséquent la vitesse de déformation de la calcite par dissolution sous contrainte à l'échelle d'un contact a été étudiée. Les résultats obtenus permettent l'identification de l'importance respective de la dissolution sous contrainte résultant de l'application de la contrainte normale et celle de la dissolution au niveau des surfaces 'libres' résultant de l'accumulation de l'énergie élastique ou plastique. Deux mécanismes différents se produisent lors de la dissolution sous contrainte de cristaux de calcite à l'échelle du grain. Dans un premier cas, la diffusion du solide en solution se produit dans le fluide présent à l'interface rugueuse entre la calcite et le poinçon. Dans un deuxième cas, la diffusion se produit le long de fractures qui se propagent du contact vers la partie du cristal soumise à des contraintes plus faibles. Les vitesses de déformation sont plus élevées dans les expériences pour lesquelles la propagation de fractures se produit. De manière générale la vitesse de déformation n'apparait pas comme étant dépendante de la contrainte, mais plutôt de la propagation ou non de fractures.

Finalement, les procédés mécaniques et chimiques actifs pendant la compaction ont été

étudiés sur des agrégats de cristaux de calcite ou de sables bioclastique. Les expériences montrent que la compaction des sables carbonatés doit être modélisée en prenant en compte à la fois la compaction mécanique et chimique. Dans toutes les expériences la nature du fluide saturant, l'organisation initiale des grains et la taille des grains sont des paramètres important contrôlant la déformation finale ainsi que la vitesse de déformation à une contrainte donnée. La déformation des échantillons saturés avec des fluides non réactifs, *e.g.* air ou décane, est moins importante qu'avec des fluides réactifs, puisque dans ce cas la compaction est seulement mécanique. Pendant la phase de chargement, la compaction chimique se produit par dissolution sous contrainte, dont la vitesse est augmentée par la présence de petites fractures au niveau des contacts intergranulaires. Cette interprétation est confirmée par l'observation des échantillons en lame-minces. Les vitesses ultrasoniques se propageant dans les agrégats saturés avec des fluides réactifs ont été mesurées et il a pu être montré que la dissolution et le transport de matière affectant la géométrie des contacts au niveau des grains, ainsi que la fracturation des grains sont probablement les raison de cette diminution de vitesse.

En conclusion, la perte de porosité dans les sédiments carbonatés est principalement due à la compaction chimique et très peu à la compaction mécanique. Les procédés chimique de la compaction sont d'une part la dissolution sous contrainte, et d'autre part la dissolution sous contrainte assistée par la propagation sous–critique de fissures. La prédominance de l'un ou l'autre de ces procédés est liée à la nature du fluide présent dans l'espace poreux ainsi qu'á la nature des grains.

Acknowledgements

First I would like to thanks Professor Knut Bjørlykke and Associate Professor Jens Jahren who gave me the opportunity to learn a lot about geology and compaction. Well beyond the scientific learning they taught me to be independent in my research which is of great value for my future professional life. I also would like to acknowledge the help I got from Professors Per Aagaard and Kaare Høeg.

Professors Dag Kristian Dysthe and François Renard shared with me their enthusiasm about research and laboratory experiments, I am forever grateful! Working with them was not only nice, but make me, I think, much more aware of how to look at scientific problems. I am also very grateful to the fact that I could always write an email or knock at the door to ask questions and always got pertinent answers.

For my stays at University of Grenoble, for interesting discussions and comments on my work I would like to thanks Professors François Renard (again!) and Jean–Pierre Gratier.

I benefited a lot from the cooperation with Stephen Ehrenberg. I learned a lot about scientific writing but also about how to present figures, etc. Stephen always had time to answer my questions and had very constructive comments on Paper 1, I am very thankful.

Saying that all the days as a PhD student the past years were great would be lying! However, I don't remember one bad day in the lab. Of course it has been quite a number of failed experiments and frustrations, but being in the lab was always a learning experience and above all fun. For that, my foremost thanks go to all my supervisors that gave me the opportunity to do a PhD with a lot of experimental work. I spend 3 years sharing my laboratory time between NGI (Norges Geoteknisk Institutt) and PGP (Physics of Geological Processes, University of Oslo).

My first day in the laboratory at NGI, I arrived unannounced and with pretty much no idea about what I was suppose to do. Rune Dyvik took time to explain me the basics of geotechnical testing, presented me to the people in the lab, and not the least helped me to fix the administrative papers. I am very thankful! The results part of Paper 1 and Paper 3 would certainly not be the same without the advises I got from Toralv Berre. I am very thankful for the fact that he shared his passion of always getting more accurate measurements and also for the time he spent explaining me all the details of triaxial testing. I would like to thanks Gudmund Havstad, Reidar Ottefor and Sven Vangbæk for all the technical help I got and also for very nice moments in the lab, my Norwegian would certainly not be the same without them.

In the lab at PGP I got started and then got a lot of help all the way from Dag Kristian Dysthe who was/is a great teacher, I'd like to thank him for all I learned and for his patience! I

had the chance to share the lab with Anja Røyne and Christophe Raufaste, I thank them both for the help, the encouragements when nothing was working and nice scientific and non–scientific discussions. Also, my gratitude goes to Olav Gundersen, for the help of course but also for discussions about sport or other subjects, that was always nice!

I would like to thanks all the students with whom I shared my office: Nazmul Mondol, Manzar Fawad and Tom Erik Maast. And especially Christer Peltonen and Øyvind Marcussen, thanks for nice time in the office but also for showing me around on the campus when I arrived and for the encouragements both on scientific and non–scientific subjects. The pretty much constant good mood of Mattias Lundmark was always pleasant to have around. I also would like to thank him for sharing his teaching passion with me, I feel very lucky to have been teaching with you Mattias. A special thanks goes to Brit Thyberg for a lot of support and encouragements!

Because working on a PhD thesis tends to go over on your personal life, I would like also to thanks people that were not involved in my PhD.
First of all I would like to thanks Christian who had to listen to all the stories of my very difficult life of PhD student. Thank for your support, thank you for being there...
I would like to thanks my flatmates Tobi and Agnar who definitely knew at the moment I came back home in the evening if something was wrong at work :) but nonetheless the atmosphere in the flat was always good and parties great. I would like to thanks Chrystelle for hours long discussions and wine drinking :) Thanks also to Jarkko for 4 years of chatting and nice company in the basement of the geology building. I also would like to thanks Anne, Diğdem, Jan Hendrik, Julien, Vincent, Binyam, Connie, Lukas, Olav, Karen and Liv Hege. I know I am forgetting people but I have to keep the acknowledgements under 2 pages... So...A special thanks goes to all the PhD students of the geology building!!

My stay in Oslo would not have been the same without the basket Girls!! Thank you all for nice moments on and maybe especially outside the court!!

I guess they know, but maybe I should say it 'merci papa, merci maman'. I would like to thanks my parents for their supports throughout the years. I am not sure they were very thrilled when I told them that I would spend some more years at university after my master... to crush rocks in a laboratory... in Oslo... Norway. But nonetheless they were always there when I needed, and always supportive.

If one person always believed on me, even when I didn't, always encouraged me to go for what I wanted and that since 25 years, that's my young brother. Well Pascal (don't worry I'm not gonna ask you to read the thesis) I hope you know what I think.

Contents

Introduction: Problem statement, main findings and conclusions of the thesis

1.1 Introduction

Sedimentary rocks are formed by deposition or precipitation of particles which are then compacted in sedimentary basins. Carbonate rocks represent one of the major sedimentary materials and are economically important as for instance for hydrocarbons reservoirs. Despite this, many questions remains regarding the evolution of their petrophysical properties with stress, temperature, and pore fluid composition changes. The present thesis investigates the relative roles of mechanics and chemistry on the porosity loss of carbonates under stress. Three different experimental setups were used to quantify the effects of various parameters on compaction. Since different sediments have different mechanical and chemical properties leading to various compaction trends, four types of carbonates were studied: cemented limestones, cemented dolostones, calcite single crystals, and bioclastic sand. Carbonate rocks containing clay, such as marl that may contain up to 75% carbonate, were not studied. Chalk is characterized by mechanical and chemical compaction processes relatively different than for other carbonates (*Scholle and Halley*, 1985), it was therefore also excluded from the present study.

Understanding the evolution of sediments petrophysical properties as a function of the pore fluid composition, the mineralogy, or the applied stress is of importance for several fields. For instance, compaction curves, *i.e.* porosity or density versus depth curves, are used as an input for basin modelling, and prediction of reservoir properties (*Sclater and Christie*, 1980; *Audet and Fowler*, 1992; *Goldhammer*, 1997; *Giles*, 1997; *Heydari*, 2000; *Ehrenberg*, 2004); or for backstripping analyses that require to take separately into account the various mineralogy (*Watts and Ryan*, 1976; *Marcussen et al.*, 2010). Compaction processes may drastically modify the rock permeability and affect the fluid flow (*Budd*, 2002; *Revil et al.*, 2002). Therefore the effect of the variation of mechanical and chemical conditions in a reservoir during production or injection also need to be evaluated.

To invert seismic and well log data, a good understanding of the relation between seismic and rock properties is needed (*Christensen and Szymanski*, 1991). Compaction processes affect porosity, permeability, grain contact stiffness or produce microstructures which in turn affect the acoustic signal. The variety of grain size, shape, type of pore and chemical reaction affecting the carbonates makes the relation between acoustic wave velocity and sediment properties especially difficult (*Rafavich et al.*, 1984; *Anselmetti and Eberli*, 1993; *Vanorio et al.*, 2010).

The data presented in this thesis can be mainly used to interpret compaction in sedimentary basins. However, most of the present study considers unconsolidated carbonate and processes affecting such granular materials are also of interest in other research areas. For instance fault gouges are restrengthening during interseismic periods (*Rice*, 1983; *Marone et al.*, 1995). One

of the major process leading to the sealing of wet active fault is pressure solution (*Renard et al.*, 2000; *Tondi*, 2007). An other example is the prediction of gravity driven instabilities. To achieve it, processes leading to more or less cohesion in granular media and rock mass need to be studied, one of them is stress corrosion (*Faillettaz et al.*, 2010). Pressure solution creep and cracks propagation in aggregates are processes also occurring during sediment compaction and studied in the present thesis.

In the first part of this thesis a brief scientific background of the work is given. It includes an introduction to compaction of sediments, including mechanical and chemical compaction as well as their effects on acoustic velocities. Characteristics specific to carbonates are shortly reviewed. Secondly, based on this scientific background the scope of the thesis is described, an introduction to the experimental methods used is given and the main results of the study are presented. Finally this chapter is closed by concluding remarks and suggestions are given for further research within carbonates rock mechanics and rock physics. In the following chapter carbonate compaction is reviewed. Then three individual papers present in more details the work carried out during this PhD project.

1.2 Compaction of sediments

Compaction of sediments during burial involves decrease of the bulk volume occurring mainly by progressive decrease in porosity with increasing depth and/or temperature. Overall sediments are driven toward higher mechanical and thermodynamical stability (*Bjørlykke*, 1999). Compaction is generally divided into two regimes, that is mechanical and chemical compaction. In siliceous sediments these two regimes are rather well separated. In those sediments, mechanical compaction dominates at shallow depth, while chemical compaction becomes predominant at depth corresponding to 60–80 °C ($\sim$ 2–3 km) (*Bjørlykke et al.*, 1989). In carbonate sediments, these two effects are difficult to separate.

1.2.1 Mechanical compaction

Mechanical compaction starts immediately after deposition and is driven by the effective stress applied on the sediments. The effective stress is the stress applied by the overlying sediments from which the pore pressure is subtracted (*Terzaghi*, 1925). Increasing stress leads to water expulsion when possible, if not then overpressure develops and reduces or stop mechanical compaction. In the case of unconsolidated loose sediments, mechanical compaction occurs mainly by grain sliding, rearrangement, and eventually grain crushing. The strain achieved

by mechanical compaction is then dependent on the grain size, the grain sorting and the clay content. Conversely, cemented porous rocks undergo less mechanical compaction, most of the deformation is then elastic and is usually analysed using poroelasticity theory (*Wong et al.*, 2004).

Mechanical compaction ceases to be the main mechanism for compaction when sediments become cemented and therefore over-consolidated with respect to the applied effective stress. Mechanical compaction may, however, be reactivated during reservoir depletion as it was for instance demonstrated by the famous subsidence cases of Wilmington or Ekofisk oil fields (*Nagel*, 2001).

1.2.2 Chemical compaction

Chemical compaction is controlled by thermodynamics and kinetics of fluid–rock interactions. In carbonates, dissolution, conversion of aragonite to calcite, and cementation processes occur at shallow depth. Then pressure solution creep becomes the main active process during chemical compaction. It is driven at the micro-scale by chemical potential differences between the stressed and unstressed part of the solid which causes i) dissolution of minerals along the contact, ii) diffusion toward the pore space, and iii) precipitation on the less-stressed faces of the grains (*Sorby*, 1863; *Weyl*, 1959). The overall rate of deformation is controlled by the slowest of these three processes. Pressure solution may therefore be controlled by the kinetics of either dissolution or precipitation reactions, or by the rate of diffusion along the grain boundary. Diffusive transport along the grain contact is driven by the chemical potential gradient existing between the liquid in the contact and the one in the pore space, the rate of transport also depends on the geometry, i.e. thickness and microstructure, of the grain-to-grain contacts. Intergranular pressure solution creep may be associated with crack propagation in which case the rate of deformation by chemical compaction will be faster.

1.2.3 Rock physics and compaction processes

One goal of rock physics is to link seismic properties to geologic properties by providing quantitative interpretation of physical rock properties, lithologies and pore fluids (*Avseth et al.*, 2005). This goal can only be achieved by first undertaking studies that correlate mineralogy to well–log or seismic data, and second by linking compaction processes, or evolution of various type of porosity with increasing effective stress; this can be done using a combination of laboratory data and rock physics modelling.

In the North Sea, a correlation between mineralogical or geochemical changes and seismic

response was observed (*Thyberg et al.*, 2000). There for instance, quartz cementation in mudstones was linked to seismic velocity increase (*Peltonen et al.*, 2009; *Thyberg et al.*, 2009). In carbonates, lithology and pore type influence acoustic velocities (*Anselmetti and Eberli*, 1993; *Eberli et al.*, 2003; *Agersborg et al.*, 2008). The influence of the pore type might be linked to the surface available for reactions between fluid and rock. For instance the increase or decrease of shear wave moduli between dry and brine saturated carbonates is attributed to the change in surface energy of the pore walls and to dispersion effects (*Verwer et al.*, 2010). More experimental and modelling data need however to be collected to better take into account changes affecting the carbonate framework due to chemical reactions (*Vanorio et al.*, 2010).

1.3 Specificities of carbonate sediments

Porosity versus depth curves for carbonates are less understood than for siliciclastic sediments. This situation is mostly due to the high variability of the carbonates deposition environments (*Bathurst*, 1971) as well as their great chemical reactivity (*Moore*, 2001). Various chemical processes inducing porosity loss have to be considered in carbonate compaction studies. These processes include dissolution, conversion of aragonite to calcite, cementation and dolomitization. Dissolution by meteoric water at the surface may however create high porosities, for instance by the formation of karst.

Compared to siliciclastic sediments, grain shapes in carbonates are highly variable and grains can contain microscopic or macroscopic pores. Therefore individual carbonate grains show varying strength, and aggregates can retain much higher porosity than siliciclastic sands (*Braithwaite*, 2005). Uncemented carbonates have higher friction angles than siliciclastic sand, with φ = 40 (*Coop*, 1990), and limestones are usually less compressible than sandstones (*Wong et al.*, 2004). The mean value for compressive strength of limestones is 100 MPa, a wide range of value is observed, however (*Braithwaite*, 2005).

The various carbonate minerals have different thermodynamics properties (*Morse and Mackenzie*, 1990), therefore chemical compaction affects them differently. Aragonite, $CaCO_3$, is about 1.5 times more soluble than calcite. Calcite, $CaCO_3$, is thermodynamically stable and, unlike quartz, its solubility decreases with increasing temperature in the range 25–350 °C (*Morey*, 1962). Dolomite, $CaMg(CO_3)_2$, is thermodynamically more stable than the two other phases. Solid solutions between calcite and magnesite, Mg–calcites, are often found in shallow water marine sediments, where they are derived from skeletons of organisms and by direct precipitation of marine cements. Their magnesium content has a strong influence on their solubility, for instance, in seawater biogenic magnesian calcite containing about 11 mol % $MgCO_3$ may have

the same solubility as aragonite (*Morse and Mackenzie*, 1990). In this thesis dolomite, calcite and high Mg–calcite are studied.

1.4 Scope of the thesis

A survey of the published literature in the following chapter gives an overview of what is known, and what is not, about carbonate compaction. Based on this knowledge, two main objectives are defined for this thesis. The first objective is to separate and quantify the relative role of mechanical and chemical compaction during carbonate sediments burial. A general question regarding burial of carbonates is: Why is there still porosity left in deeply buried limestones? Based on this the second objective of the thesis is to understand the various mechanisms responsible for porosity loss in carbonate sediments and especially chemical compaction processes.

In nature mechanical and chemical compaction act together (see section 2.2). To be able to separate their effects it is therefore necessary to study them with specifically designed laboratory experiments. Mechanical compaction proceeds differently whether it acts on unconsolidated or consolidated sediments (see section 2.3.1) and, in carbonates, cementation can occur right at the surface. Therefore mechanical compaction of both cemented limestones and dolostones from shallow buried bioclastic carbonate platforms (Paper 1) and unconsolidated carbonate sands (Paper 3) are studied by carrying out uniaxial compression tests.

The main controlling parameters for chemical compaction are stress, temperature, advective and diffusive flow and the pore water composition (see section 2.2.2). The main chemical compaction mechanism is pressure solution associated, or not, with crack propagation. Theoretical compaction laws for aggregates compacting by pressure solution are found in the literature, however no good agreement between theory and experiments has yet been found for carbonates (see section 2.3.2). This points out the need for a better understanding of pressure solution mechanisms at the grain scale. To this end, single contact indentation experiments are carried out on calcite crystals (Paper 2). How chemical compaction acts on aggregates subjected to effective stresses equivalent to 2–3 km burial depth is investigated on calcite and bioclastic carbonate sand by varying the parameters controlling chemical compaction (Paper 3).

During all the uniaxial compression tests (Papers 1 and 3) ultrasonic P- and S–waves velocities were recorded in order to link compaction processes to elastic wave velocities evolution.

1.5 Experimental setups used

Three different experimental setups were used (Figure 1.1). Two different types of uniaxial compression tests were carried out: K_0 triaxial tests and œdometer tests. Uniaxial compression tests are used for compaction studies because they prevent lateral strain which is also prevented in sedimentary basins (*Fjær et al.*, 1992; *Giles*, 1997). To investigate the mechanisms of calcite dissolution under stress at the micrometer scale, a simple setup was designed in which a half–ball lens was pressed against a calcite crystal (Figure 1.1).

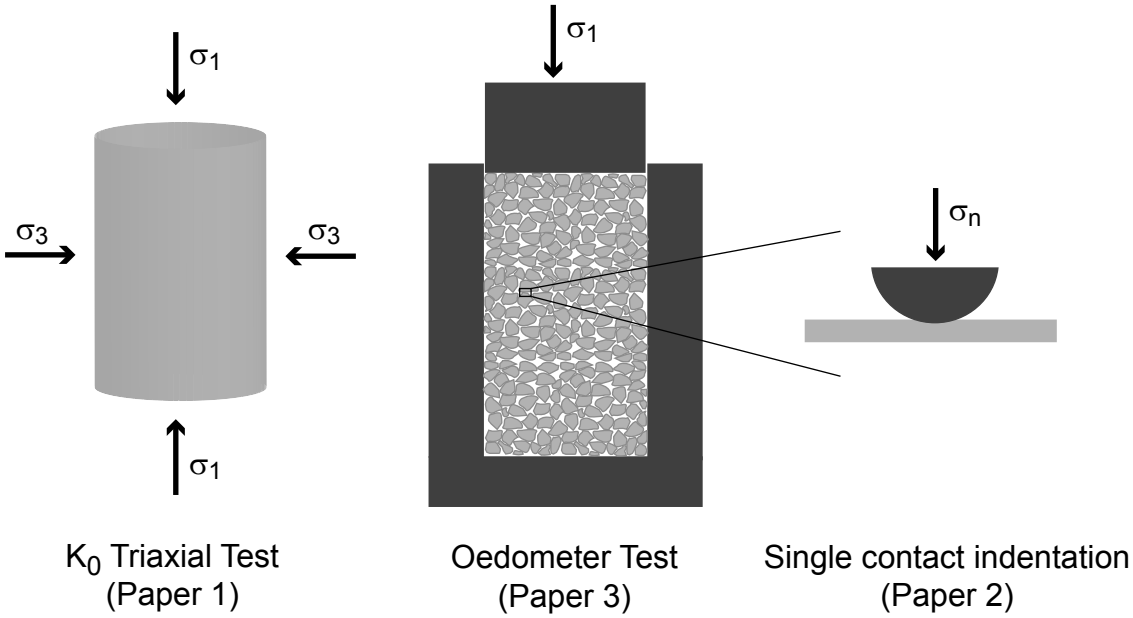

Figure 1.1: Schematic description of the three experimental setups used. The grey colour represents carbonates.

Following the linear elasticity theory, stresses applied on elastic material are linked to the resulting strain by a linear relationship. This enables the determination of two important static material characteristics, that is the elastic modulus, or Young's modulus and the Poisson ratio. In the case of uniaxial strain, the static Young's modulus, E_{stat}, is defined as follows (Turcotte and Schubert, 1982),

$$E_{stat} = \frac{(1+\nu)\cdot(1-2\nu)}{(1-\nu)} \cdot \frac{\sigma_1'}{\epsilon_1}, \tag{1.1}$$

with σ_1' the vertical effective stress, ϵ_1 the vertical strain, and ν_{stat} the static Poisson ratio which can be expressed as follows,

$$\nu_{stat} = \frac{\sigma_3'}{\sigma_1' + \sigma_3'}, \tag{1.2}$$

with σ_3' representing the minimum horizontal stress. From these two parameters it is then pos-

sible to determine the material resistance to compression, the bulk modulus, as well as the material resistance to shear stress, the shear modulus.

In K_0 triaxial tests, both the vertical and horizontal stresses are known, the determination of the material elastic moduli is then straightforward. In the case of œdometer tests, only the vertical applied stress is known, the Poisson ratio would therefore have to be assumed to enable the determination of the other material characteristics.

During uniaxial compression tests, ultrasonic elastic wave propagation through the samples were monitored. Because elastic waves mechanically disturb the samples, their velocity are linked to the elastic moduli and the bulk density, ρ, by the wave equation. Elastic moduli calculated from P- and S–wave velocities, V_p and V_s, respectively, are the dynamic moduli. The dynamic Young's modulus, E_{dyn}, is obtained by,

$$E_{dyn} = 2\rho V_s^2(1+\nu), \tag{1.3}$$

with the dynamic Poisson ratio, ν_{dyn}, expressed as,

$$\nu_{dyn} = \frac{V_p^2 - 2V_s^2}{2(V_p^2 - V_s^2)}. \tag{1.4}$$

The material resistance to compressive and shear stress may then also be expressed as a function of V_p and V_s.

In this thesis, carbonate sediments were characterised by either static moduli (Paper 1) or dynamic moduli (Paper 3). Theoretically, calculation of static and dynamic moduli should give the same values. However, in reality they are significantly different and thus hardly comparable. Several reasons may explain this discrepancy, the main one is certainly that geological materials are often characterised by a non strictly linear stress–strain relationship. Therefore the stress–to–strain ratio over a large strain measurement is different than for a very small one. This results in a strain amplitude of about 10^{-2} during static moduli measurements compared to a strain amplitude of 10^{-7} or less during static moduli measurements, and therefore significant differences between static and dynamic moduli (*Fjær et al.*, 1992; *Mavko et al.*, 2009).

During experiments the influence on final strains or strain rates of various parameters such as pore fluid composition, temperature or stress, was quantified. Then the samples were observed *ex situ* using optical microscopy, scanning electron microscopy or white light interferometry, so that stress–strain relationships during mechanical compaction or strain rates during chemical compaction could be linked to the resulting microstructures.

1.6 Main findings

Paper 1

Petrophysical properties of bioclastic platform carbonates: implications for porosity controls during burial (Marine and Petroleum Geology)

This experimental study investigates the potential for porosity loss by mechanical compaction of platform carbonate strata. To this end sixteen core–plugs samples from two Miocene carbonate platforms on the Marion Plateau, seaward of the Great Barrier Reef, offshore northeast Australia (ODP Leg194) were tested. The samples include eleven bioclastic limestones and five bioclastic dolostones that were deposited in platform-top settings having paleo-water depths of less than 10 to 90 m. They were variably cemented with low-Mg calcite and five of the samples were dolomitized before burial to present depths of 39-635 m below sea floor with porosities of 8 to 46 %.

K_0 tests were carried out and the vertical effective stress, σ_1', was increased from 0 to 70 MPa. Ten samples tested under dry conditions had up to 0.22 % strain at σ_1' = 50 MPa, whereas six samples tested saturated with brine, under drained conditions, had up to 0.33 % strain. The yield strength was reached in five of the plugs.

Overall velocities increased with decreasing porosity. V_p ranged from 3640 to 5660 m/s and V_s from 1840 to 3530 m/s. Poisson coefficient was 0.20-0.33 and Young's modulus at 30 MPa ranged between 5 and 40 GPa. Water saturated samples had lower shear moduli and slightly higher P- to S-wave velocity ratios. Mechanical creep at constant stress was observed only in samples that reached their yield strength, indicating a slow propagation of microcracks.

Although deposited as loose carbonate sand and mud, the studied carbonates acquired reef-like petrophysical properties by early calcite and dolomite cementation. The main conclusions of the study are:

- Total porosity and early cementation are fundamental controls on carbonate rock strength and compressibility, as well as on other parameters like elastic moduli.
- Early cementation of bioclastic carbonate sediments created a stable cemented framework with a high degree of over-consolidation and low compressibility.
- Water saturation of the samples produced weakening of the mechanical strength and greater scatter in the correlation of P-wave velocity versus porosity.
- Variation in mineralogy does not influence the compressibility of the plugs strongly, but acoustic velocities of dolostones are systematically higher than in limestones.

- Most of the present carbonate sediments were already so strongly cemented at 30–400 meters that further porosity loss during burial up to 4–5 km depth must occur mainly by chemical rather than mechanical processes. The more porous samples, however, would respond to increased burial by failure due to crack propagation.

Paper 2

Calcite dissolution under stress: Evolution of grain contact microstructure during pressure solution creep (Journal of Geophysical Research)

This experimental study investigates the rate of calcite deformation by pressure solution creep at a single contact, and determines the evolution of the contact geometry during dissolution under stress. Iceland spar calcite crystals were indented by half–ball lenses made of either glass or sapphire. The surface area of the samples was about 2*2 mm^2 and their thickness varied in the range 150–680 μm. Water was present at the calcite/lens interface. Two nanometre resolution techniques both *in situ* and *ex situ* were used to measure deformation and their results compared.

From these results it was possible to identify the relative importance of pressure solution driven by normal load, and free surface dissolution driven by strain energy, and how these mechanisms couple to mass transport in fluid films and fractures. The main conclusions of the study are:

- Two different processes occur during pressure solution of calcite crystals at the grain scale. The occurrence of one or the other mechanism does not appear to be ruled by the applied stress but is most likely dependent on the presence or not of a flaw in the crystal. In one case, diffusion of the dissolved solid takes place in the pore fluid present along a rough interface between calcite and the indenter. In the second case, diffusion occurs through cracks that propagate from the contact toward the less stressed part of the crystal.

- Strain rates are higher for experiments in which crack propagation occurred. This in agreement with earlier experimental studies, which show that for experiments conducted on aggregates or single crystals, strain rates increase by one to two orders of magnitude when crack propagation occurs.

- Overall it seems strain rates are not really stress dependent but rather dependent on the grain size or whether crack propagation occurs or not.

Paper 3

Experimental mechanical and chemical compaction of carbonate sand (submitted to Journal of Geophysical Research)

This experimental study determines mechanical and chemical compaction processes active during compaction of carbonate sands saturated with various fluids. Carbonate sand petrophysical properties and their evolution during burial or fault zones processes are quantified.

Two types of samples were used in this study. Firstly, Holocene shell fragments from beaches near Tromsø, northern Norway were compacted. These samples contain small amount of siliceous impurities and are characterised by a large amount of mollusc shells having internal porosity. Secondly, calcite single crystals were crushed and then compacted. Three grain sizes were used in the range 63–500 μm. The samples were saturated with air, decane, glycol, water in equilibrium with carbonate, or a solution of 5% NH_4Cl in equilibrium with carbonate. The samples were uniaxially compacted up to 32 MPa effective stress. Creep tests were also carried out on bioclastic sands at effective stress of 10, 20 and 30 MPa. P- and S–waves were monitored during both loading and creep phase.

Experimental compaction has shown that compaction of carbonates sands should be modelled as a function of both mechanical and chemical compaction also at relatively shallow depth and low temperature. In all cases, the nature of the fluid, the initial grain packing, and the grain size represent important control parameters of the final strain and the strain rates at a given stress. The main conclusions of the study are:

- In samples saturated with reactive fluids, *e.g.* water in equilibrium with carbonate or glycol/water mixture, significant chemical compaction was documented during the loading phase. Samples saturated with non–reactive fluids, *e.g.* air or decane, showed less strain at the same effective stress since the compaction was only mechanical.

- During the loading phase, chemical compaction occurred by pressure solution creep which was enhanced by the presence of cracks at the grain–to–grain contacts. This is also supported by the identification of compaction related microstructures in thin–sections.

- During creep tests carried out on bioclastic carbonate sand, the deformation was mostly due to chemical reactions. Furthermore, pore water analysis, and especially the evolution of the Mg^{2+}/Ca^{2+} ratio, showed that magnesian calcite dissolved during experiments.

- In all the creep experiments, the strain versus time relation followed a power law in time, with a single exponent equal to 0.23. Overall it was found that a combination of pressure

solution creep and subcritical crack growth was responsible for strain, and strain rates in the range $2.9{\cdot}10^{-8}$–$2.8{\cdot}10^{-6}$ s^{-1}.

- During creep tests, the samples compressibility was controlled by, in order of importance, grain size, stress, and water saturation. Pressure solution was most likely the dominant mechanism of compaction in samples saturated with water. Conversely, in samples saturated with glycol or anisole, subcritical crack growth was most likely the main mechanism of deformation.

- Ultrasonic velocity measurements showed that P- and S–waves velocities were in the range of 705 to 2440 m/s and 535 to 1250 m/s, respectively. Low velocities were especially observed in samples saturated with reactive fluids. Dissolution and transport affecting the grain–to–grain contacts geometry and crack propagation are likely to be the reason for such velocity alteration.

1.7 Conclusions

Mechanical compaction was studied during uniaxial compression tests of samples saturated with air or decane. Cemented limestones and dolostones samples having up to 32% inital porosity showed almost no porosity loss at effective stresses up to 50 MPa ($\sim$ 3–4 km). Their compaction was close to purely linear–elastic until those stresses. Loose bioclastic carbonate sands starting with 60% porosity had still about 40% porosity at 32 MPa effective stress, and crushed calcite samples having initial porosities of about 46% had still about 25% porosity when compacted up to 32 MPa ($\sim$ 2–3 km). Looking at natural compaction trends for carbonate sediments, porosity at such depth are found to be around 10-20%. This allows the conclusion that in sedimentary basins carbonates would probably loose most of their porosity through chemical compaction and that this starts at shallow depth.

In the samples studied and within the range of stresses investigated, chemical compaction occurred most of the times by a combination of pressure solution and subcritical crack growth. Whether dissolution under stress occurred by pressure solution only or by a combination of pressure solution and subcritical crack growth resulted in two different grain contact geometries. Propagation of cracks at the grain–to–grain contact affected the fluid diffusion path and therefore the strain rates. In aggregates, parameters controlling chemical compaction, and therefore strain rates, were the grain size and initial packing, the applied effective stress and the water saturation. The predominance of pressure solution or subcritical crack growth during aggregates compaction was found to be related to the fluid in presence. While propagation or not of cracks

during single contact calcite indentation was most likely related to the presence or absence of flaws near the contact.

In cemented rocks, water saturation resulted in a weakening of the mechanical strength associated with a greater scatter in the ultrasonic P–wave velocity versus porosity relation. In aggregates, ultrasonic velocities were found to be abnormally low in samples saturated with reactive fluids, probably due to dissolution modifying the grain–to–grain contact geometry, and crack propagating through the grains weakening the grain framework strength.

The present results raised questions that could not be answered within the given time or pointed out potentially interesting research topics. To be able to fully answer the question "why is there still porosity at depth up to 5 km in carbonate sediments?" a better understanding of the interaction between pressure solution and crack propagation is needed. The coupling of this two mechanisms and the derivation of strain rate laws describing compaction by mean of pressure solution associated with subcritical crack growth as initiated by *Zhang et al.* (1990) or *Yasuhara and Elsworth* (2008) should be studied in more details and extended to carbonates. This would also need more experiments investigating the relation between applied stress and crack propagation at both the grain and aggregate scale. Single contact experiments on calcite–calcite contacts investigating the potential for grain contact healing in carbonate would also be useful. To apply the knowledge obtained on carbonate compaction in the laboratory to sedimentary basins, correlation between the resulting rock properties and seismic properties need to be done. Ultrasonic waveforms were recorded during uniaxial compression tests. More could be done on these data to investigate the effect of compaction processes on ultrasonic velocities and try to link it to seismic data. To this end the relation between static and dynamic moduli in carbonates should also be investigated. In addition, specific experiments should be designed to investigate the effect of contact geometry and chemical processes at the grain–to–grain contact on ultrasonic velocities.

Bibliography

Agersborg, R., T. A. Johansen, M. Jakobsen, J. Sothcott, and A. Best (2008), Effects of fluids and dual-pore systems on pressure-dependent velocities and attenuations in carbonates, *Geophysics*, *73*(5), N35–N47.

Anselmetti, F. S., and G. P. Eberli (1993), Controls on sonic velocity in carbonates, *Pure and Applied Geophysics*, *141*(2-4), 287–323.

Audet, D., and A. C. Fowler (1992), A mathematical model for compaction in sedimentary basins, *Geophysical journal international*, *110*(3), 577–590.

Avseth, P., T. Mukerji, and G. Mavko (2005), *Quantitative seismic interpretation: applying rock physics tools to reduce interpretation risk*, Cambridge University Press, Cambridge.

Bathurst, R. G. C. (1971), *Carbonate sediments and their diagenesis*, *Developments in Sedimentology*, vol. 12, Elsevier, Amsterdam-Oxford-New York, Netherlands.

Bjørlykke, K. (1999), An overview of factors controlling rates of compaction, fluid generation and flow in sedimentary basins, in *Growth, dissolution and pattern formation in geosystems.*, edited by B. Jamtveit and P. Meakin, pp. 381–404, Kluwer Academic Publishers, Dordrecht, Netherlands.

Bjørlykke, K., M. Ramm, and G. Saigal (1989), Sandstone diagenesis and porosity modification during basin evolution, *Geologische Rundschau*, *78*(1), 243–268, doi: 10.1007/BF01988363.

Braithwaite, C. J. R. (2005), *Carbonate sediment and rocks: a manual for earth scientists and engineers*, Whittles Publ., Dunbeath.

Budd, D. A. (2002), The relative roles of compaction and early cementation in the destruction of permeability in carbonate grainstones; a case study from the paleogene of west-central florida, u.s.a, *Journal of Sedimentary Research*, *72*(1), 116–128.

Christensen, N. I., and D. L. Szymanski (1991), Seismic properties and the origin of reflectivity from a classic paleozoic sedimentary sequence, valley and ridge province, southern appalachians, *Geological Society of America Bulletin*, *103*(2), 277–289.

Coop, M. R. (1990), The mechanics of uncemented carbonate sands, *Geotechnique*, *40*(4), 607–626.

Eberli, G. P., G. T. Baechle, F. S. Anselmetti, and M. L. Incze (2003), Factors controlling elastic properties in carbonate sediments and rocks, *The Leading Edge*, *22*(7), 654–660.

Ehrenberg, S. N. (2004), Factors controlling porosity in the upper carboniferous-lower permian carbonate strata of the barents sea, *AAPG Bulletin*, *88*(12), 1653–1676.

Faillettaz, J., D. Sornette, and M. Funk (2010), Gravity-driven instabilities: Interplay between state- and velocity-dependent frictional sliding and stress corrosion damage cracking, *J. Geophys. Res.*, *115*(B3), B03,409, doi:10.1029/2009JB006512.

Fjær, E., R. M. Holt, P. Horsrud, A. M. Raaen, and R. Risnes (1992), *Petroleum related rock mechanics*, Elsevier, Amsterdam.

Giles, M. R. (1997), *Diagenesis: a quantitative perspective – Implications for basin modelling and rock property prediction*, Kluwer Academic Publishers, Dordrecht, The Netherlands.

Goldhammer, R. K. (1997), Compaction and decompaction algorithms for sedimentary carbonates, *Journal of Sedimentary Research*, *67*(1), 26–35.

Heydari, E. (2000), Porosity loss, fluid flow, and mass transfer in limestone reservoirs; application to the upper jurassic smackover formation, mississippi, *AAPG Bulletin*, *84*(1), 100–118.

Marcussen, Ø., J. I. Faleide, J. Jahren, and K. Bjørlykke (2010), Mudstone compaction curves in basin modelling: a study of mesozoic and cenozoic sediments in the northern north sea, *Basin Research*, *22*(3), 324–340, doi: 10.1111/j.1365-2117.2009.00430.x.

Marone, C., J. E. Vidale, and W. L. Ellsworth (1995), Fault healing inferred from time dependent variations in source properties of repeating earthquakes, *Geophys. Res. Lett.*, *22*(22), 3095–3098, doi: 10.1029/95GL03076.

Mavko, G., T. Mukerji, and J. Dvorkin (2009), *The Rock Physics Handbook: Tools for Seismic Analysis of Porous Media*, 2nd ed., Cambridge University Press, Cambridge.

Moore, C. H. (2001), *Carbonate reservoirs; porosity evolution and diagenesis in a sequence stratigraphic framework*, *Developments in Sedimentology*, vol. 55, Elsevier. Amsterdam-Oxford-New York, Netherlands.

Morey, G. W. (1962), Action of water on calcite, magnesite and dolomite, *American Mineralogist*, *47*(11-1), 1456–1460.

Morse, J. W., and F. T. Mackenzie (1990), *Geochemistry of sedimentary carbonates*, Elsevier, Amsterdam.

Nagel, N. B. (2001), Compaction and subsidence issues within the petroleum industry: From wilmington to ekofisk and beyond, *Physics and Chemistry of the Earth, Part A: Solid Earth and Geodesy*, *26*(1-2), 3–14, doi: 10.1016/S1464-1895(01)00015-1.

Peltonen, C., Ø. Marcussen, K. Bjørlykke, and J. Jahren (2009), Clay mineral diagenesis and quartz cementation in mudstones: The effects of smectite to illite reaction on rock properties, *Marine and Petroleum Geology*, *26*(6), 887–898.

Rafavich, F., C. H. S. C. Kendall, and T. P. Todd (1984), The relationship between acoustic properties and the petrographic character of carbonate rocks, *Geophysics*, *49*(10), 1622–1636.

Renard, F., J. P. Gratier, and B. Jamtveit (2000), Kinetics of crack-sealing, intergranular pressure solution, and compaction around active faults, *Journal of Structural Geology*, *22*, 1395–1407.

Revil, A., D. Grauls, and O. Brévart (2002), Mechanical compaction of sand/clay mixtures, *J. Geophys. Res.*, *107*(B11), 2293.

Rice, J. (1983), Constitutive relations for fault slip and earthquake instabilities, *Pure and Applied Geophysics*, *121*(3), 443–475, doi: 10.1007/BF02590151.

Scholle, P. A., and R. B. Halley (1985), Burial diagenesis; out of sight, out of mind!, in *Carbonate cements.*, *Special Publication - Society of Economic Paleontologists and Mineralogists*, vol. 36, edited by N. Schneidermann and M. Harris Paul, pp. 309–334, SEPM (Society for Sedimentary Geology), Tulsa, OK, United States.

Sclater, J. G., and P. A. F. Christie (1980), Continental stretching; an explanation of the post-mid-cretaceous subsidence of the central north sea basin, *Journal of Geophysical Research*, *85*(B7), 3711–3739.

Sorby, H. C. (1863), The bakerian lecture: On the direct correlation of mechanical and chemical forces, *Proceedings of the Royal Society of London*, *12*, 538–550.

Terzaghi, K. (1925), *Erdbaumechanik auf bodenphysikalischer Grundlage*, Deuticke, F, Leipzig/Vienna.

Thyberg, B., J. Jahren, T. Winje, K. Bjørlykke, J. I. Faleide, and Ø. Marcussen (2009), Quartz cementation in late cretaceous mudstones, northern north sea: Changes in rock properties due to dissolution of smectite and precipitation of micro-quartz crystals, *Marine and Petroleum Geology*, *In Press, Corrected Proof*, doi: 10.1016/j.marpetgeo.2009.07.005.

Thyberg, B. I., H. Jordt, K. Bjørlykke, and J. I. Faleide (2000), Relationships between sequence stratigraphy, mineralogy and geochemistry in cenozoic sediments of the northern north sea, in *Dynamics of the Norwegian Margin*, vol. 167, edited by A. Nøttvedt, pp. 245–272, Geological Society Special Publication, London.

Tondi, E. (2007), Nucleation, development and petrophysical properties of faults in carbonate grainstones: Evidence from the san vito lo capo peninsula (sicily, italy), *Journal of Structural Geology*, *29*(4), 614–628.

Turcotte, D. L., and G. Schubert (1982), *Geodynamics; applications of continuum physics to geological problems*, John Wiley & Sons, New York, NY, United States.

Vanorio, T., G. Mavko, S. Vialle, and K. Spratt (2010), The rock physics basis for 4D seismic monitoring of CO_2 fate: Are we there yet?, *The Leading Edge*, *29*(2), 156–162.

Verwer, K., G. Eberli, G. Baechle, and R. Weger (2010), Effect of carbonate pore structure on dynamic shear moduli, *Geophysics*, *75*(1), E1–E8.

Watts, A. B., and W. B. F. Ryan (1976), Flexure of lithosphere and continental-margin basins, *Tectonophysics*, *36*(1-3), 25–44.

Weyl, P. K. (1959), Pressure solution and the force of crystallization – a phenomenological theory, *Journal of Geophysical Research*, *64*(11), 2001–2025.

Wong, T.-f., C. David, and B. Menédez (2004), Mechanical compaction, in *Mechanics of Fluid - Saturated Rocks*, edited by Y. Guéguen and M. Boutéca, International geophysics series, p. 450, Elsevier Academic Press, Amsterdam.

Yasuhara, H., and D. Elsworth (2008), Compaction of a rock fracture moderated by competing roles of stress corrosion and pressure solution, *Pure and Applied Geophysics*, *165*(7), 1289–1306, doi:10.1007/s00024-008-0356-2.

Zhang, J., T. f. Wong, and D. M. Davis (1990), Micromechanics of pressure-induced grain crushing in porous rocks, *Journal of Geophysical Research, B, Solid Earth and Planets*, *95*(1), 341–352.

Carbonate compaction: A review of observations, theory, and experiments

Abstract

Carbonates are one of the major sedimentary materials. Understanding their compaction behaviour is important for porosity prediction in sedimentary basins or to improve the knowledge about sealing of active faults. In carbonates, as opposed to siliciclastic sediments, diagenesis starts at shallow depth and can contribute to the formation of a mechanically stable framework. Vertical stress, grain size and clay content are the main parameters influencing mechanical compaction. After 1-2 km burial, chemical compaction by pressure solution becomes an effective process of porosity reduction. The main parameters controlling porosity loss then become vertical stress, temperature, diffusive flow and pore fluid chemistry. Both mechanical and chemical compaction can lead to either pervasive compaction or localized deformation. The effect of the different parameters cannot easily be differentiated in observations of natural samples, as various deformation processes occur and interact simultaneously. However, control parameters may be separated in specifically designed theoretical and experimental studies.

Compaction of unconsolidated carbonate sands in laboratory occurs mostly at low stress and is mainly controlled by mineralogy and initial packing of grains. It can explain porosity reduction down to about 30% at 2.5 km. Conversely, very little porosity loss ($< 1\%$) is obtained by mechanical compaction of cemented rock. In sedimentary basins, however, much lower porosity values are usually encountered at such depth. Given that mechanical compaction does not explain satisfactorily porosity–depth trends observed in sedimentary basins, the effect of chemical compaction on porosity must be considered. Among chemical mechanisms, pressure solution involves local mass transfer by dissolution, diffusion and precipitation processes at the grain scale. Subcritical crack growth is also a fluid assisted process contributing to compaction. Pressure solution creep strain rate depends on grain size, porosity, applied stress, fluid chemistry, and temperature. So far little experimental work has been performed on pressure solution and subcritical crack growth in carbonates. However, time dependent creep experiments on calcite powder and indenter experiments on calcite crystals show that time dependent compaction is a water assisted process. Even though the different controlling parameters were tested, no clear consensus exists on the rate limiting step of deformation and, consequently, on the creep law.

Individual processes leading to porosity loss in carbonates are rather well identified. No consensus exists on their respective importance during burial, however. Even at shallow burial ($<$1 km) chemical compaction is needed to explain the gap between porosity loss obtained during experimental mechanical compaction and porosity-depth curves from sedimentary basins. This chapter provides a review of the various processes at work during carbonate compaction and synthesizes the current understanding on the respective importance of thermodynamic and

petrophysical parameters at different stages of the carbonate compaction.

2.1 Introduction

Sedimentary materials are consolidated, or compacted, during their burial history. Porosity loss in sedimentary basins has been widely studied especially due to the interest of the oil and gas industry in understanding accumulation of hydrocarbons. Even though 60% of the world oil and 40% of the world gas reserves are held in carbonates (Schlumberger market analysis, 2007) their burial compaction trends, *i.e.* porosity versus depth curves, are less understood than for siliciclastic sediments. This situation is most likely due the the high variability of the carbonates deposition environments (*Bathurst*, 1971) as well as their great chemical reactivity (*Moore*, 2001).

Principal deformation mechanisms responsible for compaction are on the one hand mechanical, *i.e.* grains sliding and fracturing, and on the other hand chemical, *i.e.* intergranular pressure solution creep in association, or not, with subcritical crack growth. Various chemical processes inducing porosity loss have to be taken into account in carbonate compaction studies. These processes include dissolution, conversion of aragonite to calcite, cementation and dolomitization.

Compaction studies based on outcrops and core materials lead to the conclusion that pressure solution creep is an important process of porosity reduction in carbonate sedimentary rocks (*Weyl*, 1959; *Schmoker and Halley*, 1982; *Rutter*, 1983; Meyers and Hill, 1983; *Scholle and Halley*, 1985). However, from natural observation, it is rather difficult to separate the influence of different parameters such has stress, temperature or pore fluid composition. Thus theoretical and experimental studies are conducted to quantify the influence of these different parameters. Understanding processes driving porosity loss in sedimentary basins is necessary to, for instance, enable prediction of porosity in geological reservoirs.

This review aims at outlining the state of knowledge on carbonate compaction based on natural observations, laboratory experiments and theoretical modelling. During diagenesis of carbonate sediments, change in porosity are induced by a combination of deformation processes, dissolution and cementation. Even though this is not the focus of the present review, dissolution and cementation at shallow depth will be covered in the extent that it affects compaction processes. In the first part an overview of natural observation of carbonate compaction is given. It is shown that by using natural observation, log and seismic data, it is possible to qualitatively separate the main deformation processes. Compaction of siliciclastic sediments is not the focus of this review but the topic will be address succinctly since comparison may help

to the understanding of carbonate compaction. In a second part theoretical models for mechanical and chemical compaction of carbonates are reviewed. These models are usually calibrated based on laboratory experiments that lead to a better quantification of the control parameters involved in natural processes.

2.2 Carbonate compaction in sedimentary basins

Compaction is a phenomenon taking place in all sedimentary basins. It involves several processes whose rates differ from one lithology to another. For instance, comparison of limestones compaction trends within the first hundred meters of burial with siliciclastic sediments shows that porosity loss is far more important in calcareous sediments (*Hamilton*, 1976). Similarly, Ehrenberg and Nadeau (2005) study of carbonate and sandstone petroleum reservoirs, show that carbonate reservoirs have lower values of median and maximum porosity for a given depth than sandstone reservoirs. Moreover, this compaction can be pervasive, where porosity reduction is quite homogeneous within the rock (*Ginsburg*, 1957), or highly localized, *i.e.* compaction bands, stylolites (*Ehrenberg*, 2003).

Within carbonates, three main lithology groups may be differentiated, that is dolomite, limestone and chalk. Dolomite and chalk can be seen as two end members as far as porosity loss with depth is concern. Porosity loss is faster in limestones than in dolomites (*Schmoker and Halley*, 1982; Ehrenberg et al., 2006b), while porosity loss in chalk occurs faster than in shallow water carbonates (*Scholle and Halley*, 1985). Dolomites are chemically (*Bathurst*, 1971) and mechanically (*Hugman and Friedman*, 1979) more stable than limestones. Thus dolomitic rocks loss less volume by compaction than limestone (*Glover*, 1968). In contrast the fine grained nature of chalk enhances mechanical reorganization. Hence high porosities and low permeabilities characteristic of chalk make them very susceptible to deform by pore collapse and hydro-fracturing (*Blanton*, 1981). These different compaction trends between various lithologies point out the necessity to analyze them separately. In the following, the focus will be primarily on limestone and, to some extent, dolomite and chalk compaction will be addressed.

Porosity of carbonate sediments ranges from 50-70% at shallow depth (e.g. few hundreds of meters) (*Hamilton*, 1976; *Schmoker and Halley*, 1982; *Fabricius*, 2003) to nearly zero at depth greater than 6 km (*Friedman et al.*, 1981; *Heydari*, 2000). It is, however, worth to mention that some carbonate reservoirs preserve high porosity even though being deeply buried, the most recent discovery being the deep water carbonate reservoir in the Santos basin, off-shore Brazil (*Caminatti et al.*, 2009).

Figure 2.1 displays some typical trends of porosity loss with depth in carbonates sediments.

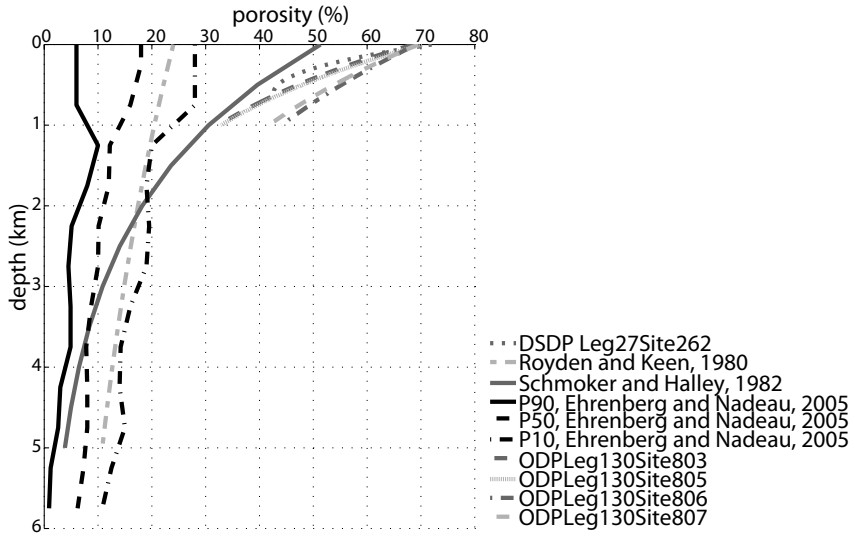

Figure 2.1: Porosity loss with depth in carbonates from different environments (Fitting curves for DSDP leg 27 from *Hamilton* (1976), and for ODP Leg 130 from *Bassinot et al.* (1993).)

Those curves illustrate the large variability of carbonate compaction, especially at shallow depth, which might partly be explained by the wide range of initial porosities 10 to 70% (Figure 2.1). These data represent carbonates from various environments, deep-sea calcareous sediments from DSDP leg 27 and ODP leg 131 (*Hamilton*, 1976), and near-surface sediments from the South Florida basin (*Schmoker and Halley*, 1982). Both data-sets indicate a fast compaction in the top 600 m and show that sediments with high initial porosity compact more readily. While within the two first kilometres porosity versus depth curves have various trends, below this depth compaction curves are more or less parallel (Figure 2.1). Although compaction trends are quite similar among the different environments represented in figure 2.1, at five kilometres depth a wide porosity range is still observable, *i.e.* from 5 to 15%.

Processes responsible for compaction involve both mechanical, *i.e.* stress dependent and time independent, and chemical, *i.e.* involving time-dependent fluid-rock interactions, mechanisms. A detailed review of their effect on porosity loss is undertaken in the following part of this section. Porosity–depth trends (Figure 2.1) are regular, indicating that porosity reduction in carbonates is a continuous process (*Scholle and Halley*, 1985). Mechanical and chemical compaction are, therefore, expected to always act together, the first one being dominant at shallow depth, while chemical compaction slowly becomes the main porosity reduction mechanism.

2.2.1 Mechanical compaction

Field observations, core and log data analysis (*Hamilton*, 1976; Enos and Sawatsky, 1981; *Scholle and Halley*, 1985; *Bassinot et al.*, 1993; Wallace et al., 2002) tend to conclude that

mechanical compaction is the principal mechanism of porosity loss during the first hundreds meters of burial. Empirical mechanical compaction law often describe porosity loss with depth as an exponential decay (*Athy*, 1930; *Sclater and Christie*, 1980),

$$\Phi = \Phi_0 e^{-bz}, \tag{2.1}$$

with Φ the porosity function of the initial porosity, Φ_0, the burial depth, z, and a constant, b. These laws can fit porosity-depth trends of grain supported carbonates from the Cenozoic platform of West-Central Florida (*Budd*, 2001), ooze limestones in the shallow waters of the Ontong Java Plateau (*Hamilton*, 1976; *Bassinot et al.*, 1993), and cold water carbonates of the Gippsland basin, Australia (Wallace et al., 2002). From these studies it seems that, even though early diagenesis and chemical compaction due to replacement of aragonite by calcite occur, mechanical compaction is the predominant mechanism of porosity loss at shallow depth in various environments.

From microstructural studies, at least four different mechanisms involved in mechanical compaction can be discriminated, that is grain sliding, grain crushing, micro-crack propagation, and pore collapse. Mechanical compaction in carbonates is affected mainly by stress, grain size and sorting, and clay content. Grain size in carbonates is related to the biological and physical origin of the carbonate (*Coogan and Manus*, 1975). Due to the increase in friction, adhesion and bridging with decreasing grain size, compaction of fine sediments is less effective than for coarse grains (*Coogan and Manus*, 1975). Heterogeneity in grain size distribution enhances mechanical compaction as well (*Chuhan et al.*, 2003). In carbonates sediments mixed with clays, mechanical compaction is more important in layers containing clays (*Ricken*, 1987). This can be explained by two mechanisms, on the one hand, clay particles increase the heterogeneity of the grain size distribution. On the other hand, clay trapped along carbonate grain contacts may prevent healing of these contacts and reduce the friction coefficient, allowing grain sliding (*Renard et al.*, 2001).

The rate of sedimentation, or sediments loading, is also a very important control of compaction. Carbonate sediments which undergone fast burial show more mechanical compaction patterns than those subjected to a slower sedimentation rate (*Scholle and Halley*, 1985). Within sediments compacting slowly enough time is available for chemical compaction processes to be operative. This may therefore reduce the effect of mechanical compaction. In natural environments, mechanical compaction is very effective to reduce porosity down to 30-40 %. To reduce further the porosity, either large differential stresses, producing pore collapse or fracturing, are needed, or chemical compaction has to play a role (*Scholle and Halley*, 1985).

2.2.2 Chemical compaction

Chemical compaction involves early meteoric and marine diagenesis, as well as crack propagation in presence of reactive fluid and dissolution - precipitation resulting from pressure solution. While early diagenesis is not a function of the stress, pressure solution and crack propagation are strongly dependent on stress. All these mechanisms are also strongly dependent on the fluid chemistry.

Pressure solution produces characteristic microstructures such as stylolites (Figure 2.2A, B) or grain–to–grain indentation (Figure 2.2D). Crack propagating in grains can then be sealed by calcite precipitating in the veins (Figure 2.2C). Petrographic studies allow some quantification of the respective role of mechanical and chemical compaction in natural carbonate through observation of microstructures (*Meyers*, 1980; *Gratier et al.*, 1999; *Budd*, 2002).

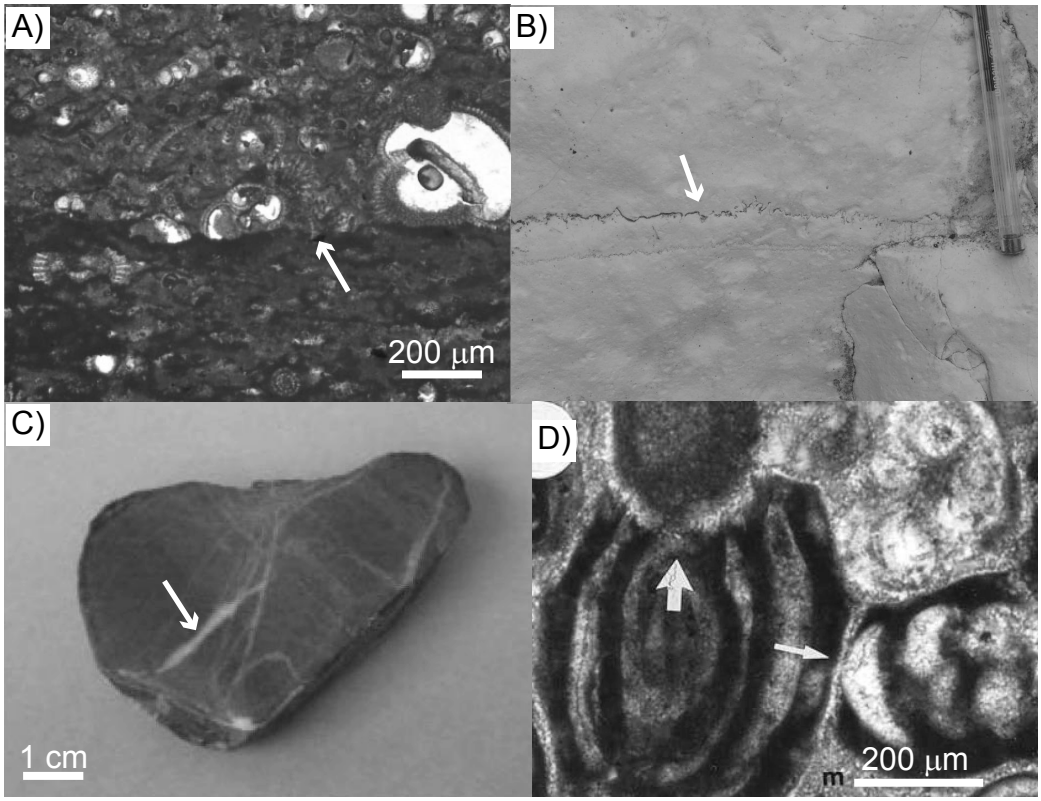

Figure 2.2: A) Microstylolite (white arrow), foraminifers are truncated by enhanced dissolution adjacent to a thin clay seam (picture from ODP Leg 192, Site 1183). B) Stylolite (white arrow) in Flamborough chalk, Yorkshire, UK. C) Limestone pebble fractures fill with calcite (white arrow), area of grenoble, France (picture from *Gratier et al.* (1999)). D) Avon park grainstones, USA, m = microspar cement, large arrow = grain interpenetration (Picture from *Budd* (2002)).

High permeability favours water-rock interaction and thus porosity loss. In some cases, highly permeable shallow water carbonates may be affected by dissolution and thus porosity gain, however. High permeability are found in coarse sands or grain supported carbonates (Enos

and Sawatsky, 1981; *Budd*, 2001). Conversely, carbonate muds are highly porous but have very low permeability, thus carbonate muds are less affected by early cementation than carbonate sands (Enos and Sawatsky, 1981; *Goldhammer*, 1997). Nevertheless when reactive flow conditions required for early cementation are met, precipitation of matter in the pore space contribute to the formation of a mechanically stable framework which prevents further compaction. For instance the Upper Jurassic Smackover Formation (Alabama) is constituted of oolitic and pelletal grainstones, which were strongly affected by early cementation. In these reservoirs a stable framework was built (*Kopaska-Merkel et al.*, 1994), therefore very little mechanical compaction occurred and an average porosity of 17 % was preserved at about 3600 m depth.

Burial depth, or effective vertical stress applied on sediments plays an important role on porosity reduction. Interactions with other controlling parameters such as temperature, pore water chemical composition, clay content are significant. Time is of course an important parameter for chemical compaction since it involves the chemical reaction kinetics. However, considering the fast kinetics of carbonate reactions, geological time is not a limiting factor and therefore this parameter is not taken into account here. In the following paragraphs, the role of stress, temperature, water flow and pore fluid chemistry are discussed separately. A special emphasis is made on their relative importance in carbonate compaction by pressure solution creep.

Effect of stress

From field observations, decrease of porosity in carbonates appears to be primarily a function of depth rather than time (*Royden and Keen*, 1980; *Schmoker and Halley*, 1982). In other words stress appears as the main driving force for compaction in carbonate sedimentary sequences. Vertical effective stress acting at the grain-to-grain contact is the main driving force for pressure solution creep. As a matter of fact intergranular pressure solution initiates with stress and to some extent with temperature increase. Once initiated it then becomes a very effective mean of porosity reduction (Meyers and Hill, 1983). In their study of Oligocene-Holocene cool water carbonates, Wallace et al. (2002) noticed that calcite cement increased with depth. In this same study, few signs of pressure solution were observed at depths less than one kilometre. Conversely, at greater depth, intergranular pressure solution was well developed and was the most obvious deformation mechanism in skeletal packstones (Wallace et al., 2002). Carbonate rocks from Anadarko basin (south-west Oklahoma), or ooid grainstones of the Upper Jurassic Smackover Formation (Alabama) (*Friedman et al.*, 1981; *Heydari*, 2000) were exposed to high vertical stresses, *i.e.* burial depth of 6 and 9 km respectively, but also to high temperatures

exceeding 200°C. In those formations, combination of mechanical and chemical compaction acted to reduce porosity. Macro- and microscopic observations of these sediments show extensive twin development on large calcite crystals, cataclastic textures, pressure solution features, cementation and grain deformation (*Friedman et al.*, 1981; *Heydari*, 2000), making difficult to separate the effects of all these mechanisms. The combination of all these processes reduced porosity to almost zero in these formations. A common feature of these different studies is that, while very little signs of pressure solution are observed at shallow depth, the number of pressure solution features increase significantly with depth. This might be an indication that pressure solution starts to be an active process of porosity reduction when a minimum amount of stress is reached.

Effect of temperature

Comparison of siliciclastic and carbonate sediments show that carbonate compaction is more sensitive to stress and to a lesser extend to temperature (*Giles*, 1997). Dissolution and precipitation processes in calcite are affected by the temperature in two manners. On the one hand, solubility of calcite decreases with temperature, on the other hand kinetics of calcite dissolution is activated by a temperature increase. These two effects compete each other, and almost cancel for pressure solution creep (*Renard et al.*, 2000). Several field observations, however, indicate that porosity loss with increasing depth can be related to increasing thermal exposure in several carbonate reservoirs (*Friedman et al.*, 1981; *Heydari*, 2000; Ehrenberg and Nadeau, 2005; *Bolås et al.*, 2008).

Effect of advective and diffusive fluid flow

Advective flow in sedimentary basin is in general rather slow (*Bjørlykke*, 1993). However, shallow water circulation plays, in some cases, an important role for early cementation (Enos and Sawatsky, 1981; *Budd*, 2001). Since low porosity reservoirs are more often found in carbonate than in sandstone, it is inferred that fractures occur more in carbonate (Ehrenberg and Nadeau, 2005), if not it would be too difficult to produce from carbonate reservoirs. This observation is significant since fracture propagation can, in some cases, control fluid flow in sedimentary basin. Fractures that are not sealed are in fact a preferential area for dissolution and therefore diffusion of matter to the surrounding area.

Local diffusion of solute is an important process since it keeps pore water under-saturated with respect to calcite, allowing further dissolution and therefore compaction. The two main structures enabling fast diffusion rate are fractures and stylolites. Local dissolution along stylo-

lites induces diffusion of matter in the surrounding media and participates to porosity occlusion (*Finkel and Wilkinson*, 1990), leading to the observation that porosity loss by cementation is actually positively correlated to the presence of stylolite (*Ehrenberg*, 2006; *Bjørlykke*, 2006). Field observations also suggest that stylolitic dissolution is enhanced by clay minerals or phyllosilicates (*Weyl*, 1959; *Ehrenberg*, 2004, 2006).

Effect of pore water composition

In formation waters, concentration of dissolved elements is a function of initial pore water chemistry which tends to equilibrate with minerals in presence (*Bjørlykke*, 1993). The degree of saturation with respect to minerals in the shallow depth pore water is of importance, since it will favour or not reactions. For instance the low degree of saturation, with respect to calcite, of Mississippian skeletal limestones paleo-groundwater is shown to favour porosity loss by intergranular pressure solution rather than mechanical grain repacking and plastic deformation (Meyers and Hill, 1983).

At shallow depth, pore waters equilibrate and become saturated with respect to carbonate minerals. In Figure 2.3 evolution of the Mg^{2+} to Ca^{2+} ratio and of the Ca^{2+} to Sr^{2+} ratio as a function of depth are displayed for few shallow and deep carbonate formations. The Mg^{2+} to Ca^{2+} ratio decreases at shallow depth which can be interpreted by the dissolution of carbonate and progressive saturation of pore water with respect to calcite. The increase of the Ca^{2+} to Sr^{2+} ratio is related to incorporation of strontium into aragonite structure. Magnesium content is also of prime importance, since it is known to inhibit dissolution of calcite (*Arvidson et al.*, 2006). For instance in shallow-water carbonates rocks of South Florida, porosity is inversely related to magnesium content of pore water (*Schmoker and Halley*, 1982).

At greater depth, *i.e.* below 100 meters, pore water composition might be less important since it is already saturated with respect to minerals. Low variability of the Mg^{2+} to Ca^{2+} ratios at greater depth (Figure 2.3) demonstrates that water became saturated with respect to calcite. The lowest values of this ratio can be explained by the increase of the calcium carbonate solubility with pressure. The Ca^{2+} to Sr^{2+} ratios are slightly lower in subsurface than at shallow depth, indicating that, once the substitution of Sr^{2+} into the mineral has occurred, strontium - carbonate reaction vanishes. At these depths, the different ratios only evolve due to local dissolution by pressure solution creep.

From natural observations several questions remain unanswered on the dynamics of mechanical and chemical compaction. The amount of overburden necessary for pressure solution to become the main process of porosity loss is difficult to determine from field observations.

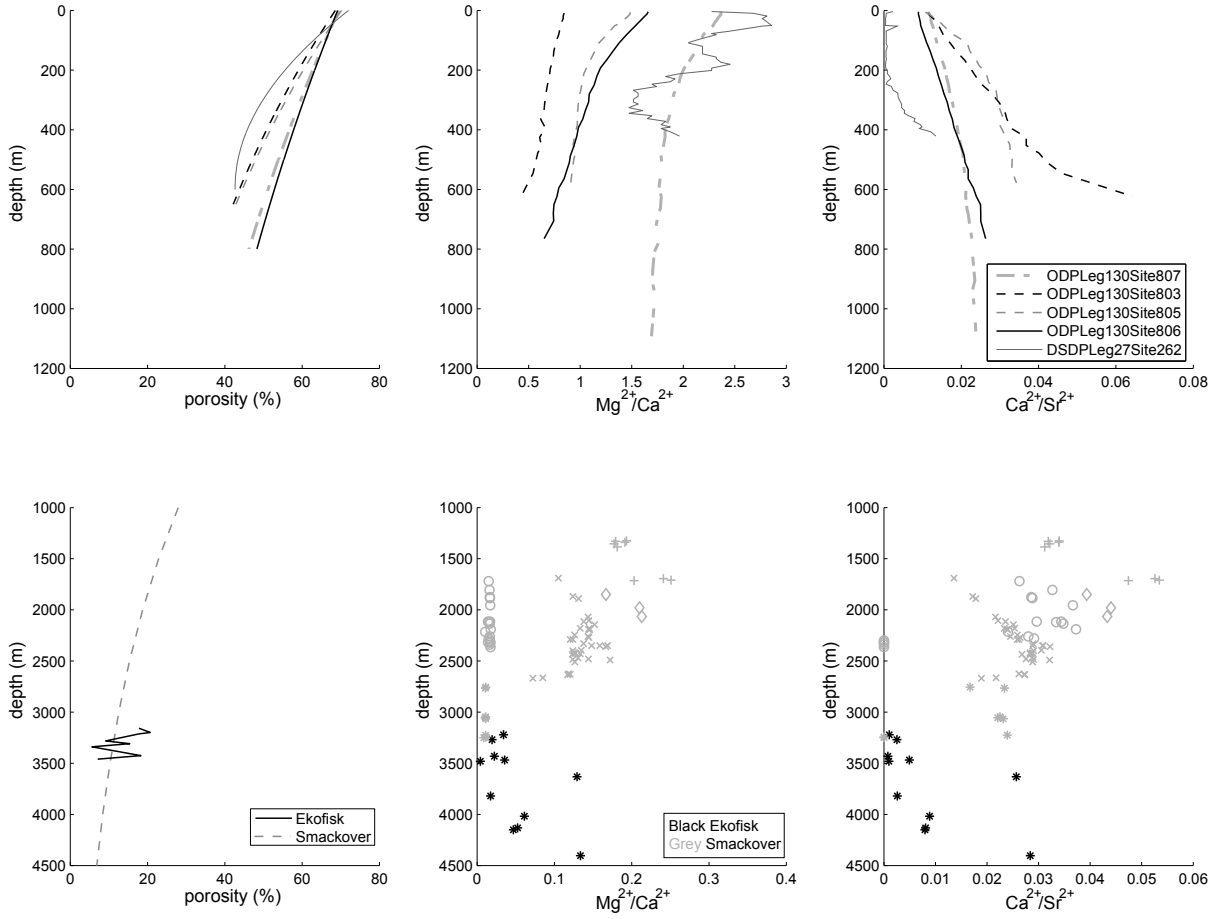

Figure 2.3: Comparison of porosity-depth trends with formation water chemistry. Upper graphs: shallow depth carbonates. Lower graphs: deep carbonates. (Smackover data: *Schmoker and Halley* (1982); *Moldovanyi and Walter* (1992); Ekofisk data: *Lubanzadio et al.* (2002); *Warren and Smalley* (1994).)

The role of temperature on chemical processes in carbonates is rather ambiguous, and the rate limiting step of pressure solution can not be determined from field observations. Answering these questions is not easy especially since once chemical compaction is operative, it is difficult to separate its effect from mechanical compaction processes on the porosity-depth data sets or in microstructures observations. In order to understand the influence of these various compaction mechanisms, and their interactions, several laboratory experiments and theoretical developments were pursued. These theoretical and experimental development are the topic of the following section.

2.3 Compaction of carbonate: theory and experiments

2.3.1 Mechanical compaction

Theoretical background

As sediments get buried, the applied vertical stress increases, which in turn leads to reduction of sediments thickness, porosity loss and increase in the bulk density. The principal component of the stress field is usually the vertical stress. The reduction in sediments thickness occurs mainly without lateral strain because surrounding sediments exert lateral stresses that prevent it (*Giles*, 1997). Taking this into consideration while describing mechanical compaction in this section, the assumption is made that deformation in sedimentary basins is uniaxial.

At shallow depth, without early cementation processes, carbonate sediments compaction can be modelled using soil mechanics approaches. At early stage of sediment deposition, when cementation has not occurred yet, the main process conducting to volumetric strain is grain rearrangement and expulsion of water. The consolidation theory, first expressed by *Terzaghi* (1925), states that the increase of effective stress leads to the expulsion of water and therefore to consolidation of soil. The effective stress, σ', is defined by,

$$\sigma' = \sigma - P_p, \tag{2.2}$$

where σ is the applied stress and P_p the pore pressure. Following Therzaghi's consolidation theory, a logarithmic relation is found between the void ratio, e, and the effective stress, σ' (*Terzaghi and Peck*, 1967),

$$e_0 - e_f = C_c \cdot log(\frac{\sigma'_f}{\sigma'_0}), \tag{2.3}$$

the indices 0 and f indicate the initial and final states of the sediment void ratio respectively,

the void ratio can be related to porosity through $\Phi = e/(1+e)$. The compression index, C_c, is a phenomenological coefficient used to characterize the different soils compaction.

If cementation occurs early then soil strength overcomes burial stresses, and mechanical compaction processes are slowed down. Once sediments are consolidated and cemented, then their deformation may be described by rock mechanics theories. Elastic deformation is then the main deformation process up to much higher stresses than for soils. Rock mechanics divide deformation induced by mechanical compaction into three main regions, *i.e.* linear-elastic, ductile, and brittle (Figure 2.4). In geological materials, the ductile phase is usually very small and restricted to situations of very high temperatures and stresses (*Jaeger et al.*, 2007). Moreover, in tectonically calm sedimentary basins most of deformation occurs in the elastic domain and the strain is usually proportional to the applied stress and a function of the sediments intrinsic properties (Figure 2.4).

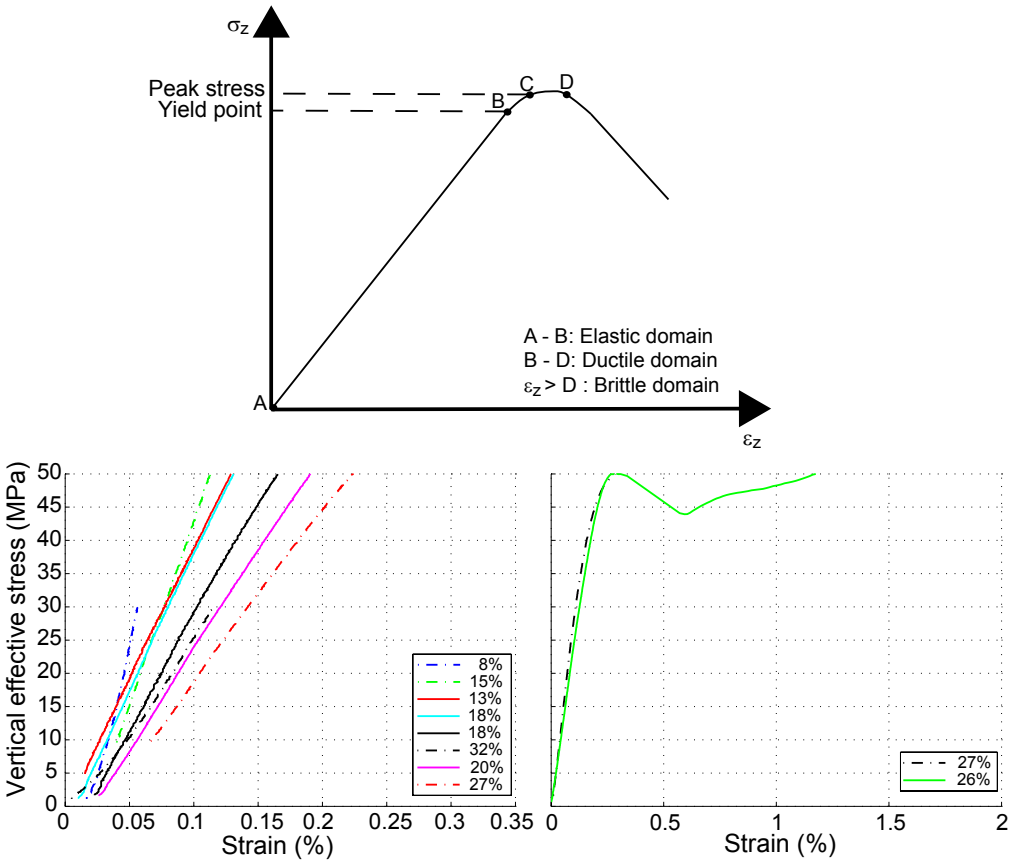

Figure 2.4: Top: Stress - strain relationship in the case of uniaxial compression. Bellow: Example of stress–strain relationship from uniaxial compression tests in dry limestones (solid lines) and dolostones (dashed lines), the porosity of the samples is indicated in the legend (data from *Croizé et al.* (2009)).

Considering sediments to be linear–elastic, uniaxial deformation can be described by a linear stress–strain relationship function of the Young's modulus, E, and the Poisson ratio, ν, of the

sediment (Turcotte and Schubert, 1982),

$$\epsilon_1 = \sigma_1 \cdot \frac{(1+\nu)\cdot(1-2\nu)}{E\cdot(1-\nu)}, \tag{2.4}$$

where σ_1 is the applied vertical stress and ϵ_1 the vertical strain.

Poroelasticity is an extension of linear elasticity that takes into account the presence of a diffusive fluid (*Biot*, 1941; *Rice and Cleary*, 1976). Poroelasticity theory is commonly used to analyse compaction of fluid saturated rocks (*Fjær et al.*, 1992; *Guéguen et al.*, 2004). The strain may then be expressed as follows,

$$\epsilon = \frac{1}{K}\cdot(\sigma_p - b\cdot P_p); \tag{2.5}$$

where K is the rock bulk modulus, σ_p the isotropic stress and b the Biot coefficient given by,

$$b = 1 - \frac{K}{K_s}; \tag{2.6}$$

with K_s the bulk modulus of the solid phase. The uniaxial bulk compressibility, β_1, and, therefore, the porosity loss are then described as a function of the effective stress and the Biot parameter (*Giles*, 1997; *Wong et al.*, 2004),

$$\beta_1 = \frac{b\cdot(1+\nu)}{3\cdot K\cdot(1-\nu)}. \tag{2.7}$$

Typical values of the Biot parameter and bulk compressibility in limestones are given in Table 2.1.

Failure occurs when peak stress is reached (Figure 2.4). Unconsolidated sediments, first need to reach a locked state then, when the vertical stress reaches a critical value, crushing starts. Particle breakage occurs when the stress along the grain contact overcomes the yield stress of the material. As force distribution is strongly dependent on the packing structure (*Chan and Ngan*, 2005) and the geometry of the contact force network (*Mair and Hazzard*, 2007), the locking state of the grains determines the localization of breakage onset.

The stress value at which brittle failure starts in limestone is influenced by temperature. Increase in temperature promotes ductility and increases the strain rate sensitivity (*Paterson and Wong*, 2004). However, up to fracture limestone strength is relatively independent of strain rate (*Paterson and Wong*, 2004). As in other type of rocks, failure in limestone involves strain softening and strain localization (*Evans et al.*, 1997). Since, in sedimentary basins, stress is mostly vertical, fracture development is usually vertical or subvertical, unless a localized high pore pressure fluid source initiate hydraulic fracture (*Rozhko et al.*, 2007). Plastic pore collapse,

Table 2.1: Some elastic moduli values for particular Limestones and Chalk found in the literature.

Rock	ϕ	ρ	E	ν	K	b	β	σ_c[a]	ref.
	%	g/cm^3	GPa		GPa		GPa^{-1}	MPa	
Limestones:									
Solenhofen	3	2.62	64	0.29			0.016	245	1, 3
Villeperdue	6.4				36	0.41			2
Tonnerre	13				19.3	0.53	0.052	72.4	2, 3
Chauvigny	17				16.3	0.69	0.061	42	2,3
Lavoux	21.9				13.8	0.77	0.072	30.4	2,3
Majella	30							37[a]	4
Saint Maximin	37							17[a]	4
Adana/Ceyhan		2.71	26.5					78	5
Adana/Karaisali		2.43	14.4					39	5
Hatay/Iskenderun		2.96	43.1					117	5
Adana/Pozanti		2.97	45.4					121	5
Chalk:									
Lixhe	42.8				3.8	0.91	0.263	7.7	2, 3

[a] σ_c: Uniaxial compressive strength
[b] Effective pressure at the onset of grain crushing
[1] : *Fjær et al.* (1992)
[2] : *Fabre and Gustkiewicz* (1997)
[3] : Vajdova et al. (2004)
[4] : *Baud et al.* (2009)
[5] : *Yasar and Erdogan* (2004)

grain breakage and failure occur at stresses above the yield stress (*Carroll and Holt*, 1972; *Curran and Carroll*, 1979). During compaction, changes in pore shape, structure or connection influence fluid flow in sedimentary basin (*Evans et al.*, 1997).

Following is a description of some experimental studies done on carbonate sand and rocks. Both types of material start compacting with quite a similar elastic behaviour. However, both type of materials have different mechanical response when considering inelastic behaviours and failure modes.

Experimental compaction of carbonate sand

The particular response of carbonate sand to loading was, first, mainly investigated within geotechnical engineering studies. Triaxial testing of uncemented (*Coop*, 1990) and naturally cemented (*Airey*, 1993) carbonate sands were carried at low stresses, *i.e.* below 8 MPa. Compaction studies being of geological interest, carbonate sands were also compacted at vertical stresses corresponding to greater burial depths. Hydrostatic triaxial tests on modern carbonate sediments from the great Bahamas bank (*Fruth et al.*, 1966), compression tests on sand with various grain size and carbonate content (*Ebhardt*, 1968; *Chuhan et al.*, 2003), and confined compression tests on shallow-water limestones cores from various sedimentary environments (*Shinn and Robbin*, 1983) were carried out at vertical stresses up to 100 MPa.

Those tests focused on porosity decrease with increasing stress and studied the mechanical strength of carbonate sands. The main results are, that carbonate sands have a stiff response up

to a yield point and have higher friction angle, $\varphi \approx 40°$, than usually encountered in soils (*Coop*, 1990). The effective angle of friction, φ', is an important parameter of the Mohr–Coulomb failure criteria which might be defined as,

$$\tau_f = c' + \sigma'_f tan\varphi' \tag{2.8}$$

with τ_f the shear strength at failure, c' the effective cohesion, and σ'_f the effective stress at failure. After yielding, carbonate sands become very compressible resulting in large volumetric strains. Carbonate sand compressibility can be related to the relatively high initial porosity usually encountered in those soils and to their yield stress (*Coop*, 1990; *Airey*, 1993).

Tests conducted at more than 20 MPa effective stress showed that most of compaction occurred in the early stage of loading, then, at effective stress greater than 5–10 MPa, the strain rate decreased (*Fruth et al.*, 1966; *Ebhardt*, 1968; *Shinn and Robbin*, 1983; *Chuhan et al.*, 2003). At low stress level, 5–10 MPa , where most of the compaction occurred, the stress–strain relationship strongly depends on the grain size and stiffness. For instance the five facies of the great Bahamas bank, *i.e.* oolite, oolitic, grapestone, skeletal and mud facies, tested by *Fruth et al.* (1966) showed different compaction behaviour up to 25 MPa. They compacted more or less readily depending on their composition and initial porosity. Parameters controlling mechanical compaction at these stresses are the composition of the sand and its initial stiffness (*Fruth et al.*, 1966), the initial packing and therefore porosity (*Fruth et al.*, 1966; *Shinn and Robbin*, 1983), and the grain size. Finer sediments are less compressible (*Ebhardt*, 1968; *Chuhan et al.*, 2003) which is due to the fact that stress is distributed between more grain–to–grain contacts. *Ebhardt* (1968) reported that temperature had some effect on compaction as well, more intense compaction was observed in experiments conducted at 90°C than on those conducted at room temperature. However no more investigation has been done on the effect of temperature on mechanical compaction. In **Paper 3** mechanical compaction of bioclastic carbonate sand was found not to be affected by temperatures in the range 20 to 70 °C.

At stresses higher than 25 MPa, stress–strain curves for different carbonate sands are much more alike than at lower stresses, meaning that porosity loss in carbonate sediments is influenced mainly by initial sorting and initial compaction (*Fruth et al.*, 1966). Mechanical compaction of unconsolidated carbonate sediments is a very effective process of porosity loss at low effective stress, but once a locking state is attained, then the strain rate is much slower.

The amount of mechanical strain achieved in carbonate sand can be rather important. *Shinn and Robbin* (1983) showed that lime sediments can compact as much as 50% of their initial thickness within first hundreds meters. However due to very large initial porosities, residual

porosities higher than 30% are reported in carbonate sands and mud after mechanical compaction under effective stresses higher than 30 MPa (*Fruth et al.*, 1966; *Shinn and Robbin*, 1983). These results show that if mechanical compaction is the only process responsible for porosity loss, one could expect to find 30% porosity in limestones buried at 3 km. However compaction curves of natural limestones show much lower porosity at this depth (Figure 2.1).

After mechanical compaction, microstructures observed in tested samples were very similar to those observed in naturally compacted carbonates. Grain fracturing was very common, as well as grain penetration and buckling of spalled margins (*Fruth et al.*, 1966); rotation of shells towards the horizontal, reorganization of organic material, conversion of part of the core from wackestone to packstone, obliteration of birdseyes and fenestral voids, flattening of fossils (*Shinn and Robbin*, 1983) were also observed. Comparison of features produced experimentally and naturally may enable a better understanding of when does cementation occur in natural environment. Features produced by mechanical compaction are certainly sites of enhanced chemical compaction in nature.

Since cementation can occur very early in carbonate, effect of cement on sand mechanical behaviour has to be taken into account. Cementation increases the shear modulus of the soil as well as its yield strength (*Airey*, 1993).

Experimental compaction of carbonate rock

At small stresses, experimental mechanical deformation of carbonate rock is usually characterized by a non–linear stress–strain relationship, interpreted to be the closure of cracks, pores and other defects (Vajdova et al., 2004). This early phase can be related to *in situ* stresses to which the rock was subjected (*Couvreur et al.*, 2001). Ultrasonic P- and S-waves velocity and quality factor calculations enables also the monitoring of the end of the crack closure phase (*Couvreur et al.*, 2001). For salt water filled porosity, the electrical conductivity decreases at the beginning of the test, that can be related to the closure of pores and sub-horizontal cracks (*Jouniaux et al.*, 2006). After this early phase, compaction is characterized by a linear elastic stress–strain relationship. This linear elastic phase can occur at different stress stages depending on the porosity of the rock and the geometry of the pore space. Using Walsh's model (*Walsh and Brace*, 1966), the non–linear stress–strain relationship can be related to the amount of cracks and various type of pores (Baud et al., 2000).

Vajdova et al. (2004) carried out hydrostatic triaxial tests on three limestones, the main structural difference between them being the porosity. Solnhofen limestone has a porosity of 3 %, porosity of Tavel limestone is 10.4 %, porosity values of indiana limestones are 16, 18

or 20 %. The compressibility of these limestones is increasing with porosity. Solnhofen limestone has a compressibility of 0.016 GPa^{-1} (Baud et al., 2000; Vajdova et al., 2004), Tavel limestone a compressibility of 0.033 GPa^{-1} and Indiana limestone a compressibility of 0.075 GPa^{-1} (Vajdova et al., 2004).

The main domain of investigation of experimental studies on carbonate rock compaction is the onset of failure occurrence and on the failure mode. Fracture propagation in rocks is an important mechanism of compaction, but is also of importance for fluid flow. A failure plane creates a path for dissolution and transport of matter or can be a place of enhanced cementation and fluid flow barrier.

Different mechanical parameters control failure in carbonates. These poro-elastic parameters are usually inferred from mechanical triaxial tests (*Renner and Rummel*, 1996; Baud et al., 2000; Palchik and Hatzor, 2002; Vajdova et al., 2004), compressional and shear waves propagation measurements (*Couvreur et al.*, 2001; *Eberli et al.*, 2003; *Vanorio et al.*, 2008) or electrical conductivity measurements in fluid saturated samples (*Jouniaux et al.*, 2006). These different methods allow to better constrain the mechanisms responsible for carbonate mechanical compaction. Hydrostatic triaxial tests (Baud et al., 2000; *Couvreur et al.*, 2001; Vajdova et al., 2004), uniaxial compression tests (Palchik and Hatzor, 2002; *Jouniaux et al.*, 2006) and triaxial compression tests with various confining pressure (*Renner and Rummel*, 1996; *Couvreur et al.*, 2001) were performed on limestones and dolomites. Carbonates tested had grain size ranging from 5 to 400 μm, various chemistry, *i.e.* calcite, aragonite, dolomite, and various pore space arrangement. Due to differences in the experimental procedures and microstructural properties of the tested samples, the different tests are difficult to compare (*Renner and Rummel*, 1996). The critical stress varies from 5 to more than 500 MPa in theses different studies. Porosity seems to be the main controlling factor on the onset of failure, even though the scattering of the critical stress as a function of the porosity is rather high (Figure 2.5). When samples are saturated, water saturation increases preferentially in cracks and enhances formation of sub–vertical fractures (*Jouniaux et al.*, 2006). Therefore, critical stress is reached earlier in water saturated samples (Figure 2.5).

Different failure modes were identified as a function of confining pressure (*Renner and Rummel*, 1996; Baud et al., 2000). For confining pressure lower than 50 MPa, *i.e.* equivalent to less than 3-4 km burial, dilatancy started and acted as precursor of brittle faulting. For intermediate confining pressure, an initial stage of strain hardening could be measured. And for confining pressure higher than 350 MPa, samples failed by cataclastic flow associated with shear enhanced compaction and strain hardening (Baud et al., 2000). Compactive cataclastic flow was commonly observed to be a transient phenomenon which evolved with increasing

strain to dilatant cataclastic flow and ultimately shear localization (Baud et al., 2000).

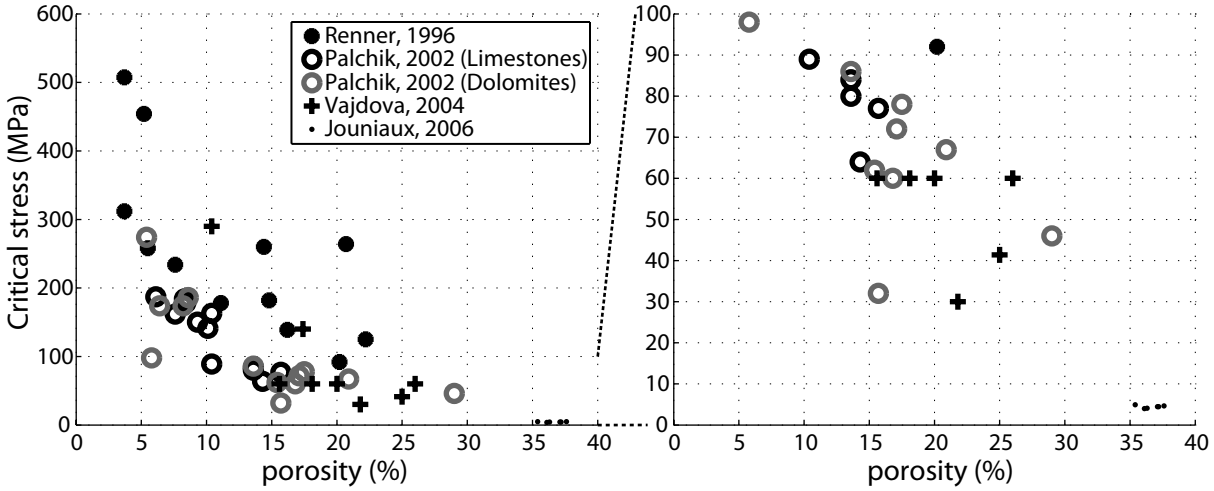

Figure 2.5: Critical axial stress in various carbonates as a function of porosity. The graph on the right side is a zoom of the lower stress part of the left side graph (All the tests were conducted under dry conditions, expected for the data from Jouniaux et al., 2006).

In very porous limestones a critical pressure beyond which stress-strain behaviour becomes non-linear was observed, this limit corresponds to pore collapse and grain crushing (Vajdova et al., 2004). Elastic, inelastic and failure properties of carbonate rocks can be related to their porosity, and carbonate compressibility increases with porosity. Critical stresses for the onset of pore collapse under hydrostatic and non-hydrostatic loading decrease with increasing porosity (Vajdova et al., 2004). Mechanical twinning dominates in the most porous limestone, while dislocation slip is activated in the most compact limestone (Vajdova et al., 2004). Elastic stiffness and porosity are the main parameters influencing the onset of dilatation (Palchik and Hatzor, 2002).

In all these experiments, small strains were obtained for rock compaction. Carbonate are in general less compressible than sandstones (*Wong et al.*, 2004). In both carbonate sand and rock compaction, the starting porosity is a crucial parameter, as the maximum compressibility was obtained for samples with the highest initial porosity. All these experiments demonstrate that loss of porosity in basin limestones are to some extend due to mechanical compaction. However, mechanical compaction is mainly operative for sands or high porosity limestones. For rocks with low porosities or in which a mechanically stable framework was built during early diagenesis (**Paper 1**), the stresses needed to achieve grain crushing and shear fracturing are usually higher than effective stresses usually encountered in sedimentary basins (Figures 2.4 and 2.5). Finally, mechanical compaction usually explains the decrease of porosity down to 20–30% at stresses equivalent to burial depths of 2 to 4 km. In sedimentary basins, porosity values are lower at those depths (Figure 2.1), therefore chemical compaction must play a key

role in carbonate compaction to lower porosities below these values.

2.3.2 Chemical compaction

Theoretical background

Pressure solution: Pressure solution is an important process of porosity elimination in sedimentary basins (*Sorby*, 1863; *Rutter*, 1983; *Tada and Siever*, 1989) or compaction and healing of active fault (*Angevine et al.*, 1982; *Hickman and Evans*, 1995; *Renard et al.*, 2000; *Yasuhara et al.*, 2003). Various type of microstructures are associated with pressure solution, *e.g.* sutured grain contact, grain truncation, indentation, clay seams or stylolites (*Wanless*, 1979; *Buxton and Sibley*, 1981; *Dysthe et al.*, 2002). The nature of microstructures associated with pressure solution is a function of the rock lithology and structural resistance (*Wanless*, 1979; *Buxton and Sibley*, 1981).

Pressure solution is a water assisted physico–chemical process occurring in relation to the stress variation along the grain surface. First the increase of solubility of minerals with pressure was observed, and the term pressure solution was created to describe the dissolution and diffusion processes (*Sorby*, 1863). The term pressure solution was later associated with three serial processes: i) dissolution at grain contact, ii) diffusion of solute matters toward the pore space and iii) precipitation on the stress–free faces of grains and/or transport by diffusion or advection (*Weyl*, 1959; *Raj*, 1982; *Rutter*, 1983; *Tada and Siever*, 1989; *Lehner*, 1990, 1995; *Gundersen et al.*, 2002). The rate of pressure solution is determined by the slowest of the three reaction, *i.e.* dissolution, diffusion or precipitation (*Rutter*, 1983).

The driving force for pressure solution is the chemical potential gradient between the highly stressed grain boundary and the pore space where stress is lower (Figure 2.6A). Numerous rate laws for aggregates compacting by pressure solution have been derived. Theoretical equations for creep rate due to intergranular pressure solution were first derived using a equilibrium approach (*Paterson*, 1973; *Durney*, 1976; *Rutter*, 1983). In order to describe the processes in a more physically realistic way, a non-equilibrium approach was then used to develop models for creep by grain boundary diffusional pressure solution, taking also into account the role of precipitation on the overall strain rate (*Lehner and Bataille*, 1984; *Lehner*, 1990; *Spiers and Schutjens*, 1990).

The grain boundary structure must be dynamically stable (*Lehner and Bataille*, 1984), *i.e.* while continuous dissolution or precipitation occurs within a representative elementary volume in the grain-to-grain contact, the average grain boundary structure remains constant. The equilibrium between the solid phase under stress and the solution of the component forming the

solid phase at the grain-to-grain contact is given by,

$$\mu_1 = f^s + \sigma_n/\rho^s; \tag{2.9}$$

where f^s is the mass specific Helmotz free energy of the solid phase, ρ^s the density of the solid phase, μ_1 the chemical potential of the dissolved solid, σ_n is the stress normal to the grain to grain contact, which is considered to be equal to the pressure, p, of the fluid within the grain boundary (*Lehner*, 1990; *Spiers and Schutjens*, 1990). The chemical potential of the solute in the pore space is therefore described by $\mu_1^{eq} = f^s + p^f/\rho^s$ with p^f the pressure of the fluid in the pore space. From there,

$$(\sigma_n - p^f)/\rho^s = \mu_1 - \mu_1^{eq}. \tag{2.10}$$

Considering the above equations (eq. 2.9 and 2.10) in the case of equilibrium, supersaturation in the pore space is attained. Precipitation might then heal the grain boundary and thus stop pressure solution which will not be able to restart once the grain boundary is healed (*Hickman and Evans*, 1991). Since in nature a grain boundary remains permeable to fluid, therefore equilibrium cannot exist at the grain boundary and equation 2.9 and 2.10 must be considered for wet boundary approaching a state of equilibrium but not reaching it (*Lehner*, 1990).

Once dissolution occurred the chemical potential gradient, $\nabla\mu_1$, between the grain boundary and the pore phase will drive diffusion. Diffusion occurs following Fick's law which relates the diffusive mass flux vector, J_1, to the chemical potential gradient (*Lehner*, 1990),

$$J_1 = -\frac{l}{1 - c_1}\nabla\mu_1, \tag{2.11}$$

with $c_1 = \rho_1/\rho$ the mass fraction and $l > 0$ a phenomenological coefficient taking into account the geometry of the grain-to-grain contact. For diffusion to occur the water film confined at the grain–to–grain contact needs to support shear stress and enable diffusion of solutes (*Weyl*, 1959). The transport properties of the trapped thin film are somewhat different from those of the pore fluid. The diffusion flux is proportional to the water film thickness at the grain–to–grain contact (*Durney*, 1976), which is a function of the effective stress (*Renard and Ortoleva*, 1997), and the diffusion coefficient of the thin film is also assumed to be lower than the one of bulk water (*Rutter*, 1983). The actual diffusion coefficient is difficult to estimate, according to the literature it is 2 to 10 times lower than for bulk water (*De Meer and Spiers*, 1999).

Grain boundary structure is a critical parameter allowing diffusion of dissolved material outside of the contact area. Several types of grain boundary structures are debated in the litera-

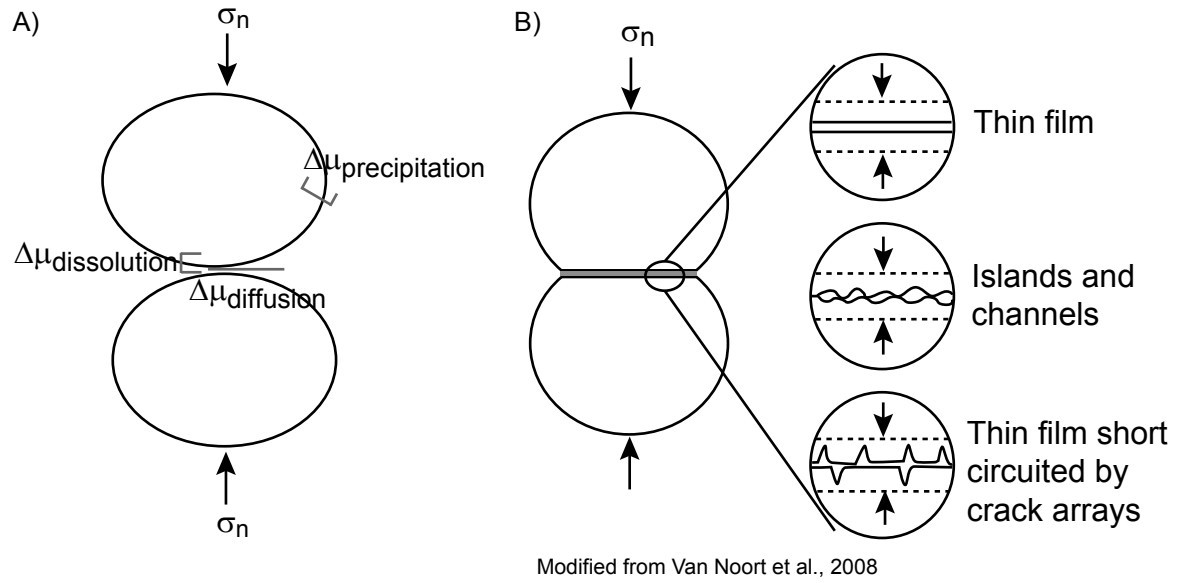

Figure 2.6: A) Schematic view of the three pressure solution steps. B) Three different grain boundary geometries considered in the literature.

ture (*Tada and Siever*, 1986; *Gratz*, 1991; *De Meer and Spiers*, 1999; *Dysthe et al.*, 2002; *van Noort et al.*, 2008). Pressure solution might occur as a combination of plastic deformation at the grain-to-grain contact and free face dissolution at the edge of the contact (*Tada and Siever*, 1986; *Karcz et al.*, 2006). A number of studies have assumed that water is present at the grain boundary and have discussed several geometries (Figure 2.6B). The first one is an adsorbed thin film which can support shear stresses (*Weyl*, 1959; *Rutter*, 1983). Secondly, and the one mostly used in recent models, is the island and channel structure (*Lehner*, 1990), there stresses are transmitted through solid-solid contacts. In this structure, the fluid is at hydrostatic pressure and has pore fluid transport properties. A third type of structure is a clay filled grain boundary, clays by increasing the water film thickness enhance diffusion (*De Meer and Spiers*, 1999). The last structure, discussed here, is a thin-film short-circuited by cracks arrays (*van Noort et al.*, 2008).

Due to removing of matter by diffusion the diffusion path becomes longer, the change in the diffusion path may then induce a change in the rate limiting step of pressure solution (*Yasuhara et al.*, 2003). The presence of stylolites is also important due to their role in diffusive mass transfer. The diffusive transfer activity of stylolites increases with increasing presence of fine-grained non-diffusible debris which increase the width of the stylolite (*Hickman and Evans*, 1995; *Renard et al.*, 2001).

The solutes transported by diffusion from the contact to the pore space may be transported out of the pore space by diffusion or advection (*Lehner*, 1995; *Gundersen et al.*, 2002). In the case of closed systems, the pore fluid becomes supersaturated with respect to the solid in

solution and then precipitation occurs on the stress-free face of the grains. In some cases precipitation may be inhibited, for instance the presence of a large amount of clay minerals in the sediments retard the precipitation (*Tada and Siever*, 1989), or in the case of quartz precipitation does not occur at temperature below 80 °C due to the low reaction's kinetics below this temperature (*Bjørlykke*, 1999); in those cases supersaturation build up in the pore space. If the pore fluid becomes largely supersaturated, the diffusion is no longer proportional to the normal stress and pressure solution becomes interface controlled (*Lehner*, 1990).

From fundamentals thermodynamics relationships characterizing the solid, aqueous and boundary phase, taking into account the three serial processes above described, macroscopic Gibbs equations were derived for granular aggregates deforming by pressure solution (*Lehner*, 1990; *Spiers and Schutjens*, 1990; *De Meer and Spiers*, 1999). Even though some differences exist between the different rate laws, especially in the definition of the parameters characterizing the grain boundary geometry, they more or less all take the following form (*Spiers and Schutjens*, 1990; *van Noort and Spiers*, 2009),

$$\dot{\epsilon} = \frac{GC(T)}{d^m} \frac{\sigma_e \Omega_s}{RT} f(\phi), \tag{2.12}$$

where $\dot{\epsilon}$ is the volumetric strain rate of the aggregate, G is a geometric constant function of the grain packing, Ω_s is the molar volume of the solid, R the gas constant and T the temperature. $f(\phi)$ is a dimensionless function of porosity, ϕ, taking into account the porosity dependent changes in grain contact and pore wall area. σ_e is the effective stress and d is the grain diameter. $C(T)$ is the thermally activated rate coefficient of the rate controlling process. $C(T)$ takes different form depending on which of dissolution, diffusion or precipitation rate is the controlling rate of deformation. m is the grain size coefficient which varies depending on the rate limiting process. In the case of a diffusion controlled compaction rate $m = 3$, while for an interface-reaction controlled rate $m = 1$.

Various parameters such has grain size, clay, stress, time, cementation or solution chemistry influence the rate of pressure solution (*Tada and Siever*, 1989). Intergranular pressure solution theory (eq. 2.12) states that the compaction strain rate increases with decreasing grain size (*Weyl*, 1959; *Rutter*, 1983; *Tada and Siever*, 1989; *Lehner*, 1990). In sediments with a wide range of grain size, dissolution occurs preferentially within the small grain size and solute are then transported towards areas of the sediments with coarser grain size where precipitation is easier (*Weyl*, 1959; *Tada and Siever*, 1989). However, theory does not account very well for wide grain size distribution (*Niemeijer et al.*, 2009).

Clay minerals are not necessary for pressure solution to take place but certainly promote

it (*Tada and Siever*, 1989). Strain rate increase due to clay mineral may be related to the increase of the water film thickness which facilitate diffusion (*Weyl*, 1959) or to the fact that clay minerals prevent grain boundary healing by maintaining the contacts open (*Renard et al.*, 2001). For stylolites, however, if the clay layer within the stylolite becomes thick compared to the grain size, then the rate of pressure solution decreases (*Weyl*, 1959). The volumetric strain rate is proportional to the effective stress (eq. 2.12).

Some theoretical works also state that a critical stress is needed to initiate pressure solution and when, due to dissolution, the grain-to-grain contact becomes large enough so that the normal stress at the boundary is low enough then pressure solution will stop and grain boundary healing starts (*Tada and Siever*, 1989; *Yasuhara et al.*, 2003; *van Noort et al.*, 2008). This critical stress is a function of the mineralogy of the compacting material. In sedimentary basins, therefore, the amount of burial depth is an important factor controlling compaction by pressure solution. To predict porosity loss by pressure solution, the burial history of the sediments needs to be taken into account since dissolution, diffusion and precipitation are time dependent phenomenons. The solution chemistry also plays a major role in controlling the rate of pressure solution. In the case of an under-saturated pore fluid, free-face dissolution might occur (*Engelder*, 1982; *Tada and Siever*, 1989). In the case of supersaturation building up in the pore space then the rate of dissolution will slow down and be a function of the precipitation kinetics (*Lehner*, 1990).

Critical parameters to be studied are grain boundary structures (**Paper 2**) and their diffusivity, dissolution and precipitation kinetics of the studied mineral in different solution's composition. Relation between compaction strain rate and applied stress, grain size or strains would also give information about the process.

Subcritical crack propagation: Crack propagation is described using fracture mechanics theory and would therefore have its place in the mechanical compaction section. However, as it will be presented here, crack propagation in rocks is affected by the environment and the fluid chemistry and can be seen as a chemical phenomenon induced by mechanical forces. Crack propagation may occur at low stress and is usually characterized by a slow propagation, it is then called subcritical crack propagation or stress corrosion. A short review of the fundamentals of crack propagation in linear elastic material is given, followed by a discussion on the effect of environmental conditions on propagation.

To study fracture mechanics, three important variables have to be taken into account: the applied stress, the size of the flaw and the fracture toughness (*Anderson*, 1995). Fracture occurs when the applied stress is sufficient to break its atomic bounds (*Anderson*, 1995; *Scholz*, 2002).

Crack propagation may be described using the energy criterion theory (*Griffith*, 1920) based on thermodynamic and energy balance. It shows that a crack will propagate in order to lower the total energy of the system.

From the energy criterion theory, the crack will propagate when the energy needed for crack to propagate is sufficient to overcome the resistance of the material. The energy release rate, G, is the change in potential energy with crack area for a linear elastic material,

$$G = \frac{\pi \sigma^2 a}{E}, \tag{2.13}$$

with σ the tensile stress, E the Young's modulus of the considered material, and the crack's length is equal to $2a$. For material having a linear elastic material the fracture toughness is independent of the size and geometry of the cracked body, the theory is therefore applicable at different scales. G is the mechanical driving force for crack propagation at equilibrium it is equal to R the material resistance (*Olagnon et al.*, 2006).

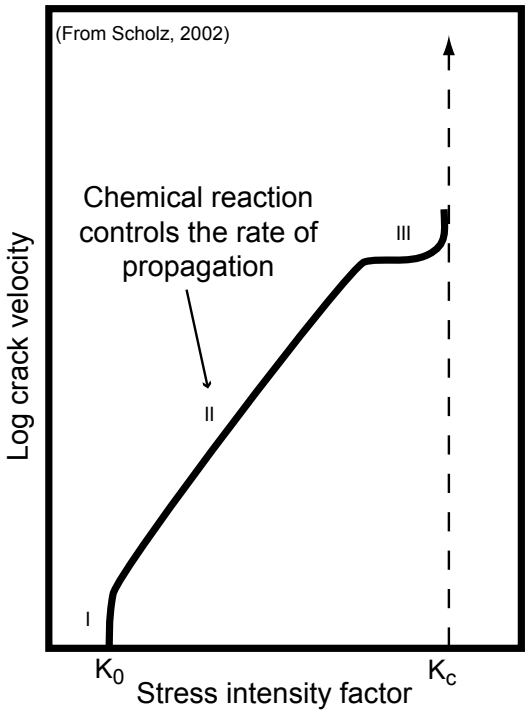

Figure 2.7: Evolution of the crack propagation velocity at stress intensity factor lower than the critical stress intensity factor.

The stress intensity factor $K_I = \sigma\sqrt{\pi a}$ characterizes the crack tip conditions in a linear elastic material. K_I is also a size independent material property. The relation between the energy release rate and the stress intensity factor is,

$$G = \frac{K_I^2}{E}. \tag{2.14}$$

The velocity of the crack propagation can be related to G or K_I leading to the so-called $v - K_I$ or $v - G$ curves (Fig 2.7). For crack to propagate, the energy release rate needs to overcome the material resistance to cracking, R. In general R may be set equal to the surface energy, γ, and therefore $R = 2\gamma$ under vacuum. Thus at equilibrium in a given environment,

$$G = R_e = \gamma_e, \tag{2.15}$$

with $\gamma_e < \gamma$ (*Olagnon et al.*, 2006). The above relations (eq. 2.13, 2.15) show that the crack propagation is dependent on the local stress as well as on the environment. Due to pre-existence of cracks in rocks, crack propagation may occur at stresses lower than required for slip or twinning (*Atkinson*, 1982; *Olagnon et al.*, 2006). The velocity may also be limited by the reaction rate between the corrosive species and the material bounds.

Propagation of cracks occurring at stresses lower than the critical stress required for fracture is an important fracture mechanism in the upper 20 km of the Earth's crust (*Atkinson*, 1982). The presence of water at the crack tip promotes weakening reactions and therefore make crack propagation easier. Different terminologies are associated with this mechanism, in particular stress corrosion or subcritical crack growth.

Subcritical growth occurs between stress intensity factors K_0 and K_c (see Figure 2.7). K_0 is the stress intensity factor below which, theoretically, no crack growth can occur, while at K_c the cracks starts to propagate dynamically (*Atkinson*, 1982; *Scholz*, 2002).

For subcritical crack growth the crack velocity is usually described by a power law defined by *Charles* (1958):

$$v = v_0 \cdot exp\left(\frac{-\Delta H}{RT}\right) \cdot K_I^n, \tag{2.16}$$

with v_0 being a pre-exponential factor, ΔH the activation enthalpy and n is the stress corrosion index, which is a material constant. Since crack propagation is a function of the reaction rate at the crack tip, it might be affected by pH (*Lawn and Wilshaw*, 1975). How crack propagation affects pressure solution creep rates in calcite is studied in **Paper 2**.

Experimental work on carbonate chemical compaction

Experimental studies on chemical compaction by pressure solution aim at finding out what is the rate limiting step of the process, *i.e.* dissolution, diffusion, precipitation. This is done in order to determine creep laws suitable for the material studied and easily applicable to natural systems as it was for instance done for quartz by *Gratier et al.* (2009).

If pressure solution is the deformation mechanism, the strain rate is influenced by the manipulation of dissolution, diffusion or precipitation. Following the theory of grain boundary diffusional pressure solution the influence of parameters such as grain size, stress, porosity, temperature, grain packing or the presence of clays, should be studied to discriminate which of the three step is the rate limiting one. Experimental work was conducted on carbonate rocks (*Baker et al.*, 1980), and recent studies were carried on the one hand on fine grained (3 to 80μm) super-pure calcite powder compacted using a microœdometer (*Zhang et al.*, 2002; *Zhang and Spiers*, 2005,b), and on the other hand on calcite crystals indented by glass (*Zubtsov et al.*, 2005).

Experiments on calcareous oozes were conducted at effective stresses in the range 4 to 100 MPa (*Baker et al.*, 1980). Experiments on fine grained calcite were carried under effective stress ranging from 1 to 4 MPa (*Zhang et al.*, 2002; *Zhang and Spiers*, 2005,b). In these studies, test experiments were conducted to ensure that pressure solution was the main deformation process in wet experiments. Three main aspects were studied, that is the influence of effective stress, grain size and pore fluid chemistry on carbonate compaction by pressure solution.

Increasing the effective stress increases the strain rate, and the rate of calcite recrystallisation (*Baker et al.*, 1980). In the different experiments the stress–strain rate relationship does not allow to determine the controlling step of calcite pressure solution. Nevertheless in one set of experiments the strain rate versus stress shows a slope of 2 (*Zhang et al.*, 2002), which according to *De Meer and Spiers* (1999) favours the precipitation controlled intergranular pressure solution.

A wider grain size distribution enhances the compaction rate (*Zhang and Spiers*, 2005,b) and decreasing the grain size increases the strain and the strain rate at fixed strains (*Zhang et al.*, 2002; *Zhang and Spiers*, 2005b). In *Zhang and Spiers* (2005) the strain rate is linked to the grain size by an inverse power law with an exponent equal to three, this indicates that diffusion is most likely the rate limiting step of the process. Compaction of carbonate rocks also lead to the conclusion that dissolution controls the rate of pressure solution (*Baker et al.*, 1980). However, the sensitivity to grain size in other experiments does not allow any conclusion on which of the precipitation, diffusion or dissolution is the rate limiting step (*Zhang and Spiers*, 2005b).

In calcite aggregates, the strain rate is decreased by addition of Mg^{2+} in the pore fluid at concentration ranging from 0.01 to 1 mol (*Zhang et al.*, 2002; *Zhang and Spiers*, 2005). Addition of PO_4^{3-} at 0.0001 to 0.001 mol/l (*Zhang and Spiers*, 2005), and $NaHPO_4$ with concentration ranging from 10^{-6} to 10^{-3} mol/l (*Zhang and Spiers*, 2005b) also decrease the strain rate. On the contrary, compaction creep increases with NaCl at 0.1 to 0.5 mol/l (*Zhang and*

Spiers, 2005). Some of these results favour precipitation as a rate limiting step for pressure solution, however the diffusion controlled hypothesis is never completely ruled out.

In carbonate environments where pore fluids are constituted of meteoric or organic poor water, calcite pressure solution should be a really active diagenetic process. This process is certainly much slower in environments where pore fluids are derived from seawater or are phosphate rich due to organic reactions or biological activity (*Zhang and Spiers*, 2005b).

Zubtsov et al. (2005) carried out indentation experiments at effective stresses ranging from 50 to 200 MPa and at temperatures of either 27°C or 40°C. In some experiments the applied stress was constant and the deformation was measured *ex situ*. In experiments conducted with a weak acid solution, a correlation was found between the depth of the hole and the applied stress. *Zubtsov et al.* (2005) also carried out high-resolution pressure solution creep experiments with continuous deformation recording. In that case, indenters were glass spheres, therefore the contact area between the indenter and the crystal increases with strain and therefore the effective applied stress decreases. In presence of a fluid in equilibrium with calcite, a direct relation between the dead weight and the deformation rate is found. Dissolution of calcite forms holes beneath indenters and dissolved calcite precipitates then around these holes.

In both methods pressure solution was established as the main deformation mechanism. In these experiments, diffusion was found to be the rate limiting step for calcite pressure solution. The deformation rate of calcite is more important when the solution contains NH_4Cl which enhances the solubility of calcite. The development of microcracks beneath the indenters shortened the diffusion transport at the indenter/calcite interface increased the strain rate (*Zubtsov et al.*, 2005).

Overall, no consensus on the rate limiting step of pressure solution in carbonates was obtained. This is to some extent related to the absence of good agreement between macroscopic strain rate laws and experimental results. A possible explanation is that present models do not take grain–size distribution or packing of aggregates accurately into account. In addition, the grain–to–grain geometry employed in the macroscopic models might not be suitable for carbonates.

In some experimental work the combination of pressure solution and subcritical crack growth was observed both at the grain scale and at the aggregate scale (*den Brok*, 1998; *den Brok et al.*, 2002; *Liteanu and Spiers*, 2009). The effect of this combination on calcite grain contact geometry was investigated in **Paper 2** and on the overall compaction behaviour of carbonate aggregates in **Paper 3**.

2.4 Implications for porosity prediction

Early cementation is an important particularity of carbonate rocks. Initial mineralogy, *i.e.* calcite or aragonite, and saturation index of pore waters with respect to those minerals represent important control parameters for porosity loss by chemical compaction at shallow depth (Meyers and Hill, 1983; *Bjørlykke*, 1993). It participates to an early loss of porosity but also plays an important role on stabilization and strengthening of the framework (cf. section 2.2). This process can, to some extent, inhibit or retard mechanical compaction at shallow depth (*Kopaska-Merkel et al.*, 1994; *Budd*, 2001). If early cementation does not affect carbonate sediments, then soil mechanics can be used to model compaction within the first 200 meters of burial (*Audet*, 1995; *Goldhammer*, 1997). Mechanical compaction is affected by the grain size, the clay content and the presence of different lithologies leading to differential compaction (cf. section 2.2). Experimental mechanical compaction shows the importance of porosity in the mechanical strength of the sediments and that mechanical compaction can usually not explain porosity values observed in nature.

Porosity loss as a function of the applied effective stress can be expressed by the consolidation theory (*Terzaghi*, 1925) or the poroelasticity theory (*Biot*, 1941; *Rice and Cleary*, 1976) whether unconsolidated sediments or rocks are taken into account. These theories involve elastic moduli that are determined experimentally for the different sediments (see subsection 2.3.1). The determination of the elastic parameters of rocks is crucial to understand their compaction during increasing burial and therefore for porosity prediction.

In carbonate sands most of the compaction occurs at low stress, *i.e.* less than 5 MPa. Then a locked state is reached and mechanical compaction proceeds by grain crushing with lower strain rates. Compaction of sand depends on the initial packing, the sand composition and the grain size, with finer grain–sized samples being less compressible. The shear modulus and the yield strength increases with cementation. Rocks tested in the laboratory show a non–linear stress–strain relationship which can be related to the amount of cracks and various types of pore present (Baud et al., 2000). Porosity seem to be the main controlling factor on rock compressibility. And overall carbonate rocks are less compressible than sandstones (*Wong et al.*, 2004). Understanding mechanical compaction and the determination of rocks elastic moduli is important. However, these parameters are affected by chemical compaction processes that affect the grain to grain contacts and modify the grain or rock framework stiffness.

Stress is the main drive of porosity loss by mechanical compaction, and it also triggers chemical compaction. Pressure solution intensity is related to the amount of applied stress or overburden (*Royden and Keen*, 1980; *Schmoker and Halley*, 1982; *Spiers and Schutjens*, 1990).

Finally grain size and sorting is important because stress concentration at grain contact depends on these parameters and control the onset of pressure solution creep (*Heydari*, 2000). At depth greater than 500–800 meters, chemical compaction becomes the main mechanism of porosity reduction in carbonates.

The main factors influencing carbonate pressure solution are stress, temperature, advective and diffusive flow and the pore fluid composition (cf. section 2.2). Once pressure solution is initiated, various factors control its kinetics. The effect of temperature pressure solution in carbonates is not clear from natural data. The increase of temperature enhances dissolution and precipitation kinetics, but diminishes calcite solubility. Hence *Rutter* (1983) demonstrated that temperature is not a dominant control process for pressure solution. The diffusion part of pressure solution is enhanced by the presence of open fractures, and especially by the presence of stylolites. Stylolites are more present in part of the sediments where clays and siliciclastic grains are present (*Weyl*, 1959; *Ehrenberg*, 2004, 2006). Formation waters composition seem less important in the subsurface than at shallow depth, but might however play a role.

Models for pressure solution takes into account different grain–to–grain contact geometry such as thin films or islands and channels models. However, some important effect are not taken well enough into account in those theories, for instance the effect of grain size distribution (*Niemeijer et al.*, 2009), or the fact that the grain contact geometry and therefore the diffusion path might be affected by the presence of cracks. The presence of cracks at the grain to grain contact will fasten the strain rates. The velocity of crack propagation is found to be dependent of the fluid in presence, since crack propagation at low stresses is controlled by the rate of chemical reactions at the crack tip. Most of the experimental work on carbonate has focused on trying to find the rate limiting step of pressure solution. However, comparing experimental data with theory, no consensus was found so far. One explanation might be that the grain contact geometry is not described well enough to be able to apply theory to experimental work. Also the effect of grain size distribution and crack propagation oat the grain contact need to be accounted for.

2.5 Conclusion

Mechanical compaction in carbonates does not play a major role on porosity loss. Already at burial depth shallower than 1 km pressure solution might control the rate of sediments compaction. Therefore, unlike siliceous sediments, carbonate compaction can not be modelled by mechanical compaction at depths corresponding to potential hydrocarbon reservoirs.

However, understanding mechanical compaction in carbonates is important. At shallow

depth, non–cemented sediments first loose porosity by mechanical compaction and reach a locked–state. The configuration in which sediments are after initial mechanical compaction determines the amount of grain to grain contacts and therefore further porosity loss by chemical compaction.

Natural and experimental observations agree to say that pressure solution is the main process of porosity loss in carbonates. Theory and experiments show that pressure solution is dependent of effective stress, porosity, grain size and pore fluid chemistry. Although most experimental studies state that the rate limiting step for calcite pressure solution is diffusion, no firm conclusion can be formulated. The rate limiting step might be of different nature depending on compaction condition, but that still has to be explored more thoroughly. Under which conditions does this process starts and stops in limestone, is also not fully understood.

Bibliography

Airey, D. W. (1993), Triaxial testing of naturally cemented carbonate soil, *Journal of Geotechnical Engineering*, *119*(9), 1379–1398.

Anderson, T. L. (1995), *Fracture mechanics: fundamentals and applications*, CRC Press, Boca Raton, 2nd ed.

Angevine, C. L., D. L. Turcotte, and M. D. Furnish (1982), Pressure solution lithification as a mechanism for the stick-slip behavior of faults, *Tectonics*, *1*(2), 151–160.

Arvidson, R. S., M. Collier, K. J. Davis, M. D. Vinson, J. E. Amonette, and A. Luettge (2006), Magnesium inhibition of calcite dissolution kinetics, *Geochimica et Cosmochimica Acta*, *70*(3), 583–594.

Athy, L. F. (1930), Density, porosity, and compaction of sedimentary rocks, *AAPG Bulletin*, *14*(1), 1–24.

Atkinson, B. K. (1982), Subcritical crack propagation in rocks: theory, experimental results and applications, *Journal of Structural Geology*, *4*(1), 41–56, doi: 10.1016/0191-8141(82)90005-0.

Audet, D. M. (1995), Modelling of porosity evolution and mechanical compaction of calcareous sediments, *Sedimentology*, *42*(2), 355–373.

Baker, P. A., M. Kastner, J. D. Byerlee, and D. A. Lockner (1980), Pressure solution and hydrothermal recrystallization of carbonate sediments; an experimental study, *Marine Geology*, *38*(1-3), 185–203.

Bassinot, F., J. Marsters, L. Mayer, and R. Wilkens (1993), Variations of porosity in calcareous sediments from the ontong java plateau, in *Proc. ODP, Sci. Results*, vol. 130, edited by L. W. Kroenke, W. H. Berger, T. R. Janecek, et al., pp. 653 – 661, College Station, TX (Ocean Drilling Program), doi:10.2973/odp.proc.sr.130.058.1993.

Bathurst, R. G. C. (1971), *Carbonate sediments and their diagenesis*, *Developments in Sedimentology*, vol. 12, Elsevier, Amsterdam-Oxford-New York, Netherlands.

Baud, P., A. Schubnel, and T. f. Wong (2000), Dilatancy, compaction, and failure mode in solnhofen limestone, *Journal of Geophysical Research, B, Solid Earth and Planets*, *105*(8), 19,289–19,303.

Baud, P., S. Vinciguerra, C. David, A. Cavallo, E. Walker, and T. Reuschle (2009), Compaction and failure in high porosity carbonates: Mechanical data and microstructural observations, *Pure and Applied Geophysics*, *166*(5-7), 869–898, doi: 10.1007/s00024-009-0493-2.

Biot, M. A. (1941), General theory of three-dimensional consolidation, *Journal of Applied Physics*, *12*(2), 155–164.

Bjørlykke, K. (1993), Fluid flow in sedimentary basins, in *Basin analysis and dynamics of sedimentary basin evolution.*, *Sedimentary Geology*, vol. 86; 1-2, edited by S. Cloetingh, W. Sassi, F. Horvath, and C. Puigdefabregas, pp. 137–158, Elsevier, Amsterdam, Netherlands.

Bjørlykke, K. (1999), An overview of factors controlling rates of compaction, fluid generation and flow in sedimentary basins, in *Growth, dissolution and pattern formation in geosystems.*, edited by B. Jamtveit and P. Meakin, pp. 381–404, Kluwer Academic Publishers, Dordrecht, Netherlands.

Bjørlykke, K. (2006), Effects of compaction processes on stresses, faults, and fluid flow in sedimentary basins; examples from the norwegian margin, in *Analogue and numerical modelling of crustal-scale processes.*, edited by S. J. H. Buiter and G. Schreurs, Geological Society of London. London, United Kingdom.

Blanton, T. L. (1981), Deformation of chalk under confining pressure and pore pressure, *Society of Petroleum Engineers Journal*, *21*(1), 43–50.

Bolås, H. M. N., C. Hermanrud, T. A. Schutter, and G. M. G. Teige (2008), Stress-insensitive chemical compaction responsible for high overpressures in deeply buried north sea chalks?, *Marine and Petroleum Geology*, *25*(7), 565–587.

Budd, D. A. (2001), Permeability loss with depth in the cenozoic carbonate platform of west-central florida, *AAPG Bulletin*, *85*(7), 1253–1272.

Budd, D. A. (2002), The relative roles of compaction and early cementation in the destruction of permeability in carbonate grainstones; a case study from the paleogene of west-central florida, u.s.a, *Journal of Sedimentary Research*, *72*(1), 116–128.

Buxton, T. M., and D. F. Sibley (1981), Pressure solution features in a shallow buried limestone, *Journal of Sedimentary Petrology*, *51*(1), 19–26.

Caminatti, M., J. L. Dias, and B. Wolf (2009), From turbidites to carbonates: Breaking paradigms in deep water, in *Offshore Technology Conference*, Houston, Texas, doi: 10.4043/20124-MS.

Carroll, M. M., and A. C. Holt (1972), Static and dynamic pore-collapse relations for ductile porous materials, *Journal of Applied Physics*, *43*(4), 1626–1636.

Chan, S. H., and A. H. W. Ngan (2005), Statistical distribution of contact forces in packings of deformable spheres, *Mechanics of Materials*, *37*(4), 493–506.

Charles, R. J. (1958), Dynamic fatigue of glass, *Journal of Applied Physics*, *29*(12), 1657–1662.

Chuhan, F. A., A. Kjeldstad, K. Bjørlykke, and K. Høeg (2003), Experimental compression of loose sands; relevance to porosity reduction during burial in sedimentary basins, *Canadian Geotechnical Journal = Revue Canadienne de Geotechnique*, *40*(5), 995–1011.

Coogan, A. H., and R. W. Manus (1975), Compaction and diagenesis of carbonate sands, in *Compaction of coarse-grained sediments I : Developments in Sedimentology*, vol. 18A, edited by A. Chilingarian and K. H. Wolf, pp. 79 – 166, Elsevier, New York.

Coop, M. R. (1990), The mechanics of uncemented carbonate sands, *Geotechnique*, *40*(4), 607–626.

Couvreur, J. F., A. Vervoort, M. S. King, E. Lousberg, and J. F. Thimus (2001), Successive cracking steps of a limestone highlighted by ultrasonic wave propagation, *Geophysical Prospecting*, *49*(1), 71–78.

Croizé, D., S. N. Ehrenberg, K. Bjørlykke, F. Renard, and J. Jahren (2009), Petrophysical properties of bioclastic platform carbonates: implications for porosity controls during burial, *Marine and Petroleum Geology*, *In Press, Corrected Proof*, doi: 10.1016/j.marpetgeo.2009.11.008.

Curran, J. H., and M. M. Carroll (1979), Shear-stress enhancement of void compaction, *Journal of Geophysical Research*, *84*(NB3), 1105–1112.

De Meer, S., and C. J. Spiers (1999), On mechanisms and kinetics of creep by intergranular pressure solution, in *Growth, dissolution and patterns formation in geosystems*, edited by B. Jamtveit and P. Meakin, Kluwer Academic Publishers, Dordrecht, The Netherlands.

den Brok, B., J. Morel, and M. Zahid (2002), In situ experimental study of roughness development at a stressed solid/fluid interface, in *Deformation Mechanisms, Rheology and Tectonics: Current Status and Future Perspectives*, vol. 200, edited by S. DeMeer, M. R. Drury, J. H. P. DeBresser, and G. M. Pennock, pp. 73–83, The Geological Society, London.

den Brok, S. W. J. B. (1998), Effect of microcracking on pressure-solution strain rate; the gratz grain-boundary model, *Geology*, *26*(10), 915–918.

Durney, D. W. (1976), Pressure-solution and crystallization deformation, *Philosophical Transactions of the Royal Society of London, Series A: Mathematical and Physical Sciences*, *283*(1312, A discussion on natural strain and geological structure), 229–240.

Dysthe, D. K., Y. Podladchikov, F. Renard, J. Feder, and B. Jamtveit (2002), Universal scaling in transient creep, *Physical Review Letters*, *89*(24), 246,102.

Eberli, G. P., G. T. Baechle, F. S. Anselmetti, and M. L. Incze (2003), Factors controlling elastic properties in carbonate sediments and rocks, *The Leading Edge*, *22*(7), 654–660.

Ebhardt, G. (1968), Experimental compaction of carbonate sediments, in *Recent developments in carbonate sedimentology in central Europe*, pp. 58–65, Springer-Verlag, New York, NY, United States.

Ehrenberg, S. N. (2003), Carbonate porosity control by aluminosilicate distribution; finnmark carbonate platform (pennsylvanian-permian), offshore north norway, in *2003 AAPG annual convention with SEPM.*, edited by J. Chidsey Thomas, C., American Association of Petroleum Geologists and Society of Economic Paleontologists and Mineralogists. Tulsa, OK, United States. 2003.

Ehrenberg, S. N. (2004), Factors controlling porosity in the upper carboniferous-lower permian carbonate strata of the barents sea, *AAPG Bulletin*, *88*(12), 1653–1676.

Ehrenberg, S. N. (2006), Porosity destruction in carbonates platforms, *Journal of Petroleum Geology*, *29*(1), 41–52, doi:10.1111/j.1747–5457.2006.00041.x.

Ehrenberg, S. N., and P. H. Nadeau (2005), Sandstone vs. carbonate petroleum reservoirs; a global perspective on porosity - depth and porosity - permeability relationships, *AAPG Bulletin*, *89*(4), 435–445.

Ehrenberg, S. N., G. P. Eberli, M. Keramati, and S. A. Moallemi (2006), Porosity-permeability relationships in interlayered limestone-dolostone reservoirs, *AAPG Bulletin*, *90*(1), 91–114.

Engelder, T. (1982), A natural example of the simultaneous operation of free-face dissolution and pressure solution, *Geochimica et Cosmochimica Acta*, *46*(1), 69–74.

Enos, P., and L. H. Sawatsky (1981), Pore networks in holocene carbonate sediments, *Journal of Sedimentary Petrology*, *51*(3), 961–985.

Evans, B., Y. Bernabe, and W. Zhu (1997), Evolution of pore structure and permeability of rocks in laboratory experiments, in *Growth, dissolution and pattern formation in geosystems.*, edited by B. Jamtveit and P. Meakin, pp. 327–344, Kluwer Academic Publishers, Dordrecht, Netherlands.

Fabre, D., and J. Gustkiewicz (1997), Poroelastic properties of limestones and sandstones under hydrostatic conditions, *International Journal of Rock Mechanics and Mining Sciences*, *34*(1), 127–134.

Fabricius, I. L. (2003), How burial diagenesis of chalk sediments control sonic velocity and porosity, *AAPG Bulletin*, *87*(11), 1755–1778.

Finkel, E. A., and B. H. Wilkinson (1990), Stylolitization as source of cement in mississippian salem limestone, west-central indiana, *AAPG Bulletin*, *74*(2), 174–186.

Fjær, E., R. M. Holt, P. Horsrud, A. M. Raaen, and R. Risnes (1992), *Petroleum related rock mechanics*, Elsevier, Amsterdam.

Friedman, G. M., S. A. Reeckmann, and B. Borak (1981), Carbonate deformation mechanisms in the world's deepest wells (nearly equal 9 km), *Tectonophysics*, *74*(3-4), T15–T19.

Fruth, J., L S, G. R. Orme, and F. A. Donath (1966), Experimental compaction effects in carbonate sediments, *Journal of Sedimentary Petrology*, *36*(3), 747–754.

Giles, M. R. (1997), *Diagenesis: a quantitative perspective – Implications for basin modelling and rock property prediction*, Kluwer Academic Publishers, Dordrecht, The Netherlands.

Ginsburg, R. N. (1957), Early diagenesis and lithification of shallow-water carbonate sediments in south florida, in *Regional Aspects of Carbonate Deposition*, vol. 5, edited by R. J. LeBlanc and J. G. Breeding, pp. 80–99, Society of Economic Paleontologists and Mineralogists, Special publication.

Glover, J. E. (1968), Significance of stylolites in dolomitic limestones, *Nature*, *217*(5131), 835–836, doi: 10.1038/217835a0.

Goldhammer, R. K. (1997), Compaction and decompaction algorithms for sedimentary carbonates, *Journal of Sedimentary Research*, *67*(1), 26–35.

Gratier, J. P., F. Renard, and P. Labaume (1999), How pressure solution creep and fracturing processes interact in the upper crust to make it behave in both a brittle and viscous manner, *Journal of Structural Geology*, *21*(8-9), 1189–1197.

Gratier, J. P., R. Guiguet, F. Renard, L. Jenatton, and D. Bernard (2009), A pressure solution creep law for quartz from indentation experiments, *Journal of Geophysical Research-Solid Earth*, *114*, doi:10.1029/2008jb005652.

Gratz, A. J. (1991), Solution-transfer compaction of quartzites - progress toward a rate law, *Geology*, *19*(9), 901–904.

Griffith, A. A. (1920), The phenomena of rupture and flow in solids, *Philosophical Transactions of the Royal Society of London. Series A, Containing Papers of a Mathematical or Physical Character*, *221*, 163–198.

Guéguen, Y., L. Dormieux, and M. Boutéca (2004), Fundamentals of poromechanics, in *Mechanics of Fluid–Saturated Rocks*, edited by Y. Guéguen and M. Boutéca, International geophysics series, p. 450, Elsevier Academic Press, Amsterdam.

Gundersen, E., F. Renard, D. K. Dysthe, K. Bjørlykke, and B. Jamtveit (2002), Coupling between pressure solution creep and diffusive mass transport in porous rocks, *Journal of Geophysical Research, B, Solid Earth and Planets*, *107*(11).

Hamilton, E. L. (1976), Variations of density and porosity with depth in deep-sea sediments, *Journal of Sedimentary Petrology*, *46*(2), 280–300.

Heydari, E. (2000), Porosity loss, fluid flow, and mass transfer in limestone reservoirs; application to the upper jurassic smackover formation, mississippi, *AAPG Bulletin*, *84*(1), 100–118.

Hickman, S. H., and B. Evans (1991), Experimental pressure solution in halite - the effect of grain interphase boundary structure, *Journal of the Geological Society*, *148*, 549–560.

Hickman, S. H., and B. Evans (1995), Kinetics of pressure solution at halite-silica interfaces and intergranular clay films, *Journal of Geophysical Research-Solid Earth*, *100*(B7), 13,113–13,132.

Hugman, R. H. H., and M. Friedman (1979), Effects of texture and composition on mechanical behavior of experimentally deformed carbonate rocks, *AAPG Bulletin*, *63*(9), 1478 – 1489.

Jaeger, J. C., N. G. W. Cook, and R. W. Zimmerman (2007), *Fundamentals of rock mechanics*, 4th ed., Blackwell publishing.

Jouniaux, L., M. Zamora, and T. Reuschle (2006), Electrical conductivity evolution of non-saturated carbonate rocks during deformation up to failure, *Geophysical Journal International*, *167*(2), 1017–1026.

Karcz, Z., E. Aharonov, D. Ertas, R. Polizzotti, and C. H. Scholz (2006), Stability of a sodium chloride indenter contact undergoing pressure solution, *Geology*, *34*(1), 61–63, doi:10.1130/G21722.1.

Kopaska-Merkel, D. C., S. D. Mann, and J. W. Schmoker (1994), Controls on reservoir development in a shelf carbonate; upper jurassic smackover formation of alabama, *AAPG Bulletin*, *78*(6), 938–959.

Lawn, B., and R. Wilshaw (1975), Indentation fracture - principles and applications, *Journal of Materials Science*, *10*(6), 1049–1081.

Lehner, F. K. (1990), Thermodynamics of rock deformation by pressure solution, in *Deformation Processes in Minerals, Ceramics and Rocks*, edited by D. J. Barber and P. G. Meredith, p. 423, Unwin Hyman Ltd, London, United Kingdom.

Lehner, F. K. (1995), A model for intergranular pressure solution in open systems, *Tectonophysics*, *245*(3-4), 153–170.

Lehner, F. K., and J. Bataille (1984), Nonequilibrium thermodynamics of pressure solution, *Pure and Applied Geophysics*, *122*(1), 53–85.

Liteanu, E., and C. J. Spiers (2009), Influence of pore fluid salt content on compaction creep of calcite aggregates in the presence of supercritical CO_2, *Chemical Geology*, *265*(1-2), 134–147, doi:10.1016/j.chemgeo.2008.12.010.

Lubanzadio, M., N. R. Goulty, and R. E. Swarbrick (2002), Variation of velocity with effective stress in chalk; null result from north sea well data, *Marine and Petroleum Geology*, *19*(8), 921–927.

Mair, K., and J. F. Hazzard (2007), Nature of stress accommodation in sheared granular material: Insights from 3D numerical modeling, *Earth and Planetary Science Letters*, *259*(3-4), 469–485.

Meyers, W. J. (1980), Compaction in mississippian skeletal limestones, southwestern new mexico, *Journal of Sedimentary Research*, *50*(2), 457–474.

Meyers, W. J., and B. E. Hill (1983), Quantitative studies of compaction in mississippian skeletal limestones, new mexico, *Journal of Sedimentary Petrology*, *53*(1), 231–242.

Moldovanyi, E. P., and L. M. Walter (1992), Regional trends in water chemistry, smackover formation, southwest arkansas; geochemical and physical controls, *AAPG Bulletin*, *76*(6), 864–894.

Moore, C. H. (2001), *Carbonate reservoirs; porosity evolution and diagenesis in a sequence stratigraphic framework*, *Developments in Sedimentology*, vol. 55, Elsevier. Amsterdam-Oxford-New York, Netherlands.

Niemeijer, A., D. Elsworth, and C. Marone (2009), Significant effect of grain size distribution on compaction rates in granular aggregates, *Earth and Planetary Science Letters*, *284*(3-4), 386–391, doi: 10.1016/j.epsl.2009.04.041.

Olagnon, C., J. Chevalier, and V. Pauchard (2006), Global description of crack propagation in ceramics, *Journal of the European Ceramic Society*, *26*(15), 3051–3059, doi: 10.1016/j.jeurceramsoc.2005.11.004.

Palchik, V., and Y. H. Hatzor (2002), Crack damage stress as a composite function of porosity and elastic matrix stiffness in dolomites and limestones, *Engineering Geology*, *63*(3-4), 233–245.

Paterson, M. S. (1973), Nonhydrostatic thermodynamics and its geologic applications, *Reviews of Geophysics*, *11*(2), 355–389.

Paterson, M. S., and T. f. Wong (2004), *Experimental rock deformation; the brittle field*, 2nd ed., Springer-Verlag. Berlin, Federal Republic of Germany.

Raj, R. (1982), Creep in polycrystalline aggregates by matter transport through a liquid-phase, *Journal of Geophysical Research*, *87*(NB6), 4731–4739.

Renard, F., and P. J. Ortoleva (1997), Water films at grain-grain contacts; debye-hueckel, osmotic model of stress, salinity, and mineralogy dependence, *Geochimica et Cosmochimica Acta*, *61*(10), 1963–1970.

Renard, F., J. P. Gratier, and B. Jamtveit (2000), Kinetics of crack-sealing, intergranular pressure solution, and compaction around active faults, *Journal of Structural Geology*, *22*, 1395–1407.

Renard, F., D. Dysthe, J. Feder, K. Bjørlykke, and B. Jamtveit (2001), Enhanced pressure solution creep rates induced by clay particles; experimental evidence in salt aggregates, *Geophysical Research Letters*, *28*(7), 1295–1298.

Renner, J., and F. Rummel (1996), The effect of experimental and microstructural parameters on the transition from brittle failure to cataclastic flow of carbonate rocks, *Tectonophysics*, *258*(1-4), 151–169, doi:10.1016/0040-1951(95)00192-1.

Rice, J. R., and M. P. Cleary (1976), Some basic stress diffusion solutions for fluid-saturated elastic porous-media with compressible constituents, *Reviews of Geophysics*, *14*(2), 227–241.

Ricken, W. (1987), The carbonate compaction law: a new tool, *Sedimentology*, *34*(4), 571–584, doi:10.1111/j.1365-3091.1987.tb00787.x.

Royden, L., and C. E. Keen (1980), Rifting process and thermal evolution of the continental margin of eastern canada determined from subsidence curves, *Earth and Planetary Science Letters*, *51*(2), 343–361.

Rozhko, A., Y. Podladchikov, and F. Renard (2007), Failure patterns caused by localized rise in pore-fluid overpressure and effective strength of rocks, *Geophysical Research Letters*, *34*, L22,304, doi:10.1029/2007GL031,696.

Rutter, E. H. (1983), Pressure solution in nature, theory and experiment, *Journal of the Geological Society of London*, *140*(5), 725–740.

Schmoker, J. W., and R. B. Halley (1982), Carbonate porosity versus depth; a predictable relation for south florida, *AAPG Bulletin*, *66*(12), 2561–2570.

Scholle, P. A., and R. B. Halley (1985), Burial diagenesis; out of sight, out of mind!, in *Carbonate cements.*, *Special Publication - Society of Economic Paleontologists and Mineralogists*, vol. 36, edited by N. Schneidermann and M. Harris Paul, pp. 309–334, SEPM (Society for Sedimentary Geology), Tulsa, OK, United States.

Scholz, C. H. (2002), *The mechanics of earthquakes and faulting*, 2nd ed., Cambridge University Press, Cambridge.

Sclater, J. G., and P. A. F. Christie (1980), Continental stretching; an explanation of the post-mid-cretaceous subsidence of the central north sea basin, *Journal of Geophysical Research*, *85*(B7), 3711–3739.

Shinn, E. A., and D. M. Robbin (1983), Mechanical and chemical compaction in fine-grained shallow-water limestones, *Journal of Sedimentary Petrology*, *53*(2), 595–618.

Sorby, H. C. (1863), The bakerian lecture: On the direct correlation of mechanical and chemical forces, *Proceedings of the Royal Society of London*, *12*, 538–550.

Spiers, C. J., and P. M. T. M. Schutjens (1990), Densification of crystalline aggregates by fluid - phase diffusional creep, in *Deformation Processesin Minerals, Ceramics and Rocks*, edited by D. J. Barber and P. G. Meredith, p. 423, Unwin Hyman Ltd, London, United Kingdom.

Tada, R., and R. Siever (1986), Experimental knife-edge pressure solution of halite, *Geochimica et Cosmochimica Acta*, *50*(1), 29–36, doi:10.1016/0016-7037(86)90045-1.

Tada, R., and R. Siever (1989), Pressure solution during diagenesis, *Annual Review of Earth and Planetary Sciences*, *17*, 89–118.

Terzaghi, K. (1925), *Erdbaumechanik auf bodenphysikalischer Grundlage*, Deuticke, F, Leipzig/Vienna.

Terzaghi, K., and R. B. Peck (1967), *Soil mechanics in engineering practice*, Wiley, New York, 2nd ed.

Turcotte, D. L., and G. Schubert (1982), *Geodynamics; applications of continuum physics to geological problems*, John Wiley & Sons, New York, NY, United States.

Vajdova, V., P. Baud, and T. f. Wong (2004), Compaction, dilatancy, and failure in porous carbonate rocks, *Journal of Geophysical Research, B, Solid Earth and Planets*, *109*, B05,204, doi:10.1029/2003JB002508.

van Noort, R., and C. J. Spiers (2009), Kinetic effects of microscale plasticity at grain boundaries during pressure solution, *J. Geophys. Res.*, *114*, doi: 10.1029/2008JB005634.

van Noort, R., H. J. M. Visser, and C. J. Spiers (2008), Influence of grain boundary structure on dissolution controlled pressure solution and retarding effects of grain boundary healing, *J. Geophys. Res.*, *113*, doi: 10.1029/2007JB005223.

Vanorio, T., C. Scotellaro, and G. Mavko (2008), The effect of chemical and physical processes on the acoustic properties of carbonate rocks, *The Leading Edge*, *27*(8), 1040–1048.

Wallace, M. W., G. R. Holdgate, J. Daniels, S. J. Gallagher, and A. Smith (2002), Sonic velocity, submarine canyons, and burial diagenesis in oligocene-holocene cool-water carbonates, gippsland basin, southeast australia, *AAPG Bulletin*, *86*(9), 1593–1607.

Walsh, J. B., and W. F. Brace (1966), Elasticity of rock: a review of some recent theoretical studies, *Rock Mechanics and Engineering Geology*, *4*, 283–297.

Wanless, H. R. (1979), Limestone response to stress; pressure solution and dolomitization, *Journal of Sedimentary Petrology*, *49*(2), 437–462.

Warren, E. A., and P. C. Smalley (1994), The ekofisk field, in *North Sea formation waters atlas*, *Memoir - Geological Society of London*, vol. 15, edited by E. A. Warren and P. C. Smalley, p. 29, Blackwell [for the] Geological Society of London, London, United Kingdom.

Weyl, P. K. (1959), Pressure solution and the force of crystallization – a phenomenological theory, *Journal of Geophysical Research*, *64*(11), 2001–2025.

Wong, T.-f., C. David, and B. Menédez (2004), Mechanical compaction, in *Mechanics of Fluid - Saturated Rocks*, edited by Y. Guéguen and M. Boutéca, International geophysics series, p. 450, Elsevier Academic Press, Amsterdam.

Yasar, E., and Y. Erdogan (2004), Correlating sound velocity with the density, compressive strength and young's modulus of carbonate rocks, *International Journal of Rock Mechanics and Mining Sciences (1997)*, *41*(5), 871–875.

Yasuhara, H., D. Elsworth, and A. Polak (2003), A mechanistic model for compaction of granular aggregates moderated by pressure solution, *Journal of Geophysical Research-Solid Earth*, *108*(B11).

Zhang, X., and C. J. Spiers (2005a), Compaction of granular calcite by pressure solution at room temperature and effects of pore fluid chemistry, *International Journal of Rock Mechanics and Mining Sciences*, *42*, 950–960.

Zhang, X., and C. J. Spiers (2005b), Effects of phosphate ions on intergranular pressure solution in calcite: An experimental study, *Geochimica et Cosmochimica Acta*, *69*(24), 5681–5691.

Zhang, X., J. Salemans, C. J. Peach, and C. J. Spiers (2002), Compaction experiments on wet calcite powder at room temperature; evidence for operation of intergranular pressure solution,

in *Deformation mechanisms, rheology and tectonics; current status and future perspectives*, *Geological Society Special Publications*, vol. 200, edited by S. de Meer, R. Drury Martyn, J. H. P. de Bresser, and M. Pennock Gill, pp. 29–39, Geological Society of London, London, United Kingdom.

Zubtsov, S., F. Renard, J. P. Gratier, D. K. Dysthe, and V. Traskine (2005), Single-contact pressure solution creep on calcite monocrystals, in *Deformation mechanisms, rheology and tectonics; from minerals to the lithosphere*, *Geological Society Special Publications*, vol. 243, edited by D. Gapais, P. Brun Jean, and R. Cobbold Peter, pp. 81–95, Geological Society of London, London, United Kingdom.

Paper 1: Petrophysical properties of bioclastic platform carbonates: implications for porosity controls during burial

Journal of Marine and Petroleum Geology

Petrophysical properties of bioclastic platform carbonates: implications for porosity controls during burial

Delphine Croizé[a],Stephen N. Ehrenberg[b], Knut Bjørlykke[a], François Renard[c], Jens Jahren[a]

[a] Department of Geosciences, University of Oslo, Norway

[b] Oil and Gas Research Center, Sultan Qaboos University, Muscat, Sultanate of Oman

[c] LGCA-CNRS-Observatoire de Grenoble, Université Joseph Fourier, Grenoble, France & Physics of Geological Processes, University of Oslo, Norway

Abstract

This study is based on rock mechanical tests of samples from platform carbonate strata to document their petrophysical properties and determine their potential for porosity loss by mechanical compaction. Sixteen core-plug samples, including eleven limestones and five dolostones, from Miocene carbonate platforms on the Marion Plateau, offshore northeast Australia, were tested at vertical effective stress, σ'_1, of 0-70 MPa, as lateral strain was kept equal to zero. The samples were deposited as bioclastic facies in platform-top settings having paleo-water depths of $<$10 to 90 m. They were variably cemented with low-Mg calcite and five of the samples were dolomitized before burial to present depths of 39-635 m below sea floor with porosities of 8 to 46 %. Ten samples tested under dry conditions had up to 0.22 % strain at σ'_1 = 50 MPa, whereas six samples tested saturated with brine, under drained conditions, had up to 0.33 % strain. The yield strength was reached in five of the plugs. The measured strains show an overall positive correlation with porosity. V_p ranges from 3640 to 5660 m/s and V_s from 1840 to 3530 m/s. Poisson coefficient is 0.20-0.33 and Young's modulus at 30 MPa ranged between 5 and 40 GPa. Water saturated samples had lower shear moduli and slightly higher P- to S-wave velocity ratios. Creep at constant stress was observed only in samples affected by pore collapse, indicating propagation of microcracks. Although deposited as loose carbonate sand and mud, the studied carbonates acquired reef-like petrophysical properties by early calcite and dolomite cementation. The small strains observed experimentally at 50 MPa indicate that little mechanical compaction would occur at deeper burial. However, as these rocks are unlikely to preserve their present high porosities to 4-5 km depth, further porosity loss would proceed mainly by chemical compaction and cementation.

3.1 Introduction

Shallow water carbonates are strongly affected by early diagenesis (Friedman, 1964). Widely variable early diagenetic processes affecting carbonate sediments make application of quantitative models for petrophysical properties more difficult than for siliciclastic rocks which are more stable at low temperature (*Anselmetti and Eberli*, 1993; Anselmetti and Eberli, 2001; *Eberli et al.*, 2003; Adam et al., 2006; *Vanorio et al.*, 2008). In large part because of varying early diagenesis, the Marion Plateau carbonate platforms display a wide range of petrophysical properties within a narrow range of depths (Isern et al., 2002; Ehrenberg et al., 2003, 2006c). They are therefore well suited for studying the impact of early diagenesis on mechanical compaction. Early carbonate diagenetic processes include dissolution of aragonite and magnesian calcite, precipitation of low-Mg calcite, as well as dolomitization (Meyers and Hill, 1983; *Scholle and Halley*, 1985). These processes can both add and remove large volumes of material, such that subsequent mechanical compaction during the first several hundred meters of burial depends strongly on the early diagenetic history (*Hamilton*, 1976; *Scholle and Halley*, 1985; *Bassinot et al.*, 1993; Wallace et al., 2002). Although initial porosities of carbonate sediments are very high ranging around 50 - 60 % (Enos and Sawatsky, 1981; Kroenke et al., 1991), porosities of subsurface carbonate reservoirs are generally much lower than in sandstones and commonly show trends of regular decrease as burial increases (Schmoker, 1984; Brown, 1997; Ehrenberg and Nadeau, 2005). At depth less than 2 - 2.5 km, i.e., temperature lower than 70 - 90 °C, mechanical compaction is commonly the main process of porosity loss in sandstones (Bjørlykke and Høeg, 1997; Paxton et al., 2002), but its importance in carbonates is more difficult to evaluate because of the irregular grain shapes and extensive diagenetic alteration characteristic of many carbonate sediments. Laboratory experiments showed that when carbonates are not cemented, mechanical compaction plays a major role on porosity loss (*Goldhammer*, 1997; *Chuhan et al.*, 2003). While carbonate rocks are mostly studied based on outcrop or cores from reservoirs, the present study measures the petrophysical properties of Miocene carbonate rocks buried at 39 - 635 meters below sea floor which represents their maximal burial depth. The results provide a basis for predicting porosity at greater depth and understanding the respective roles of mechanical and chemical compaction in carbonate sediments.

3.2 Samples

The samples studied are from two Miocene carbonate platforms that were cored during Ocean Drilling Program (ODP) Leg 194 on the Marion Plateau, just seaward of the Great Barrier

Reef on the northeastern Australian continental margin (Pigram et al., 1992; Isern et al., 2002). These cores are characterized by strong petrophysical heterogeneities over short vertical depth intervals, reflecting varying influence of both depositional textures and diagenesis (Ehrenberg et al., 2006b). Details regarding the units sampled and the separation of the samples into different textural classes are provided by Isern et al. (2002); Ehrenberg et al. (2006a). Fifteen horizontally oriented, 25 mm core-plugs were selected among the samples analysed by Ehrenberg et al. (2003) (Figs. 3.1 and 3.2). One additional sample, plug 1.2, is a vertically oriented plug drilled from whole-core sample EHWR1 (Ehrenberg, 2007). The samples consist of eleven limestones and five dolostones cored from depth of 39 - 365 meters below sea floor. The sediments were deposited as loose bioclastic grains and mud in paleo-water depths estimated to have been less than 10 to less than 100 meters (Isern et al., 2002). Principal bioclasts are large benthic foraminifers, red algae and bryozoans. Plugs have porosities of 8 - 46 % and permeabilities ranging from 0.04 to >50000 mD (Table 3.1). A wide scatter is observed in the permeability - porosity relationship and no clear relationship between textures and porosity - permeability trends is apparent (Fig. 3.3). Comparison between plug and whole core measurements for the Marion Plateau samples shows that plug samples, despite their smaller size, adequately represent the petrophysical properties of the studied cores (Ehrenberg, 2007). The sixteen samples selected for testing include nine plugs from site 1193, penetrating the Northern Marion Platform (NMP) and seven plugs from site 1196, on the Southern Marion Platform (SMP) (Table 3.1). The samples include eleven limestones and five dolostones, meaning that they contain 80% or more calcite or dolomite, respectively. All samples originally had bioclastic textures (packstone, grainstone, floatstone) and have negligible siliciclastic content.

3.3 Experimental method

3.3.1 K_0 triaxial tests

The experimental method used is K_0 triaxial testing under drained conditions. K_0 stands for coefficient of lateral stress at rest, $K_0 = \sigma'_3/\sigma'_1$, where σ'_3 is horizontal effective stress and σ'_1 is vertical effective stress, both are expressed in MPa. The samples are cylindrical plugs of about 25 mm in diameter and 17 - 29 mm in height. All plugs were ground at top and bottom to make the two end surfaces plane and parallel. For some plugs plaster was added on the end surfaces to fill large pores and ensure an uniform application of load on the surface. Plaster was also applied at a few places on the sample sides to prevent the confining membrane from being pressed into cavities and thereby being punctured at high cell pressures. The plugs were then

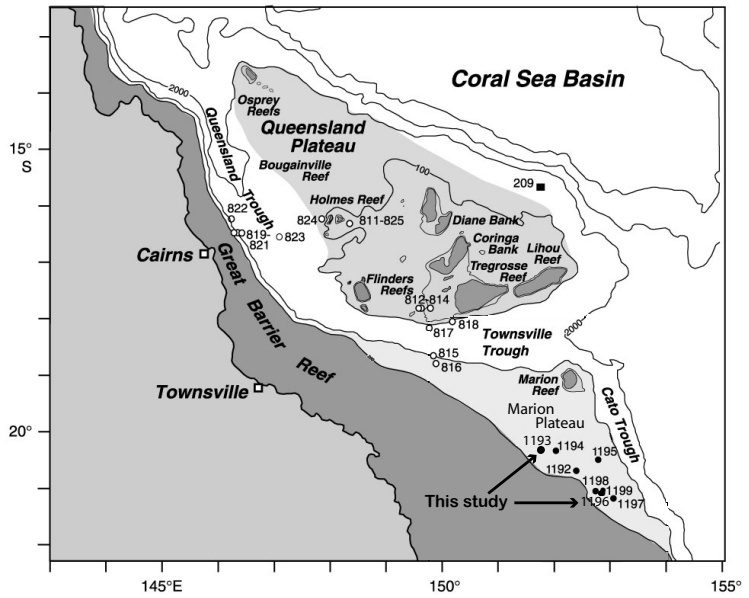

Figure 3.1: Location of ODP drilling sites 1193 and 1196 where the tested samples were taken (modified from Isern et al. (2002)).

Figure 3.2: Plugs 18, 21, 22 and 30 before compaction.

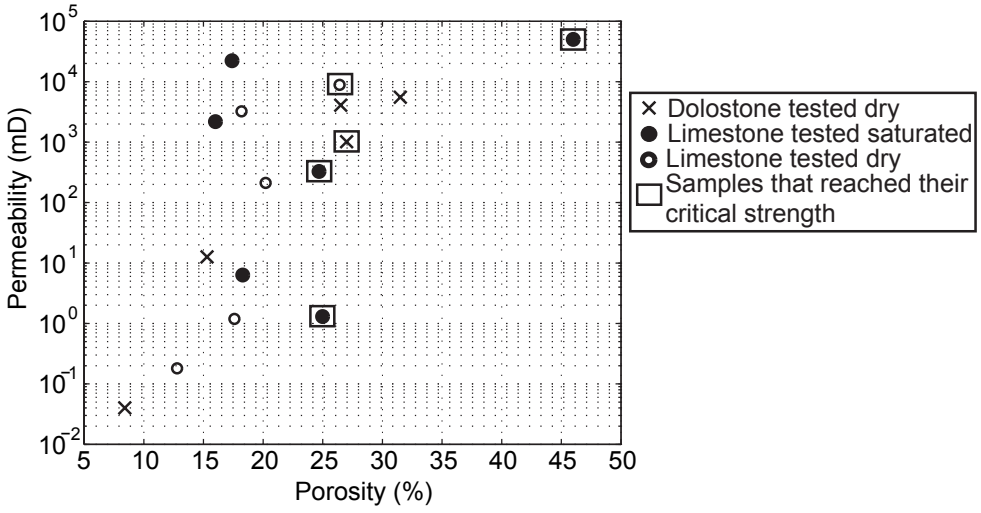

Figure 3.3: Permeability versus porosity (Actual values are to be found in Table 3.1).

Table 3.1: Sample characteristics, test conditions and calculated elastic parameters

site[a]	plug	z[b]	mineralogy	tex[c]	GD[d]	height[e]	k[f]	Φ[g]	conditions	σ'_{1ini}[h]	σ'_{3ini}[h]	σ'_{1final}[h]	E[i]	ν[i]	K[i]	μ[i]	β[i]	V_p[j]	V_s[j]
1193	18	45.97	Limestone	O	2.71	21.00	213.0	20.2	Dry	1.66	0.5	50	19.6	0.25	19.7	16.3	3.34	3927	2454
1196	69	56.97	Dolostone		2.82	21.43	1014.0	27.0	Dry	1.66	0.5	50	22.1	0.24	21.1	17.9	3.98	4081	2526
1193	21	63.74	Limestone	C	2.71	25.10	8835.0	26.4	Dry	1.25	0.5	50	19.5	0.23	11.0	20.8	4.42	3833	2774
1193	22	67.92	Limestone	X	2.72	23.60	1.18	17.6	Dry	1.66	0.5	50	21.9	0.28	11.4	23.53	2.90	4028	2899
1193	30	73.79	Limestone	O	2.70	29.25	3236.0	18.2	Dry	1.25	0.5	50	28.5	0.26	20.5	21.7	2.43	4359	2803
1196	114	316.86	Limestone	F	2.71	22.50	0.18	12.8	Dry	5	2	50	30.2	0.24	28.0	18.9	2.54	4523	2652
1196	160	539.35	Dolostone		2.73	26.27	0.04	8.4	Dry	1.25	0.5	30	33.3	0.33	39.8	35.9	1.30	5630	3542
1196	167	557.51	Dolostone		2.82	27.73	5545.0	31.5	Dry	1.25	0.5	30	20.9	0.24	28.6	17.1	3.69	4292	2497
1196	201	633.88	Dolostone		2.76	23.15	12.60	15.3	Dry	9.8	2.94	50	30.9	0.23	36.0	23.5	1.81	4934	2937
1196	203	634.98	Dolostone		2.78	21.67	4094.0	26.5	Dry	9.8	2.94	50	18.1	0.20	29.9	13.5	3.85	4129	2198
1196	1.2	38.58	Limestone	X	2.75	19.54	1.3	25.0	Saturated	1.66	0.5	70	8.63	0.30	29.7	15.3	11.7	4358	2355
1193	2	42.16	Limestone	O	2.70	22.54	22314	17.4	Saturated	1.66	0.5	70	14.9	0.27	41.1	19.3	3.57	5008	2678
1193	4	43.19	Limestone	O	2.68	19.35	2169	16.0	Saturated	1.66	0.5	70	12.4	0.29	32.3	16.3	3.60	4495	2485
1193	17	45.69	Limestone	O	2.72	21.60	325	24.7	Saturated	1.66	0.5	70	8.56	0.25	35.5	15.4	6.38	4550	2366
1193	52	61.34	Limestone	C	2.72	17.46	6.31	18.3	Saturated	1.66	0.5	50	14.2	0.26	29.1	14.3	3.84	4191	2271
1193	31	74.16	Limestone	C	2.70	24.24	>50000	46.0	Saturated	1.66	0.5	7					18.8	4264	2463

[a] ODP drilling site number

[b] Depth in meters below sea floor

[c] Texture: C = coarse grainstone, F = fine grainstone, X = packstone with isolated vugs, O = packstone with large vugs (From Ehrenberg et al., 2006a)

[d] Grain density (g/cm^3)

[e] Plug height (mm)

[f] Klinkenberg-corrected gas permeability (mD)

[g] Porosity (%)

[h] Initial and final stress values during triaxials tests (MPa)

[i] Elastic parameters calculated at σ'_1 = 30 MPa: E = Young's Modulus (GPa), ν = Poisson ratio, K = bulk modulus (GPa), μ = shear modulus (GPa), β = compressibility ($10^{-11} Pa^{-1}$)

[j] Acoustic velocity in meters per second, mean values measured at $\sigma'_1 \geq 20$ MPa (Except for plug 31 for which σ'_1 is less than 10 MPa)

dried at 50 - 60°C. Two knobs were glued, diametrically opposed, at the middle height of the sample for fixation of the radial deformation sensor. The samples were then sprayed with latex rubber to create a confining membrane.

The samples were mounted into the triaxial cell and subjected to a vacuum of about 0.1 MPa inside the confining membrane and then subjected to a confining pressure of about 0.5 MPa. The vacuum was then released by allowing air into the sample for the dry tests and brine for the saturated tests. For the saturated tests a back pressure of 5 MPa was applied by increasing confining pressure and pore pressure simultaneously to 5.5 and 5.0 MPa, respectively, to secure good saturation. The effective stresses were then increased to σ'_{1ini} and σ'_{3ini} values given in Table 3.1. Then vertical stress was increased at a rate of 3.75 MPa per hour for the dry tests and 5 MPa per hour for the saturated tests to the σ'_{1final} values given in Table 3.1, while strain in the horizontal direction was prevented by continuously adjusting the lateral stress. The effective vertical stress was calculated from the measurements of the effective confining pressure and the deviator load applied by piston through the top of the cell and measured by the internal load cell. The pressure controllers (for cell and pore pressure) and the loading press (for deviator load) were connected to a PC so that the stresses could be applied automatically. Deformations were recorded by two vertical LVDT deformation sensors and one radial LVDT deformation sensor. Considering the experimental method and accounting for false deformation, vertical deformation readings were estimated to be accurate to about $\pm$0.002 mm. The brine used to saturate the plugs consisted of 35 g dissolved NaCl per litre water. Tangent Young's modulus, E, and Poisson ratio, ν, were calculated at 30 MPa from stress and strain measurements (Table 3.1). The following relations were used to determine ν (eq. 3.1) and E (eq. 3.2) from stress and vertical strain, ϵ_1 (Turcotte and Schubert, 1982):

$$\nu = \frac{\sigma'_3}{\sigma'_1 + \sigma'_3}; \tag{3.1}$$

$$E = \frac{\sigma'_1 \cdot (1+\nu) \cdot (1-2\nu)}{(1-\nu) \cdot \epsilon_1}. \tag{3.2}$$

3.3.2 Acoustic velocity measurement

Compressional and shear wave velocities were measured throughout the tests at regular time intervals using the pulse transmission technique (*Birch*, 1960). P- and S-wave piezoelectric transducers were mounted inside the base and top plates of the triaxial cell to measure P- and S-wave velocities along the plug axis. Resonant frequency of the crystals was, according to the manufacturer, 500 kHz. Compressional and shear wave velocities measured are between 3640

- 5660 and 1840 - 3530 m/s, respectively. Although the resonant frequency of the glued crystal may deviate somewhat from the one of the pure crystal, the wavelength of the ultrasonic pulse is assumed to range from 3.7 to 11.3 mm, which is less than the plugs radius. This arrangement is assumed to be sufficient to avoid diffraction phenomena and unwanted shape mode. The signals were recorded on a computer, and first arrival times picked manually. At low stresses, S-wave first arrivals are difficult to pick, but the clarity of the signal improves as effective vertical stress increases. Correction for equipment was applied to the P- and S-wave velocities. First arrival times, t_0, were measured with no sample in between the base and top plates. This zero time was then subtracted from the picked traveltime, t_s, measured with a plug present. The plug's compressional or shear wave velocity was then calculated as: $V_{p/s} = h_s/(t_s - t_0)$, where h_s is the height of the sample. Bulk and shear modulus were calculated at 30 MPa from V_p and V_s measurements.

3.4 Results

3.4.1 Stress - strain relationship

From the stress - strain curves (Fig. 3.4) most of the deformation is interpreted to be linear elastic. The saturated tests show greater compressibility than the dry tests (Figs. 3.4 and 3.5). At σ_1' = 50 MPa, the vertical strain, ϵ_1, is less than 0.22 % for the dry tests, while ϵ_1 is greater than 0.22 % for the saturated tests (Figs. 3.4a, b). The critical strength, i.e., the stress value where failure or gradual yielding starts, of the plugs was reached for two samples during the dry tests and three samples during the saturated tests (Fig. 3.4c, d). For plug 1.2, at vertical effective stress greater than 35 MPa, the stress - strain relation is non-linear possibly indicating start of strain hardening. These five samples exhibiting the onset of failure or gradual yielding all have high porosity relative to the other samples (Fig. 3.5), suggesting that rock strength may be related to the degree of cementation. Compressibility, $\beta = \Delta\epsilon/\Delta\sigma_1'$, was calculated for dry and wet experiments. Compressibility of the dry plugs, β_{dry}, is 1.30 - 4.42 $\cdot$ 10^{-11} Pa^{-1} and compressibility of the saturated plugs, β_{sat}, is 3.57 - 18.8 $\cdot$ 10^{-11} Pa^{-1} (Fig. 3.5). Compressibility correlates with porosity in both groups. Comparison with published data for dry compressibility of carbonates (Bell, 1981; Baud et al., 2000; Vajdova et al., 2004) shows that present samples are less compressible for a given porosity (Fig. 3.5). The non-linear part of the stress - strain curves at low stresses is inferred to be due to closure of cracks (Baud et al., 2000).

Young's moduli are between 5 and 40 GPa and Poisson's ratios are in the range 0.2 - 0.33

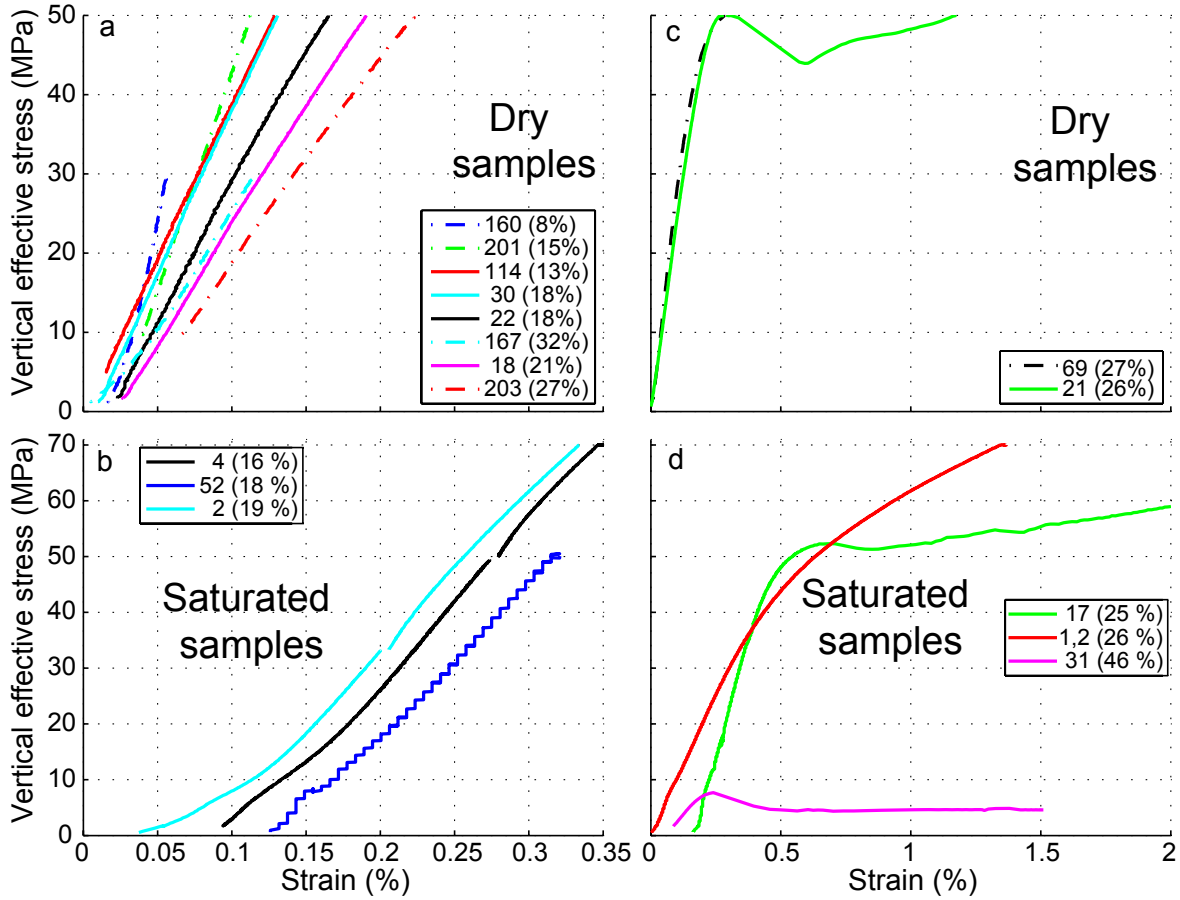

Figure 3.4: Effective stress versus strain. Line pattern indicates mineralogy, dashed lines = dolostone and solid lines = Limestone. Sample porosity is shown in parentheses.

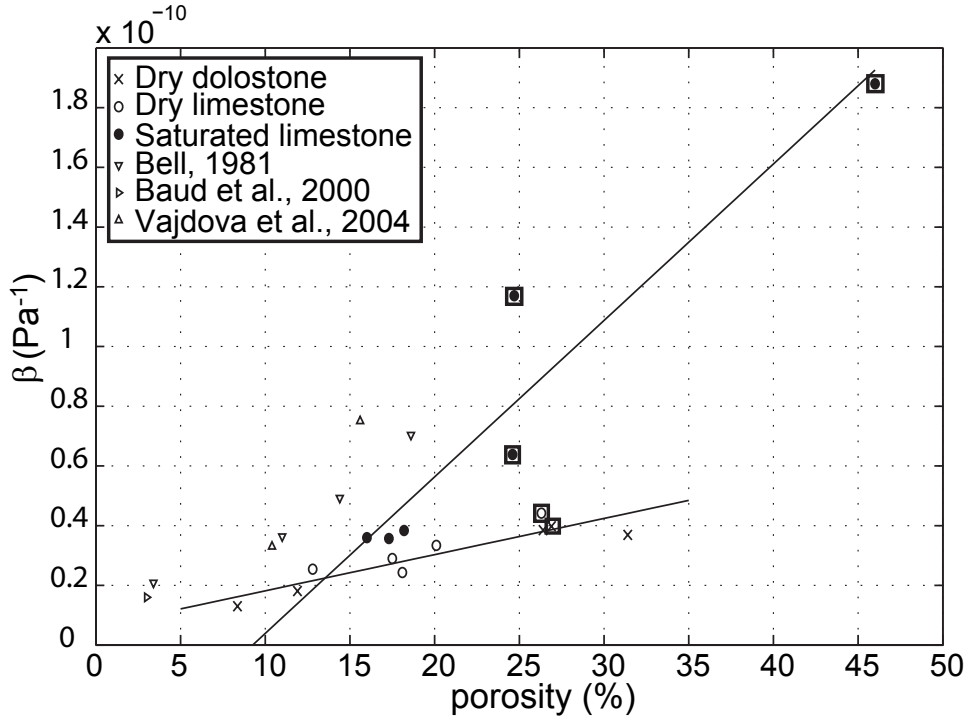

Figure 3.5: Compressibility versus porosity, comparing present results with published data. Samples that reached their yield strength are enclosed in black square. The lines correspond to best linear fit for dry and wet samples.

(Fig. 3.6 and Table 3.1). The studied samples display a more or less linear relation between horizontal and vertical effective stresses. This implies that Poisson's ratio remains almost constant during the tests, showing only minor decrease with increasing stress (Fig. 3.6). A dramatic decrease of E with increasing stress is observed for sample 21, 69, 17, 1.2 and 31, this is interpreted as the beginning of brittle deformations.

Both for dry and saturated samples, Young's modulus decreases with increasing porosity (Fig. 3.6). Dry limestones of the present study have lower Young's moduli than found in those studied by Palchik and Hatzor (2002), this is especially noticeable at low porosities (Fig. 3.6). Calculations by the modified Mori - Tanaka's relationship (Luo and Weng, 1987), using elastic constants of calcite (Bhimasenachar, 1945) and dolomite (Nur and Simmons, 1969), give higher values of both Young's modulus and Poisson ratio than the experimental data (Fig. 3.6). Lack of correlation between E or ν and porosity most likely indicates that others factors, such as pore shape and texture, play an important role in determining the mechanical strength of carbonates.

Creep was observed in the five samples in which the critical strength was reached (Fig. 5.8), whereas no creep occurred in the plugs that did not reach their critical strength. Failure was, most likely, followed by crack propagation and volume reduction, which could also be an effective means of mechanical compaction.

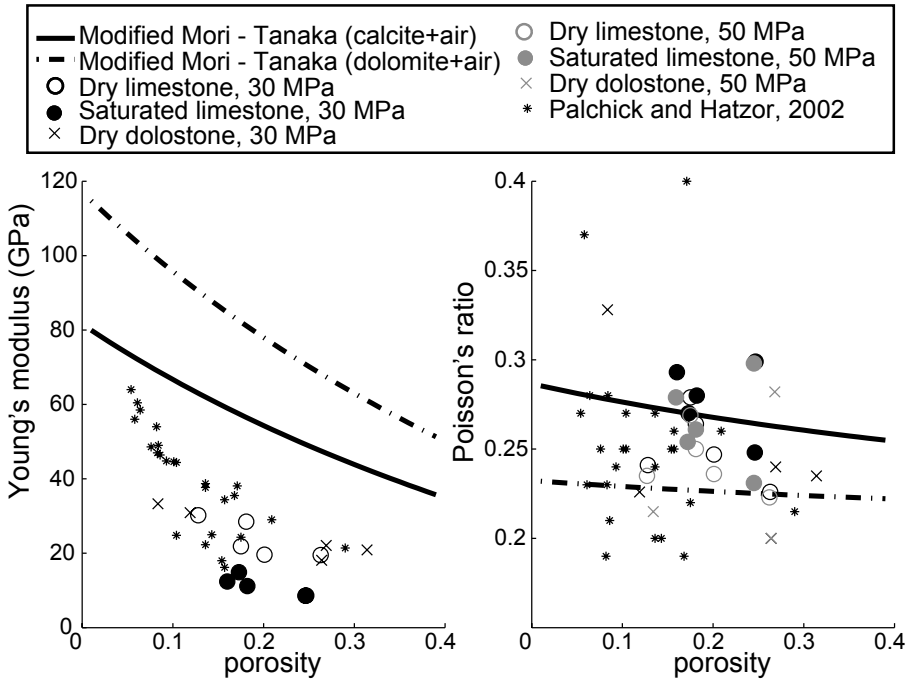

Figure 3.6: Young modulus and Poisson's ratio at σ_1' of 30 and 50 MPa versus porosity. Present results are compared with data of Palchik and Hatzor (2002) and values calculated by the modified Mori - Tanaka's method (Luo and Weng, 1987).

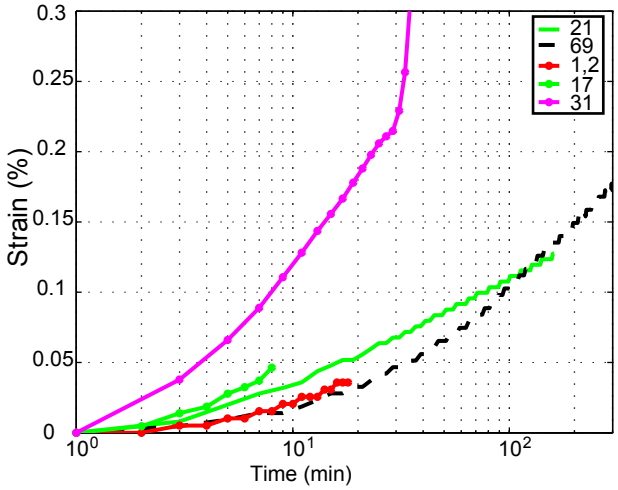

Figure 3.7: Creep at constant stress of plugs 69 and 21 at 50 MPa, plugs 1.2 and 17 at 70 MPa and plug 31 at 4.6 MPa.

3.4.2 Acoustic velocities

P and S wave velocities show little increase with stress, which should be expected since strain values are small (Fig. 3.8). Compressional velocities increase slightly at low stress, but become approximately constant above σ_1' = 10 MPa, this is more pronounced for low velocity samples (Fig. 3.8). The velocity increase is in agreement with the non linearity of the stress - strain curves at low stresses which may be related to the closure of cracks (Fortin et al., 2007). At similar porosities, higher compressional velocities are observed in saturated than in dry conditions (Fig. 3.8), in agreement with previous studies (Winkler and Nur, 1979; Yale, 1985; Tao et al., 1995; Adam et al., 2006).

Wide ranges of V_p and V_s values are observed in the present samples, with the lowest velocities occurring in the samples showing greatest strains (Figs. 3.4, 3.8). The high variability of V_p and V_s within a narrow depth range is similar to the variability observed in samples from the Great Bahama Bank (Anselmetti and Eberli, 2001). The samples with the lowest porosity have as expected (Verwer et al., 2008) the highest V_p (Fig. 3.10). Scatter in the V_p values might be due to variations in types of cement (*Eberli et al.*, 2003), and pore geometry (Tao et al., 1995; *Dürrast and Siegesmund*, 1999; Sayers, 2008; Verwer et al., 2008). V_p to V_s ratio is constant during tests and tends to be higher in the saturated plugs. V_p/V_s is 1.39-1.87 for dry samples and 1.80-1.95 for saturated samples (Fig. 3.9).

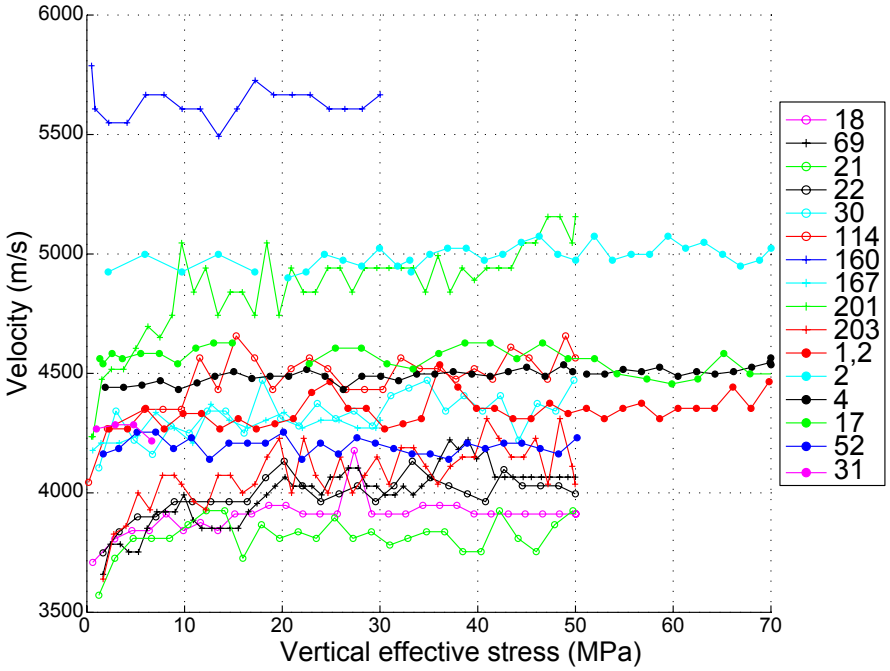

Figure 3.8: P-wave velocity versus vertical effective stress for all samples.

Bulk and shear modulus calculated from V_p and V_s measurements are plotted together with

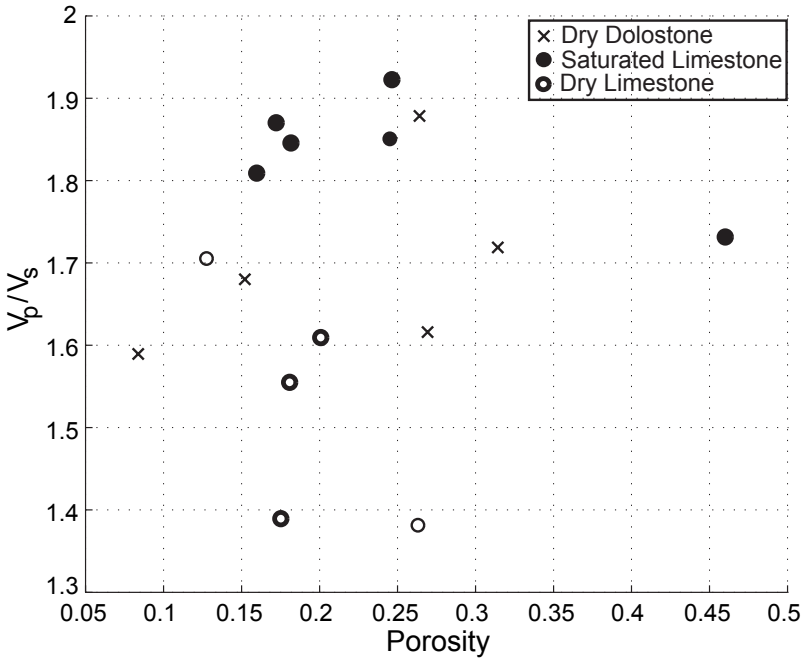

Figure 3.9: Vp to Vs ratio versus porosity. Vp to Vs ratios were calculated with mean values of Vp and Vs at vertical stress greater than 20 MPa. Plug 31 (Φ=46%) reached its critical strength at 7 MPa, therefore for this plug Vp to Vs ratio was calculated from values at vertical stress below 7 MPa.

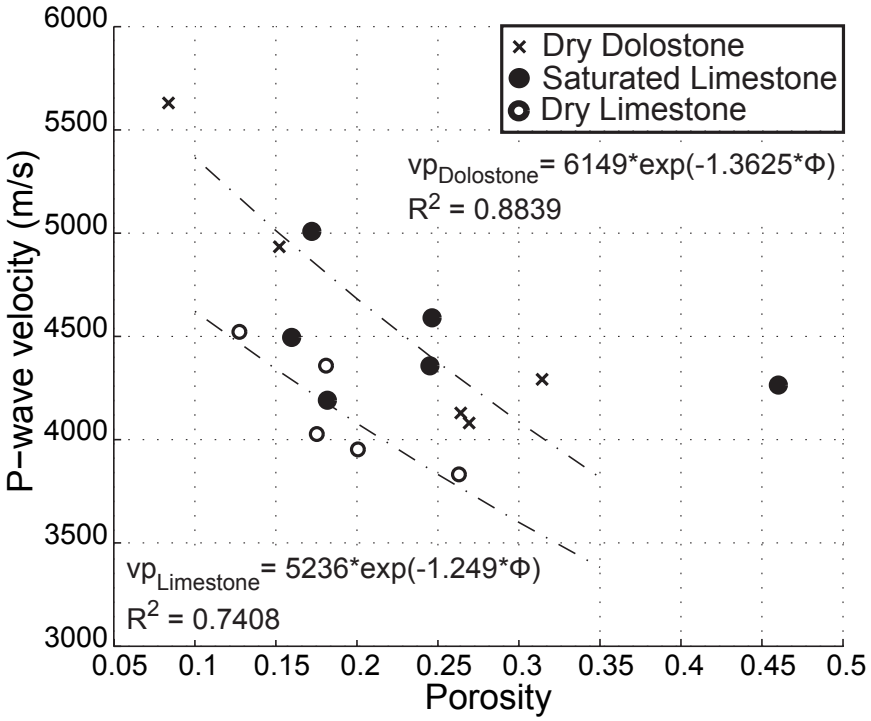

Figure 3.10: Vp at 30 MPa versus porosity. Best fits for limestone and dolostone are displayed, no good fit was found for saturated samples.

Hashin - Shtrikman bounds in Fig. 3.11. Bulk modulus data are well predicted by theory. Two limestones samples and one dolostone sample have higher shear modulus than the Hashin - Shtrikman upper bound (Fig. 3.11). Dolostones have slightly higher bulk modulus, while shear modulus does not seem to be influenced by mineralogy. The saturated tests have overall lower shear modulus than the dry tests, but there are too few data to be certain (Fig. 3.11). Such an effect is not predicted by *Gassmann* (1951), but has been noted in previous carbonate studies (Baechle et al., 2005; *Vanorio et al.*, 2008).

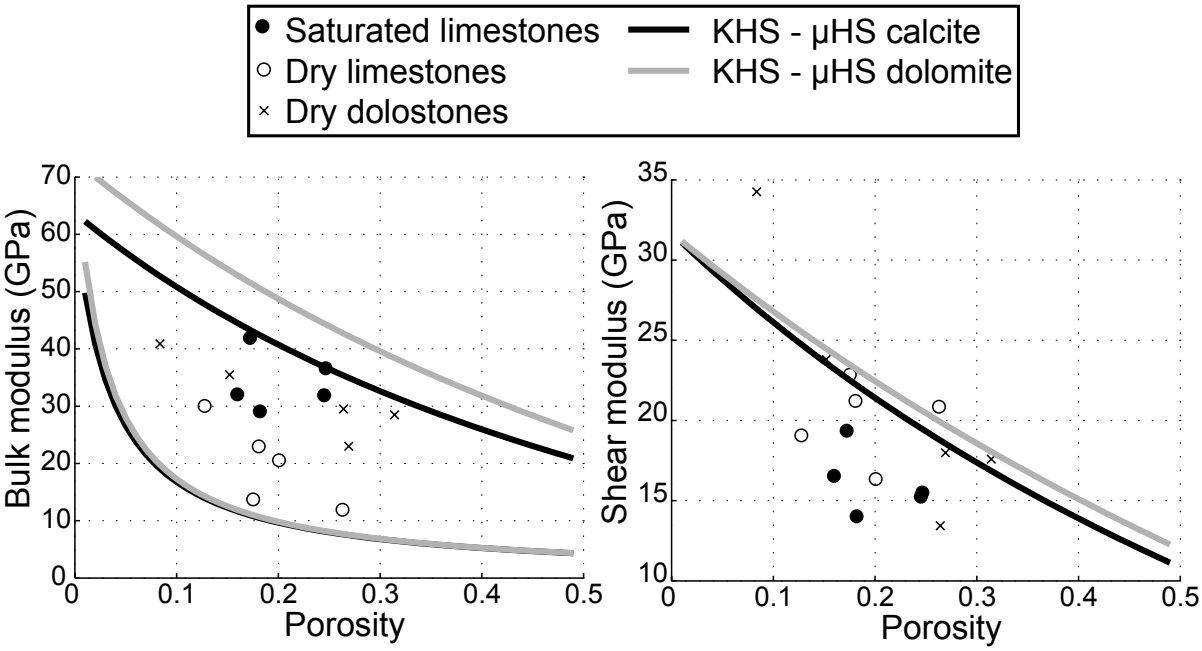

Figure 3.11: Shear and bulk modulus at 30 MPa, calculated from V_p and V_s values, versus porosity. Hashin - Shtrikman upper and lower bounds for bulk, KHS, and shear, μHS, modulus were calculated for calcite and dolomite, the pores being filled by air.

3.4.3 Relationship between microstructures and physical properties

Two features common to all the limestone samples are dominance of bioclasts and cementation by low-Mg calcite (plug 52, 18 Fig. 3.12). Dolostone samples were also constituted mainly of bioclasts, but have been replaced and cemented by dolomite.

Of the five plugs that reached their critical strength, samples 21 and 31 have pore diameters larger than encountered in most other tested plugs (see Table 3.2). The observation of *Chuhan et al.* (2003) that coarse-grained sediments are more compressible than fine grained sediments may explain the greater compaction shown by sample 1.2 which contains larger grains than other samples (Fig. 3.12). Sample 69 is cemented by micro-crystals of dolomite that have precipitated homogeneously inside the matrix, creating pores with a wide range of shapes and

providing many sites for cracks nucleation and propagation. Sample 17 contains abundant microporosity, in addition to larger pores, and inter-granular and intra-granular microcracks. Coalescence of microcracks after compression tests was observed in samples 1.2 and 17 (Fig. 3.12).

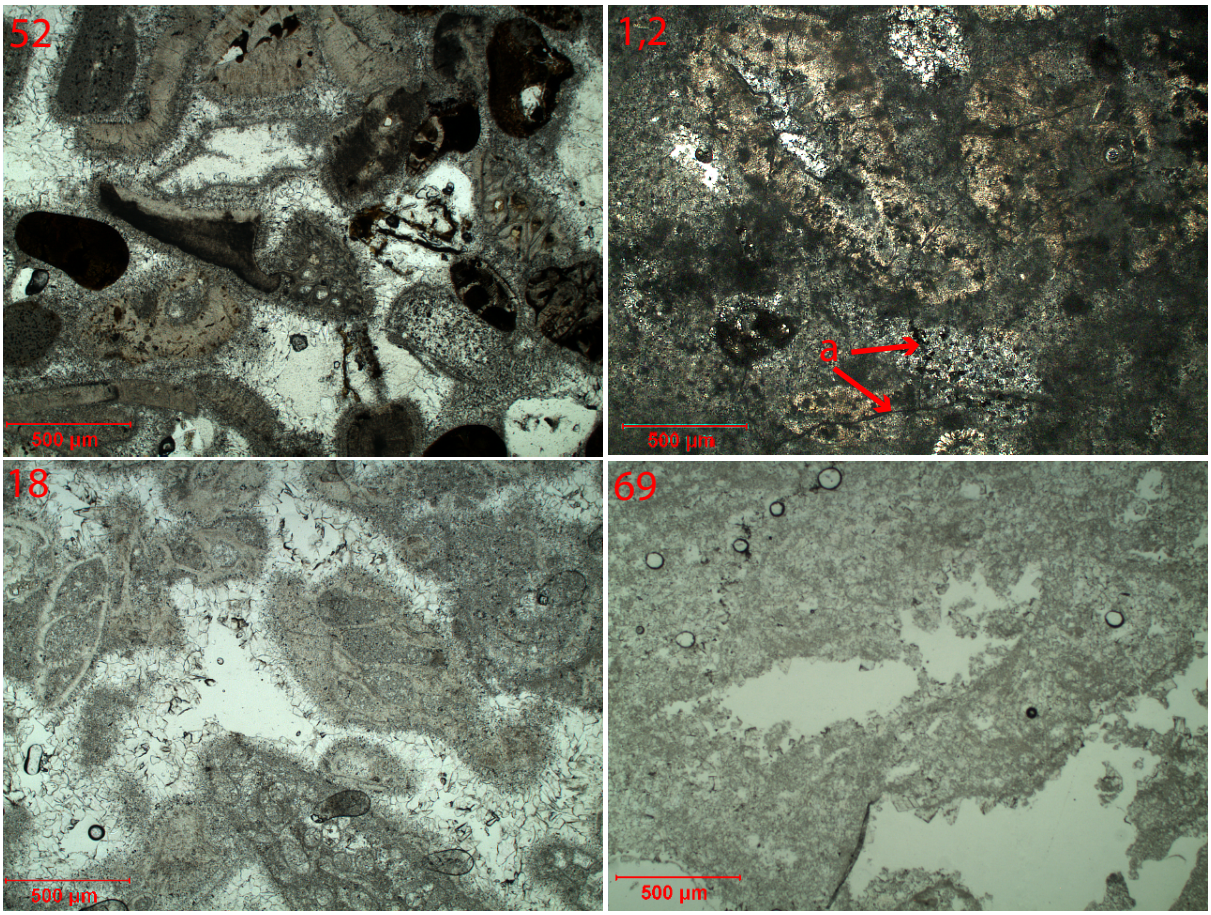

Figure 3.12: Thin sections of samples 52, 1.2, 18 and 69 before triaxial test showing the heterogeneity of the grains size and pore shapes. Samples 52 and 18 did not break, because sparitic cement reinforced the pores, forming vault like structures that could sustain the stress. Samples 1.2 (a: cracks propagation) and 69 (no cement did reinforce the pores) did show a brittle behavior at 50 MPa.

The aspect ratio of pores (long axis divided by short axis) was measured on thin section photographs (Table 3.2). The data show that brittle behaviour is associated with higher values of pore aspect ratio for given porosity (Fig. 3.13). At comparable porosity, larger pores (Table 3.2) are associated with increased likelihood of failure. This can perhaps be explained by assuming that smaller pore sizes result from higher cement contents and consequent increase in rock strength.

Plug 4 and 52 have lower velocity than the other water saturated samples (Fig. 3.10). Plug 4 has a high pore aspect ratio (Table 3.2), which may explain its low compressional velocity (Baechle et al., 2005; Adam et al., 2006; *Vanorio et al.*, 2008). However this explanation is not

Table 3.2: Mean values of the pore size and aspect ratio, and their dispersion.

Plug	N[a]	mean((a+b)/2)[b]	var((a+b)/2)[c]	mean(AR)[d]	var(AR)[c]
18	40	0.25	0.053	2.7	2.2
69	54	0.19	0.171	2.6	1.2
21	40	0.35	0.100	3.5	6.2
22	32	0.16	0.012	2.1	0.6
30	40	0.32	0.109	2.2	1.2
114	47	0.08	0.003	2.5	7.7
160	41	0.24	0.083	1.9	0.3
167	57	0.24	0.020	2.0	0.8
201	45	0.22	0.025	1.9	1.2
203	49	0.29	0.028	2.1	0.6
1.2	18	0.21	0.012	2.2	1.4
2	35	0.36	0.139	2.6	1.6
4	28	0.22	0.016	2.8	2.7
17	38	0.16	0.013	2.5	2
52	39	0.18	0.012	2.1	1.7
31	35	0.57	0.171	2.4	1.2

[a] N = number of pores measured
[b] a = long axis of the pores (mm), b = small axis of the pores (mm)
[c] var = variance
[d] AR = Pore aspect ratio, AR = a/b

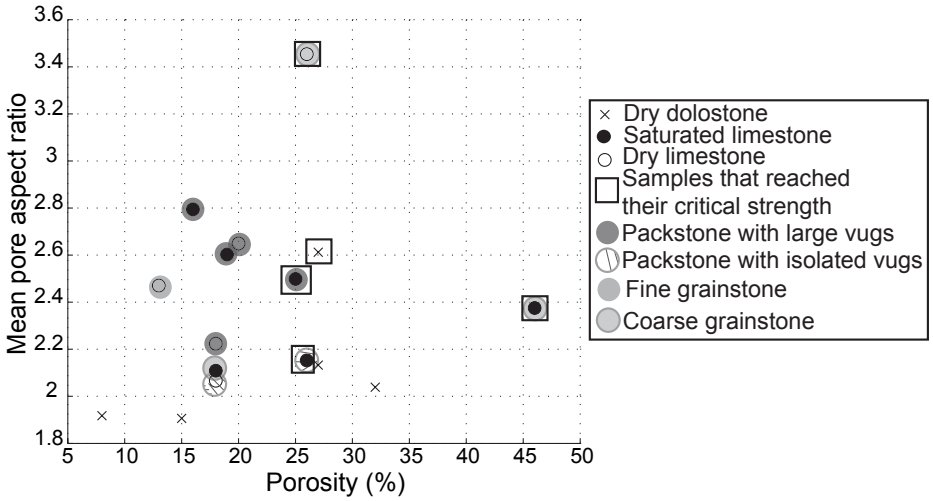

Figure 3.13: Mean pore aspect ratio versus initial porosity.

valid for plug 52. Therefore, in the present study, the scatter in acoustic velocity is not explained by changes in pore size and shape only.

3.5 Discussion

Eleven of the sixteen plug tested displayed a linear stress - strain relationship. Among those plugs, little mechanical compaction was obtained during K_0 triaxial tests at vertical effective stress up to 70 MPa (Fig. 3.4). These Marion Plateau carbonates are less compressible than carbonates with lower porosity tested in other studies. Triaxial tests on dry Solnhofen, Indiana and Tavel limestones with porosities ranging from 3 to 13 %, showed strains ranging from 0.19 to 0.46 % at confining pressure of 50 MPa (Vajdova et al., 2004). Dry tests on the Marion Plateau plugs show maximum strain at σ_1' = 50 MPa of 0.22 % while on average they are more porous than the carbonates studied by Vajdova et al. (2004) (Fig. 3.4). The lower compressibility of the Marion Plateau samples than other cemented limestones (Bell, 1981; Baud et al., 2000; Vajdova et al., 2004) is tentatively attributed to greater cementation of the former. The present study suggests that cementation has made the Marion Plateau carbonates stronger than would be expected from their porosity and depth values, resulting in only minor porosity reduction in response to the stresses applied. Although the above comparisons concern specifically limestones, the Marion Plateau dry dolostones do not display different stress - strain relationship than the dry limestones. The formation of a stable framework built during early diagenesis, makes these samples stronger than expected from porosity and depth values. Increasing applied stress on these samples produced little porosity reduction, therefore for these type of rocks mechanical compaction is not the main process of porosity reduction with burial.

The hypothesis of strength correlating with amount and, possibly, types of cementation can be tested by measuring the samples by modal analysis, i.e., point counting, of thin sections. These data are not part of the existing dataset, but are planned to be acquired, now that the probable role of cementation has been identified.

During K_0 tests, the plugs walls are prevented from collapsing by the regulation of the lateral stress. This is also prevented in sedimentary basins due to lateral stresses exerted by surrounding sediments. Nevertheless, five of the sixteen plugs reached their critical strength during testing (Fig. 3.4). For the saturated samples, the three limestones out of six that reached their critical strength, all have porosities greater than 20%. Among the saturated samples, three different textures are represented, one of each reached its critical strength. For the dry tests, two out of ten plugs failed, both having porosity greater than 20 %, although three other samples with porosity greater than 20 % did not fail. One common feature of the two dry samples

that reached their yield strength is the combination of high pore aspect ratio and high porosity (Fig. 3.13, Table 3.2). Failure seems to be most likely occurring in coarse grained samples than in fine grained ones, although this is not true in all cases. Different factors may decide on competence versus failure of these samples, but the present study clearly shows that high porosity is favourable to failure, as no failure occurred in samples with porosity less than 20 % (Fig. 3.5).

Only the data for limestones can be compared between dry and saturated states because the dolomite were only tested dry. The saturated limestones show much greater increase in compressibility at higher porosities than dry samples, such that $\beta_{sat} - \beta_{dry}$ increases with porosity (Fig. 3.5). However, the compressibility - porosity correlation is much stronger for the dry samples. As expected from the compressibility results, the saturated limestones have lower elastic moduli than the dry limestones (Fig. 3.6). Another effect of saturation is that shear moduli values are lower and bulk moduli tend to be higher in saturated samples (Fig. 3.11). The dry limestone and dolostone data define two parallel velocity - porosity trends (Fig. 3.10), whereas no trend is apparent for the saturated samples. Higher V_p to V_s ratios are also found in saturated limestones (Fig. 3.9).

Young's modulus tends to decrease with increasing porosity as predicted by theory (Fig. 3.6), even though the predicted values are higher than the measured values. Young's modulus values obtained during this study are in agreement with values obtained on limestones by Palchik and Hatzor (2002). As expected from the compressibility results, the saturated samples have lower elastic moduli than the dry samples (Fig. 3.6). Porosity is probably the main factor controlling compressibility and elasticity, but poor correlations between porosity and these mechanical properties indicates that other factors are also important. For the dry samples, bulk and shear moduli are higher in dolostones than in limestones at equivalent porosity values (Fig. 3.11, table 3.1).

V_p ranges from 3640 to 5660 m/s and V_s from 1840 to 3530 m/s for the plugs of this study. Compressional velocities are lower than most published data for which $V_{pLimestone}$ ranges from 6200 to 6500 m/s, and $V_{pDolostone}$ from 6900 to 7400 m/s (Mavko et al., 1998). Dolostone and limestone do not display different stress - strain relationship (Fig. 3.5), but dolostone samples do have significantly higher ultrasonic velocity (Fig. 3.10). As noted above, the dry limestone and dolostone data define two parallel velocity - porosity trends (Fig. 3.10). The velocities values of this study are similar to those measured on samples of equivalent porosity and depth from the Great Bahamas Bank (Anselmetti and Eberli, 2001). The results of this study confirm a strong correlation of P-wave velocity with total porosity under dry conditions and variably higher velocities for given porosity in limestones under saturated conditions (Fig. 3.10). The

minimal scatter in the dry data suggests that these samples may share basic similarities in pore geometry and matrix connectivity, as these factors are known to introduce scatter in velocity - porosity data (Anselmetti and Eberli, 2001). The considerably greater scatter in the saturated data in Figure 3.10 can be better examined when petrographic analyses become available.

Vertical stress of 50 MPa is equivalent to approximately 4-5 km burial depth under hydrostatic fluid pressure. The K_0 tests thus simulate the potential natural burial of the Marion Plateau platforms to depths corresponding to the Earth's deeper petroleum reservoirs. The present experimental results indicate that increasing burial of the Marion Plateau carbonates can therefore be expected to result in two different types of behaviour:

1. The more strongly cemented samples will experience elastic deformation and little porosity loss by mechanical compaction (Fig. 3.4a,b).

2. The less cemented or more porous samples will fail by crack propagation (Fig. 5.8), breaking grain-to-grain contacts and allowing further porosity loss by mechanical compaction.

For the majority of the samples, the observation of very little compaction at stresses up to 50 MPa, indicates that almost no porosity reduction would occur by mechanical compaction if these rocks were buried at 4 to 5 km depth. Average porosity of the set of samples is about 20 % and very little porosity loss is obtained during testing. It is unlikely that this amount of porosity would be preserved at 4-5 km burial depth. For example, Ehrenberg and Nadeau (2005) show that average porosity of carbonate petroleum reservoirs world-wide is around 8 % at 4-5 km depth. We may therefore conclude that the porosity reduction in such strata occurs mainly by chemical processes as depth increases with burial. This implies that the rate of porosity loss is a function of dissolution and precipitation processes and is unrelated to mechanical compaction. For the subordinate population of weak samples with porosity greater than 20%, failure by crack propagation will cause local porosity loss.

The stratigraphic distribution of porosity in the two Marion Platform profiles, together with the tested sample locations, provides an indication of the locations prone to mechanical failure. As the failed samples are all from depths of less than 80 meters below sea floor, it can be speculated that these weak intervals might become more strongly cemented and thus resistant to failure before burial deeper than a few hundred metres. In such case, the conclusions derived from the non-failed samples may apply to the entire section of each platform.

3.6 Conclusions

- In this study, total porosity and early cementation are identified as fundamental controls on carbonate rock strength and compressibility, as well as on other parameters like elastic Moduli.
- Early cementation of bioclastic carbonate sediments has produced a stable cemented framework with a high degree of over-consolidation and low compressibility.
- The effect of water saturation was observed in both the weakening of the mechanical strength and greater scatter in the correlation of P-wave velocity versus porosity.
- Variation in mineralogy does not influence the compressibility of the plugs strongly, but acoustic velocities of dolostones are systematically higher than in limestones.
- Most of the present carbonate sediments were already so strongly cemented at 30 - 400 meters that further porosity loss during burial to to 4 - 5 km depth must occur mainly by chemical rather than mechanical processes. The more porous samples, however, would respond to increased burial by failure due to crack propagation.

Acknowledgements

Samples used were provided by the Ocean Drilling Program, which is sponsored by the U.S. National Science Foundation and participating countries under management of Joint Oceanographic Institutions, Inc. The authors would like to thank Toralv Berre, Trude Ørbech and Sven Vangbæk from the Norwegian Geotechnical Institute for their help in the laboratory and helpful comments on an earlier version of this manuscript. The two anonymous reviewers are also thanked for their constructive comments.

Bibliography

Adam, L., Batzle, M., Brevik, I., 2006. Gassmann's fluid substitution and shear modulus variability in carbonates at laboratory seismic and ultrasonic frequencies. Geophysics 71 (6), F173–F183.

Anselmetti, F. S., Eberli, G. P., 1993. Controls on sonic velocity in carbonates. Pure and Applied Geophysics 141 (2-4), 287–323.

Anselmetti, F. S., Eberli, G. P., 2001. Sonic velocity in carbonates - a combined product of depositional lithology and diagenetic alterations. In: Ginsburg, R. (Ed.), Subsurface geology of a prograding carbonate platform margin, Great Bahama Bank: results of the Bahamas Drilling Project. SEPM special publication 70, pp. 193 – 216.

Baechle, G. T., Weger, R. J., Eberli, G. P., Massaferro, J. L., Sun, Y.-F., 2005. Changes of shear moduli in carbonate rocks: Implications for gassmann applicability. The Leading Edge 24 (5), 507–510.

Bassinot, F., Marsters, J., Mayer, L., Wilkens, R., 1993. Variations of porosity in calcareous sediments from the ontong java plateau. In: Kroenke, L. W., Berger, W. H., Janecek, T. R., et al. (Eds.), Proc. ODP, Sci. Results. Vol. 130. College Station, TX (Ocean Drilling Program), pp. 653 – 661, doi:10.2973/odp.proc.sr.130.058.1993.

Baud, P., Schubnel, A., Wong, T. f., 2000. Dilatancy, compaction, and failure mode in solnhofen limestone. Journal of Geophysical Research, B, Solid Earth and Planets 105 (8), 19,289–19,303.

Bell, F. G., 1981. A survey of the physical properties of some carbonate rocks. Bulletin of Engineering Geology and the Environment 24 (1), 105 – 110, doi - 10.1007/BF02595261.

Bhimasenachar, J., 1945. Elastic constants of calcite and sodium nitrate. Proc. Indian Acad. Sci. Sect. A.

Birch, F., 1960. The velocity of compressional waves in rocks to 10 kilobars, part 1. Journal of Geophysical Research 65 (4), 1083–1102.

Bjørlykke, K., Høeg, K., 1997. Effects of burial diagenesis on stresses, compaction and fluid flow in sedimentary basins. Marine and Petroleum Geology 14 (3), 267–276.

Brown, A., 1997. Porosity variation in carbonates as a function of depth: Mississippian madison group, williston basin. In: Kupecz, J., Gluyas, J., Bloch, S. (Eds.), Reservoir quality prediction in sandstones and carbonates: AAPG Memoir. Vol. 69. pp. 29 – 46.

Chuhan, F. A., Kjeldstad, A., Bjørlykke, K., Høeg, K., 2003. Experimental compression of loose sands; relevance to porosity reduction during burial in sedimentary basins. Canadian Geotechnical Journal = Revue Canadienne de Geotechnique 40 (5), 995–1011.

Dürrast, H., Siegesmund, S., 1999. Correlation between rock fabrics and physical properties of carbonate reservoir rocks. International Journal of Earth Sciences 88 (3), 392–408.

Eberli, G. P., Baechle, G. T., Anselmetti, F. S., Incze, M. L., 2003. Factors controlling elastic properties in carbonate sediments and rocks. The Leading Edge 22 (7), 654–660.

Ehrenberg, S. N., 2007. Whole core versus plugs: scale dependence of porosity and permeability measurements in platform carbonates. AAPG Bulletin 91 (6), 835–846.

Ehrenberg, S. N., Eberli, G. P., Baechle, G. T., 2006a. Porosity-permeability relationships in miocene carbonate platforms and slopes seaward of the great barrier reef, australia (odp leg 194, marion plateau). Sedimentology 53 (6), 1289–1318.

Ehrenberg, S. N., Eberli, G. P., Bracco, G. G. L., 2003. Data report: porosity and permeability of miocene carbonate platforms on the marion plateau, odp leg 194. In: Anselmetti Flavio, S., Isern Alexandra, R., Blum, P., et al. (Eds.), Proc. ODP, Sci. Results, 194. Texas A&M University, Ocean Drilling Program. College Station, TX, United States, pp. 1–217, doi:10.2973/odp.proc.sr.194.007.2004.

Ehrenberg, S. N., Eberli, G. P., Keramati, M., Moallemi, S. A., 2006b. Porosity-permeability relationships in interlayered limestone-dolostone reservoirs. AAPG Bulletin 90 (1), 91–114.

Ehrenberg, S. N., McArthur, J. M., Thirlwall, M. F., 2006c. Growth, demise, and dolomitization of miocene carbonate platforms on the marion plateau, offshore ne australia. Journal of Sedimentary Research 76 (1), 91–116.

Ehrenberg, S. N., Nadeau, P. H., 2005. Sandstone vs. carbonate petroleum reservoirs; a global perspective on porosity - depth and porosity - permeability relationships. AAPG Bulletin 89 (4), 435–445.

Enos, P., Sawatsky, L. H., 1981. Pore networks in holocene carbonate sediments. Journal of Sedimentary Petrology 51 (3), 961–985.

Fortin, J., Gueguen, Y., Schubnel, A., 2007. Effects of pore collapse and grain crushing on ultrasonic velocities and v-p/v-s. Journal of Geophysical Research-Solid Earth 112 (B8).

Friedman, G. M., 1964. Early diagenesis and lithification in carbonate sediments. Journal of Sedimentary Research 34 (4), 777–813.

Gassmann, F., 1951. Elasticity of high-porosity sandstone: Uber die elastizitat poroser medien. Vierteljahrsschr. Nat. Ges. Zurich 96, 1 – 23.

Goldhammer, R. K., 1997. Compaction and decompaction algorithms for sedimentary carbonates. Journal of Sedimentary Research 67 (1), 26–35.

Hamilton, E. L., 1976. Variations of density and porosity with depth in deep-sea sediments. Journal of Sedimentary Petrology 46 (2), 280–300.

Isern, A. R., Anselmetti, F. S., Blum, P., et al., 2002. Init. repts. 194. In: Shipboard Scientific Party Proc. ODP. College Station, TX (Ocean Drilling Program), pp. 1–116, doi:10.2973/odp.proc.ir.194.104.2002.

Kroenke, L. W., Berger, W. H., Janecek, T. R., et al., 1991. Proc. odp, init. repts., 130. Doi:10.2973/odp.proc.ir.130.1991.

Luo, H. A., Weng, G. J., 1987. On eshelby inclusion problem in a 3-phase spherically concentric solid, and a modification of mori-tanakas method. Mechanics of Materials 6 (4), 347–361.

Mavko, G., Mukerji, T., Dvorkin, J., 1998. The rock physics handbook: tools for seismic analysis in porous media. Cambridge University Press, Cambridge.

Meyers, W. J., Hill, B. E., 1983. Quantitative studies of compaction in mississippian skeletal limestones, new mexico. Journal of Sedimentary Petrology 53 (1), 231–242.

Nur, A., Simmons, G., 1969. Effect of saturation on velocity in low porosity rocks. Earth and Planetary Science Letters 7 (2), 183–193.

Palchik, V., Hatzor, Y. H., 2002. Crack damage stress as a composite function of porosity and elastic matrix stiffness in dolomites and limestones. Engineering Geology 63 (3-4), 233–245.

Paxton, S. T., Szabo, J. O., Ajdukiewicz, J. M., Klimentidis, R. E., 2002. Construction of an intergranular volume compaction curve for evaluating and predicting compaction and porosity loss in rigid-grain sandstone reservoirs. AAPG Bulletin 86 (12), 2047–2067.

Pigram, C. J., Davies, P. J., Feary, D. A., Symonds, P. A., 1992. Absolute magnitude of the second-order middle to late miocene sea-level fall, marion plateau, northeast australia. Geology (Boulder) 20 (9), 858–862.

Sayers, C. M., 2008. The elastic properties of carbonates. The Leading Edge 27 (8), 1020–1024.

Schmoker, J. W., 1984. Empirical relation between carbonate porosity and thermal maturity - an approach to regional porosity prediction. Aapg Bulletin-American Association of Petroleum Geologists 68 (11), 1697–1703.

Scholle, P. A., Halley, R. B., 1985. Burial diagenesis; out of sight, out of mind! In: Schneidermann, N., Harris Paul, M. (Eds.), Carbonate cements. Vol. 36 of Special Publication - Society of Economic Paleontologists and Mineralogists. SEPM (Society for Sedimentary Geology), Tulsa, OK, United States, pp. 309–334.

Tao, G., King, M. S., Nabibidhendi, M., 1995. Ultrasonic wave-propagation in dry and brine-saturated sandstones as a function of effective stress - laboratory measurements and modeling. Geophysical Prospecting 43 (3), 299–327.

Turcotte, D. L., Schubert, G., 1982. Geodynamics; applications of continuum physics to geological problems. John Wiley & Sons, New York, NY, United States.

Vajdova, V., Baud, P., Wong, T. f., 2004. Compaction, dilatancy, and failure in porous carbonate rocks. Journal of Geophysical Research, B, Solid Earth and Planets 109, B05204.

Vanorio, T., Scotellaro, C., Mavko, G., 2008. The effect of chemical and physical processes on the acoustic properties of carbonate rocks. The Leading Edge 27 (8), 1040–1048.

Verwer, K., Braaksma, H., Kenter, J. A. M., 2008. Acoustic properties of carbonates: Effects of rock texture and implications for fluid substitution. Geophysics 73 (2), B51–B65.

Wallace, M. W., Holdgate, G. R., Daniels, J., Gallagher, S. J., Smith, A., 2002. Sonic velocity, submarine canyons, and burial diagenesis in oligocene-holocene cool-water carbonates, gippsland basin, southeast australia. AAPG Bulletin 86 (9), 1593–1607.

Winkler, K., Nur, A., 1979. Pore fluids and seismic attenuation in rocks. Geophysical Research Letters 6 (1), 1–4.

Yale, D. P., 1985. Recent advances in rock physics. Geophysics 50 (12), 2480–2491.

Paper 2: Calcite dissolution under stress: Evolution of grain contact microstructure during pressure solution creep

Journal of Geophysical Research – Solid Earth (in press)

Experimental calcite dissolution under stress: Evolution of grain contact microstructure during pressure solution creep

Delphine Croizé[a,b], François Renard[b,c],Knut Bjørlykke[a], and Dag Kristian Dysthe[c]

[a] Department of Geosciences, University of Oslo, Norway

[b] Université Joseph Fourier - Grenoble I, LGCA-CNRS-Observatoire de Grenoble, France

[c] Physics of Geological Processes (PGP), University of Oslo, Norway.

Abstract

For the first time, nanometre resolution techniques both *in situ* and *ex situ* were compared in order to study calcite dissolution under stress. The results obtained enabled identification of the relative importance of pressure solution driven by normal load and free surface dissolution driven by strain energy. It is found that pressure solution of calcite crystals at the grain scale occurred by two different mechanisms. Diffusion of the dissolved solid took place at a rough calcite/indenter interface, or through cracks that propagated from the contact toward the less stressed part of the crystal. It is also found that strain rates are mostly a function of the active process, i.e. pressure solution associated or not with cracks, rather than being influenced by stress variations. Strain rates obtained in this study are in agreement with published data of experimental calcite and carbonate dissolution under stress.

4.1 Introduction

During burial, sediments are subjected to increasing stresses and temperature with depth. Their compaction results in a porosity decrease and an increase in density. Compaction processes may be either mechanical and thus a function of the effective stress, or chemical, involving dissolution and precipitation of minerals. Pressure solution creep is a chemical deformation mechanism occurring in the presence of a reactive fluid, and is responsible for slow and irreversible compaction of sediments. Intergranular pressure solution creep is an important process of porosity loss in sedimentary basins (*Rutter*, 1983; *Tada and Siever*, 1989) or of healing of active faults during the interseismic period (*Ramsay*, 1980; *Angevine et al.*, 1982; *Gratier*, 1987; *Renard et al.*, 2000). An other possible irreversible deformation mechanism during compaction of sediments is subcritical crack growth (*Atkinson*, 1982; *Liteanu and Spiers*, 2009).

Pressure solution is driven at the micro-scale by chemical potential differences between the stressed and unstressed part of the solid which cause i) dissolution of minerals along the contact, ii) diffusion toward the pore space, and iii) precipitation on the less-stressed faces of the grains (*Sorby*, 1863; *Weyl*, 1959). The overall rate of deformation is controlled by the slowest of these three processes. Pressure solution may therefore be controlled by the kinetics of either dissolution or precipitation reactions, or by the rate of diffusion along the grain boundary. Diffusive transport along the grain contact is driven by the chemical potential gradient existing between the liquid in the contact and the one in the pore space, the rate of transport also depends on the geometry, i.e. thickness and microstructure, of the grain-to-grain contact.

Theoretical relations describing the strain rate of aggregates compacting by intergranular pressure solution include phenomenological coefficients (*Weyl*, 1959; *Lehner*, 1990). They also have different dependencies on grain size and stress according to whether the process is controlled by kinetics or by diffusion. A number of experimental studies have been carried out to determine these parameters, but few experimental data exist on calcite pressure solution creep. Recent experimental studies were carried on both fine–grained (3 to 80 μm) super-pure calcite powder compacted at 2–4 MPa effective stress (*Zhang et al.*, 2002; *Zhang and Spiers*, 2005,b) and at 30 MPa (*Liteanu and Spiers*, 2009) using an œdometer, and on calcite crystals indented by glass (*Zubtsov et al.*, 2005). Either the deformation was proposed to be controlled by diffusion (*Zhang and Spiers*, 2005; *Zubtsov et al.*, 2005) or by precipitation kinetics (*Baker et al.*, 1980; *Zhang et al.*, 2002; *Zhang and Spiers*, 2005b). The lack of consensus on the rate–limiting process of pressure solution in carbonates is related to the absence of good agreement between macroscopic strain rate laws and experimental results. A possible explanation is that present models do not take grain–size distribution or packing of aggregates accurately into account. In addition, the grain–to–grain geometry employed in the macroscopic models might not be suitable for carbonates.

Macroscopic predictive theories describing aggregate compaction by pressure solution creep should be based on spatial averaging methods using micro-scale phenomenological descriptions (*Lehner*, 1990). Therefore, to predict the strain rate at aggregate or outcrop scale, a good understanding of the three serial processes at the grain scale and of the detailed microstructure of the grain contact is required. The structure of grain-to-grain contact and its effect on the rate of pressure solution creep are still not fully understood, however. Several types of grain boundary structures are debated in the literature (*Tada and Siever*, 1986; *Gratz*, 1991; *De Meer and Spiers*, 1999; *Dysthe et al.*, 2002; *van Noort et al.*, 2008). Pressure solution might occur as a combination of plastic deformation at the grain-to-grain contact and free face dissolution at the edge of the contact (*Tada and Siever*, 1986; *Karcz et al.*, 2006). A number of studies

have assumed that water is present at the grain boundary and have discussed several geometries. For instance the grain boundary may be flat and diffusion occurs through an adsorbed thin film which can support shear stresses (*Weyl*, 1959; *Rutter*, 1983; *Yasuhara et al.*, 2003) and has a slightly smaller diffusion coefficient than a free fluid. Another type of grain contact geometry is the dynamic island and channel structure (*Raj*, 1982; *Lehner*, 1990), where stresses are transmitted through solid-solid contacts. In this model, the fluid is at hydrostatic pressure and has transport properties similar to the pore fluid. A third type of structure is a thin film, short-circuited by crack arrays (*Gratz*, 1991; *den Brok et al.*, 2002).

Another process, that is less understood, is the formation of tiny cracks that grow slowly and permanently damage the solid (*Atkinson*, 1982). The propagation of such cracks at stress intensity factor lower than the critical stress intensity factor is called subcritical crack growth or stress corrosion. The three important variables to be taken into account are the applied stress, the size of the flaw and the fracture toughness (*Anderson*, 1995; *Scholz*, 2002). Following the energy criterion theory, cracks will propagate in order to lower the total energy of the system (*Griffith*, 1920). The driving force for crack propagation is the energy release rate which corresponds to the change in potential energy with crack surface area for a linear elastic material. At equilibrium the energy release rate is proportional to the material resistance to cracking, which is also equivalent to the surface energy, therefore the material resistance to cracking is affected by the environment (*Olagnon et al.*, 2006). Due to the pre-existence of flaws in the rocks, crack propagation may occur at stresses lower than required for slip or twinning (*Atkinson*, 1982; *Olagnon et al.*, 2006), and the presence of water at the crack tip may promote weakening reactions.

Grain contact healing, or neck growth, has been showed to be a mechanism taking place in pressure solution experiments where both the indenter and the indented material were halite (*Hickman and Evans*, 1991; *Zubtsov et al.*, 2004; *van Noort et al.*, 2007), this is possibly an important mechanism for calcite as well (*Yamasaki and Weiping*, 1993). The present study aims at understanding the important connection between contact geometry and strain–rate, however. To this end an experimental set–up was designed, in which a point force is applied on a calcite crystal via a hemi-spherical lens made of either glass or sapphire, to study stress–enhanced dissolution along a single contact. A film of water saturated with respect to calcite is present at the calcite/lens interface. High stresses along the contact induce dissolution of calcite below the lens and, therefore, an increase of the contact surface area. The growth of the contact and the resulting displacement are followed during several tens of hours using optical interferometry, i.e. displacement of Newton rings. This allows the determination of the rate of calcite dissolution as a function of stress. Before and after experiments, crystal surface topography was measured

down to nanometre resolution using white light interferometry, enabling determination of the resulting microstructures. The rates measured in the present study are compared with previous studies of calcite indentation or carbonate slow deformation.

4.2 Experimental method

A single indenter set-up was specifically designed to study dissolution of calcite under stress, the method is similar to the one used by *Hickman and Evans* (1995). Firstly, Iceland spar calcite crystals were cleaved and polished to start each experiment with a flat crystallographic surface. The indented plane was normal to a cleavage and miscut with respect to the calcite rhombs. Calcite samples used were natural samples mined in South-West China and manufactured by Photox Optical System Ltd. Surface roughness was measured using white light interferometry prior to the force application. The surface area of the samples was close to 2*2 mm^2. Sample thickness varied in the range 150–680 μm. Secondly, a single contact force was applied on one point of the calcite crystal using a glass or sapphire half-ball lens provided by Edmund Optics. Half-balls with three different radii were used (Table 4.1), providing different initial contact surface areas. The calcite crystal and the half-ball lens were placed between a thin cover-glass bent over the half-ball lens and glued at both ends onto a thicker cover-glass (as shown in Figure 4.1a). The applied force was a function of the bending of the thin cover-glass, i.e. of the total height of half-ball lens and calcite crystal. Thirdly, water saturated with respect to calcite was introduced in the system, i.e. after loading. After the water injection, the progression of the water at the calcite/lens interface and the complete wetting of the contact was observed with the microscope. Because the half-ball lenses were either made of glass or sapphire, these two materials being less reactive than calcite, they are assumed to be chemically inert. After validating the experimental protocol on a dozen test experiments, a series of six experiments was performed for which the experimental conditions are to be found in Table 4.1.

The relationship between applied force and deflection of the thin cover–glass was calibrated using two different cover–glasses and four different dead weights (Figure 4.1b). Since the calcite samples in the experiments were glued onto the thin cover–glass, calcite crystals of similar size were glued on the thin cover-glasses during force calibration to ensure that the elastic parameters of the set-up were similar. For calibration, a thin cover glass was initially maintained horizontally by two stands, one on each side. A dead weight was then suspended on the cover–glass using a sewing needle. For each cover–glass and weight, the deflection due to the suspended weight was measured using an LVDT LD400-5 displacement sensor provided by Omega Engineering Inc. The resulting deflection versus force curve was then used to determine

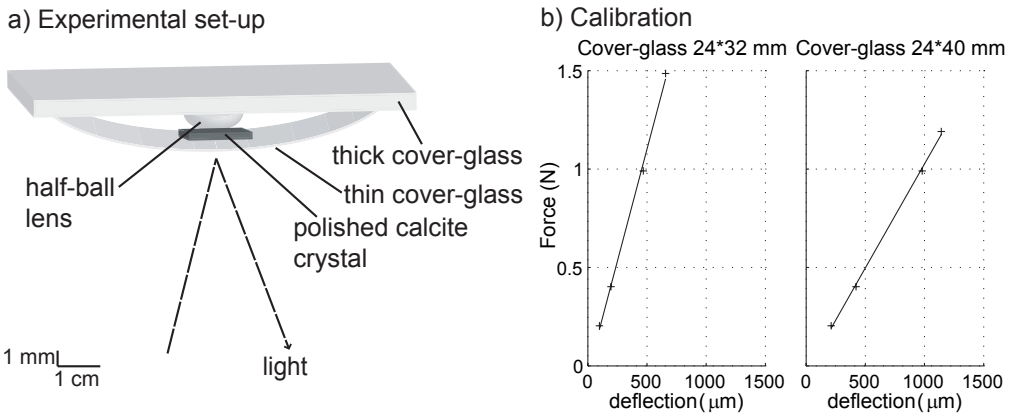

Figure 4.1: a) Experimental set-up: a flat piece of polished calcite crystal is pressed against a half-ball lens by means of a bent cover glass. b) Force calibration: deflection versus applied force relationships obtained for the two types of cover–glasses used.

the applied force, F, in each experiment (Figure 4.1b).

The calcite/lens contact was observed using an inverted reflected light microscope (Olympus GX 71). The light source was a green monochromatic LED with a specific wavelength of λ=530 nm. Light was transmitted across the loaded sample, and interference fringes formed around the contact between the calcite sample and the half-ball lens. The light rays reflected from the lens/water and water/calcite interfaces produced concentric constructive (high intensity) and destructive (low intensity) interference fringes centred on the contact (Figure 4.2). These interference fringes are called Newton rings and were produced when the distance between the two solids was of the same order of magnitude as the light wavelength (*Tolansky*, 1973). The motion of the interference fringes due to the increase of the contact was followed for several tens of hours using time-lapse photography (D100 Nikon Digital Camera). The contact surface area, A, was extracted using image processing software (ImageJ), by outlining by hand the dark centre of the picture enclosed within the first Newton ring. The applied stress was then simply calculated using $\sigma = F/A$. The picture resolution being $\lambda/4$, the actual surface area of contact might therefore be smaller than the one outlined by hand, which implies that the calculated stress values represent minimum values.

At the beginning of each experiments, water saturated with respect to calcite was introduced at the calcite/lens interface with the help of a micro-syringe. The high stress at the wetted calcite/lens interface induced a chemical potential gradient from the contact toward the non-stressed part of the fluid. The enlargement of the contact surface area resulted in a change of the set-up geometry (Figure 4.2), and the displacement of the Newton rings could then be monitored. In some experiments the water film evaporated and a new saturated water droplet was injected in the contact and the time noted. This shows that the solutions are usually super-

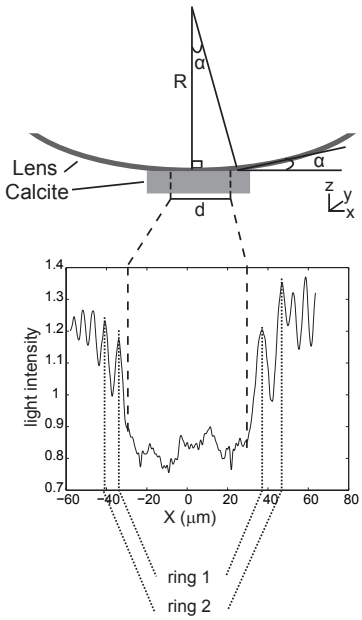

Figure 4.2: Top: Geometry of the calcite/half-ball lens interface. During experiments, a water film is present at the calcite/glass interface. R: radius of the half-ball lens used, d = contact diameter. Bottom: Light intensity (arbitrary units) along a 1D profile across the contact, showing constructive/destructive interference patterns.

saturated during experiments.

At the end of each experiment, the crystal was dried and the resulting surface topography was measured using white light interferometry (Wyko 2000 Surface Profiler from Veeco). This was done by means of a microscope with a reference arm creating interference fringes with maximum intensity at equal optical path lengths of the imaging beam and reference beam. By moving the sample vertically and simultaneously capturing an image of the interference intensity envelope, the relative height of the imaged surface at each pixel can be determined with a vertical resolution of 3 nm. The horizontal resolution depended on the lens used and was in the range 0.24 to 0.50 micrometres. A detailed topography of the indented region was obtained from these measurements. The results are displayed as a digital elevation image in which the height range is shown as a colour scale.

4.3 Data analysis

4.3.1 *In situ* measurements

Colour pictures of the contact and the Newton rings were taken at regular interval for a period of up to three days. Pictures were first split into the red, green and blue channels. Since a green light source was used, the green channel only was selected to get a better signal to noise

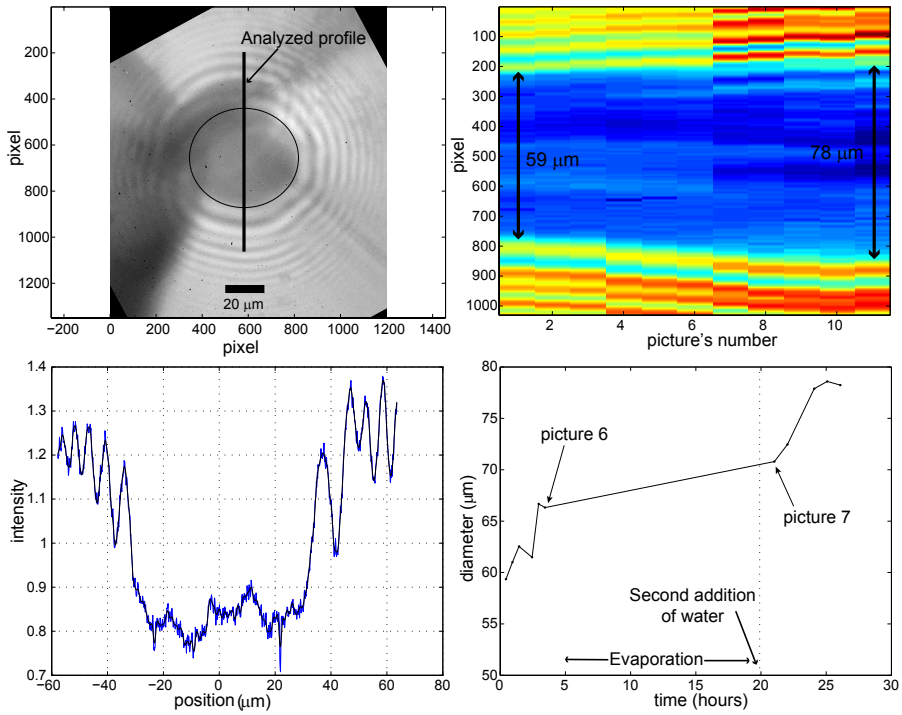

Figure 4.3: Data processing steps of the optical pictures to extract the contact diameter growth rate for experiment F01. a) green channel of the first analysed picture showing the contact surrounded by Newton rings, b) selected profile for pictures 1 to 11, c) each profile is filtered and centred on $X = 0$, d) growth of the diameter through time.

ratio. In order to optimise the data visualisation, contrast enhancement filters were also used. For each experiment, the lower and upper bounds of the recorded intensity were identified, then the same linear contrast stretch was applied on the whole set of pictures. To ensure that the Newton rings displacement was due to the contact dissolution and not to a movement of the entire crystal, a static reference point on the pictures was chosen and an image cross-correlation method was applied to the entire set of time-lapse pictures. If the cross-correlation revealed an overall displacement of the set-up, for instance due to microscope vibrations, the selected pictures were translated using the displacement vector obtained with the cross-correlation.

Figure 4.3 describes the successive data processing steps, which from the recorded pictures lead to the determination of the rate of contact surface area enlargement. A profile perpendicular to the Newton rings was chosen in each recorded picture, the profile was 10 pixels wide and stacked to suppress some noise. The selected intensity profile was smoothed using a Butterworth lowpass filter. Each profile was then centred such that the centre of the contact area was located at $X = 0$. The evolution of the diameter with time was related to the increase of the contact surface area and hence to the decrease of the applied stress, i.e. $\sigma = F/A$ with $F \approx$ constant.

The volume of dissolved calcite is equal to the volume of the half-ball lens replacing solid

calcite. To determine the volume of calcite dissolved through time, the vertical displacement of the half-ball lens was calculated at different time steps t_i. The vertical displacement occurring between t_{i-1} and t_i is expressed by $\delta_{i,n}$, with n the order of the interference fringe considered. Knowing the geometry of the set-up (Figure 4.2) and the horizontal displacement of the n^{th} Newton ring, vertical displacement is calculated as follows,

$$\delta_{i,n} = (X_{i,n} - X_{i-1,n}) \cdot \tan\left(\arcsin\left(\frac{X_{i-1,n}}{R^+}\right)\right), \tag{4.1}$$

where $X_{i,n}$ is the distance from the considered Newton ring to the centre of the contact area at t_i and R^+ the equivalent radius of the half-ball lens calculated on the assumption that the contact between the half-ball lens of radius R and the calcite crystal follows the Hertz contact theory between two elastic bodies, with $R^+ = (4Ea)/((1-\nu^2)3\pi\sigma)$ (***Fischer-Cripps***, 1999). E and ν are, respectively, the Young's modulus and Poisson's ratio of the half-ball lens, $a = ((3FR)/(4E_r))^{1/3}$ is the calculated contact radius from Hertz contact theory, with $E_r = ((1-\nu^2_{calcite})/(E_{calcite}) + (1-\nu^2_{indenter})/(E_{indenter}))^{-1}$, F being the applied force (***Johnson***, 1985). To calculate E_r, a and R^+ the following elastic constants were used: $\nu_{calcite}$ = 0.32, $E_{calcite}$ = 73 GPa, ν_{glass} = 0.25, E_{glass} = 82 GPa, $\nu_{sapphire}$ = 0.25 and $E_{sapphire}$ = 335 GPa.

From $\delta_{i,n}$ the total vertical displacement $Z_{i,n}$ at t_i is then calculated as follows:

$$Z_{i,n} = \sum_{i=1}^{j} \delta_{i,n}. \tag{4.2}$$

The largest source of error in the calculation of $\delta_{i,n}$ according to this method lies in determining the minima of the fringes, i.e. the value of X_i on the picture. This error is typically $\pm$ 3 pixels, one pixel being equivalent to 0.118 μm, it can be assumed that $\delta_{i,n}$ is accurate at $\pm$ 0.009 μm. This calculation implies the assumption that, firstly the calcite surface is flat outside the contact, secondly the calcite surface does not change outside the contact. The typical roughness over a crystal surface of 3000 μm^2 is about R_a = 50 nm both before and after experiments. Therefore the accuracy of the vertical measurements Z can be assumed to be $\pm$ 0.009 μm.

The indenter used was a half-ball lens, therefore, the volume, $V_{i,n}$, of dissolved calcite is equal to the volume of a spherical cap,

$$V_{i,n} = \pi \cdot Z^2_{i-1,n} \cdot \left(R^+ - \frac{Z_{i,n}}{3}\right). \tag{4.3}$$

The volume of dissolved calcite is then converted into a number of moles, $N = V_i * \rho/M$, where ρ = 2.7 g/cm^3 (the density of calcite) and $M = 100$ g/mol (the molecular mass of calcite). The amount of dissolved calcite was monitored as a function of time using the displacement of

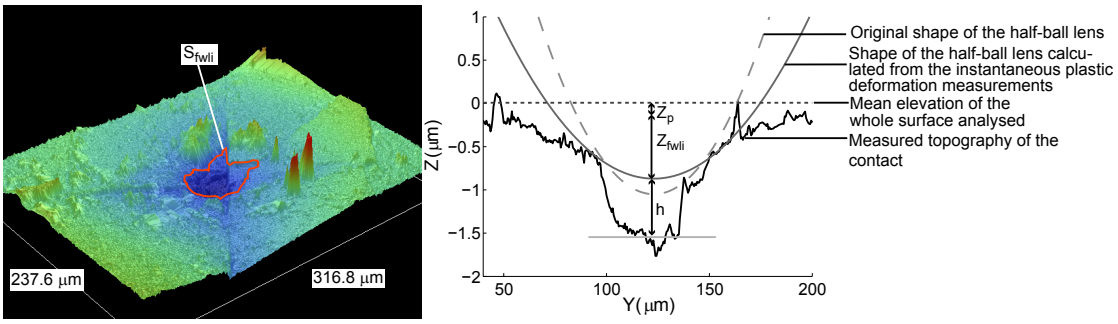

Figure 4.4: Digital elevation image where the contact surface area S_{fwli} is outlined in red. Values of Z_{fwli} and h are calculated from profiles extracted from digital elevation images.

the Newton rings. For each experiment, $\delta_{i,n}$, $Z_{i,n}$ and $V_{i,n}$ were calculated for the first two Newton rings, n = 1 and n = 2. The rate of calcite dissolution in mol/s could then be calculated as a function of time and applied stress. Strain rates, $\dot{\epsilon}$ in s^{-1}, were calculated from the increase of *in situ* vertical displacement values through time,

$$\dot{\epsilon} = \frac{\Delta Z / R_{eq}}{\Delta t} \tag{4.4}$$

$R_{eq} = \sqrt{((S_1 + S_f)/2)/\pi}$ being the equivalent contact radius, i.e. diffusion path, taken as a reference length, S_1 and S_f are the initial and final surface areas of contact, respectively. Two phases could be differentiated in the results for experiments F01, F02, F05, F06 and F07, two strain rates are therefore calculated for these experiments.

4.3.2 White light interferometry measurements

Microstructures that developed during experiments below the indenter were analysed at the end of each experiment, using digital elevation images obtained from white light interferometry. To improve the quality of the results and their interpretation, linear tilts inherent to the system and samples were removed, and pixels with no signal were interpolated. Surface areas of contact at the end of experiments, S_{fwli}, were then outlined by hand on the digital elevation image using image processing software (Figure 4.4, Table 4.1). Surface areas measured this way include only the part of the contact where enough dissolution occurred to be clearly identified, therefore stress values calculated using these surface areas would represent maximum stress. The actual applied stress therefore lies between the value calculated from the *in situ* measurements and the one calculated from the white light interferometry measurements.

Instantaneous plastic deformation occurred when the force was applied on calcite crystals. To determine the magnitude of dissolution due to pressure solution as revealed by the white light interferometry profiles, the residual imprint of the indenter after instantaneous plastic de-

formation was measured, and removed. Dry tests were performed in which a calcite sample was loaded and unloaded in the same conditions as in the experiments, i.e. similar crystals, applied forces and half-ball lenses. These tests enabled determination of the residual deformation in the crystal. The residual holes were fitted with circles of radius R_{res} (see Table 4.1). The equivalent shapes of the indenter represented on the vertical profiles obtained from white light interferometry measurements have radius R_{res}. For each half-ball lens, the depth of the residual hole resulting from plastic deformation, Z_p, was measured. The volume of the residual hole, V_p, was calculated from Z_p and R_{res}. The vertical displacement due to pressure solution creep, Z_{fwli}, was calculated as being the penetration of the equivalent sphere into the resulting hole minus the penetration depth, Z_p, due to plastic deformation (Figure 4.4).

For most of the experiments the hole created by dissolution of the calcite is deeper than the penetration of the half-ball lens; in these cases the height, h, of the hole below the indenter was measured (Figure 4.4). The total volume of the hole, V_{fwli}, from which V_p was subtracted, includes both the volume of calcite replaced by the half-ball lens and the volume of calcite dissolved below. Therefore the value of V_f which includes only the volume of calcite replaced by the half–ball lens (eq. 4.3) can not be compared to V_{fwli}. To get an idea of the three-dimensionality of the contact, two topography profiles, perpendicular to each other, were taken for each experiment. For these two profiles of the same surface, the half-ball lens was fitted so that Z_{fwli} is identical. In the case of noisy profiles an average profile was calculated including the data from the entire hole. The calculated shape of the half–ball lens was fitted onto this average profile. Therefore some points of the white light interferometry profiles can be located above the line symbolizing the half–ball lens.

The holes observed after the experiments are deeper than the penetration depth of the indenter. Two explanations are possible: this is either due to the stress application or to the dissipation of stored plastic strain energy, i.e. dislocations inducing dissolution. To determine which of these two explanations applies, wet tests were performed. Once the residual deformation due to dry indentation was measured, some crystals were left in water saturated with respect to calcite for 50 hours, without any load. At the end of the tests, some crystal reorganisation was observed but the depth and shape of the holes was the same as before the water treatment (Figure 4.5). This implies that the dissolution of calcite below the indenter and under stress is related to the applied stress, i.e. dissolution and precipitation under the effect of a stress-driven mechanism.

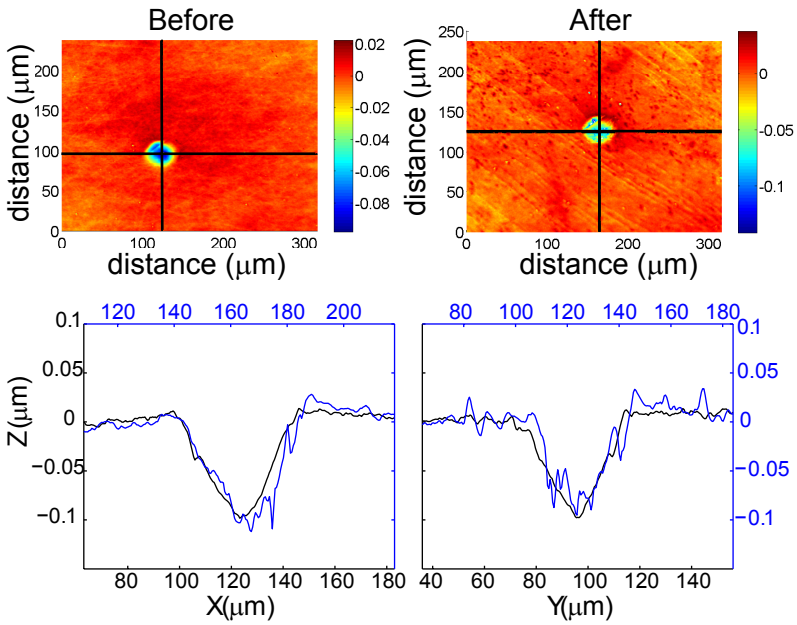

Figure 4.5: On the top left of the figure, calcite surface after dry deformation with a sapphire half-ball lens of radius 0.500 mm and an applied force F = 0.82 N. On the top right, same surface after 50 hours in water saturated with respect to calcite. On the topography profiles, the black lines correspond to the measurements before the water treatment and the grey lines to the measurements after the water treatment.

Table 4.1: Experimental conditions and results from *in situ* and white light interferometry measurements

	Conditions						*In situ* measurements						WLI measurements						
No	e[a]	IM[b]	R	R^+	R_{res}	F	S_1[c]	σ_1[d]	Z_f[e]	V_f[e]	t_f[f]	S_f[c]	Z_p	V_p	Z_{fwli}[g]	V_{fwli}	h	Duration[h]	S_{fwli}
	μm		mm	mm	mm	N	μm^2	MPa	μm	μm^3	hours	μm^2	μm	μm^3	μm	μm^3	μm	hours	μm^2
F01	300	glass	0.77	1.60	1.27	1.15	2650	434	0.19	184	26.08	3603	0.085	28.90	0.84	5610.9	0.60	64.20	2169
F02	567	glass	0.50	1.04	1.27	1.14	1974	578	0.08	23.2	34.01	2090	0.083	27.70	0.52	2069.6	0.21	52.61	785
F03	580	glass	0.25	0.52	0.37	0.88	1065	826	0.02	0.79	24.44	1086	0.340	134.3	0.07	353.9	0	28.44	973
F05	510	glass	0.50	1.04	1.25	1.08	1397	773	0.06	12.8	28.50	2363	0.075	21.90	0.67	4592.1	0.45	40.51	1335
F06	153	glass	0.50	1.04	1.33	1.46	3327	439	0.12	46.4	37.42	3492	0.160	113.4	0.05	2592.6	2.58	90.42	1169
F07	682	sapphire	0.50	2.70	0.96	1.27	1572	808	0.05	20.4	46.75	1823	0.120	43.43	0.20	1225.2	0.60	49.88	777

[a] e: thickness of the calcite crystal used
[b] IM: indenter material
[c] S_1, S_f: Initial and final surface area of contact calculated from *in situ* pictures
[d] σ_1: Initial stress $\sigma_1 = F/S_1$
[e] Z_f,V_f: The subscript f denotes values obtained from the last picture. Z_f has an accuracy of $\pm$ 0.009 μm
[f] t_f: Time of the last picture used to determine *in situ* vertical displacement
[g] Z_{fwli} has an accuracy of $\pm$ 0.003 μm
[h] Total duration of the experiments

4.4 Results

4.4.1 *In situ* vertical displacements

For each experiment, Z_i and V_i were calculated using the displacements of the two first Newton rings (Figure 4.2). Discrepancy may exist if the vertical displacements are calculated using either the first or the second Newton ring. Trends are, however, rather similar for the two rings and, except for experiments F05 and F07, the results obtained are within the same order of magnitude (Figure 4.6). Overall, noise is more important in data obtained using the second Newton ring, therefore, all the values of vertical displacement and volume of calcite dissolved, found in Table 4.1, were calculated using the displacement of the first Newton ring. For experiments F01, F02, F06 and F07 the water film at the contact evaporated during experiments; dissolution started again when water was added once more to the system (Figure 4.6). In addition, no deformation was observed before water was added to the system, thus it can be concluded that the observed deformations in the present study are due to dissolution of calcite under the effect of stress.

Since lenses with different diameters were used (Table 4.1), comparison between the different experiments is easier when vertical displacements are converted into number of moles of calcite dissolved. Evolution of calcite dissolution is then followed through time (Figure 4.6). Strain rates for the different phases of experiments are displayed next to the dissolution versus time curve (Figure 4.6). In all experiments surface areas of contact increase with time (see S_1 and S_f in Table 4.1), therefore applied stresses decrease accordingly. In experiment F01, dissolution is rather constant throughout the experiment. In this case the strain rate is insensitive to the stress variation. In experiments F06 and F07, the second parts of experiments are characterised by slower strain rates. For these two experiments strain rate slows down with decreasing stress. Hence, the decrease in stress is more important in F07 and the decrease in strain rate is also more important in F07 than in F06 (Figure 4.6). Conversely, the strain rate in F02 increases with decreasing stress. In experiment F05, the strain rate increases after the seventieth hour while stress is decreasing, and after the twenty-seventh hour no more deformation is observed (Figure 4.6). In experiment F03, very little but constant deformation is observed.

Precipitated calcite was observed on crystal surfaces after all experiments. It is, however, difficult to differentiate precipitation due to evaporation of the fluid from precipitation resulting from pressure solution. Quantification of the amount of calcite which precipitated due to pressure solution was therefore not possible.

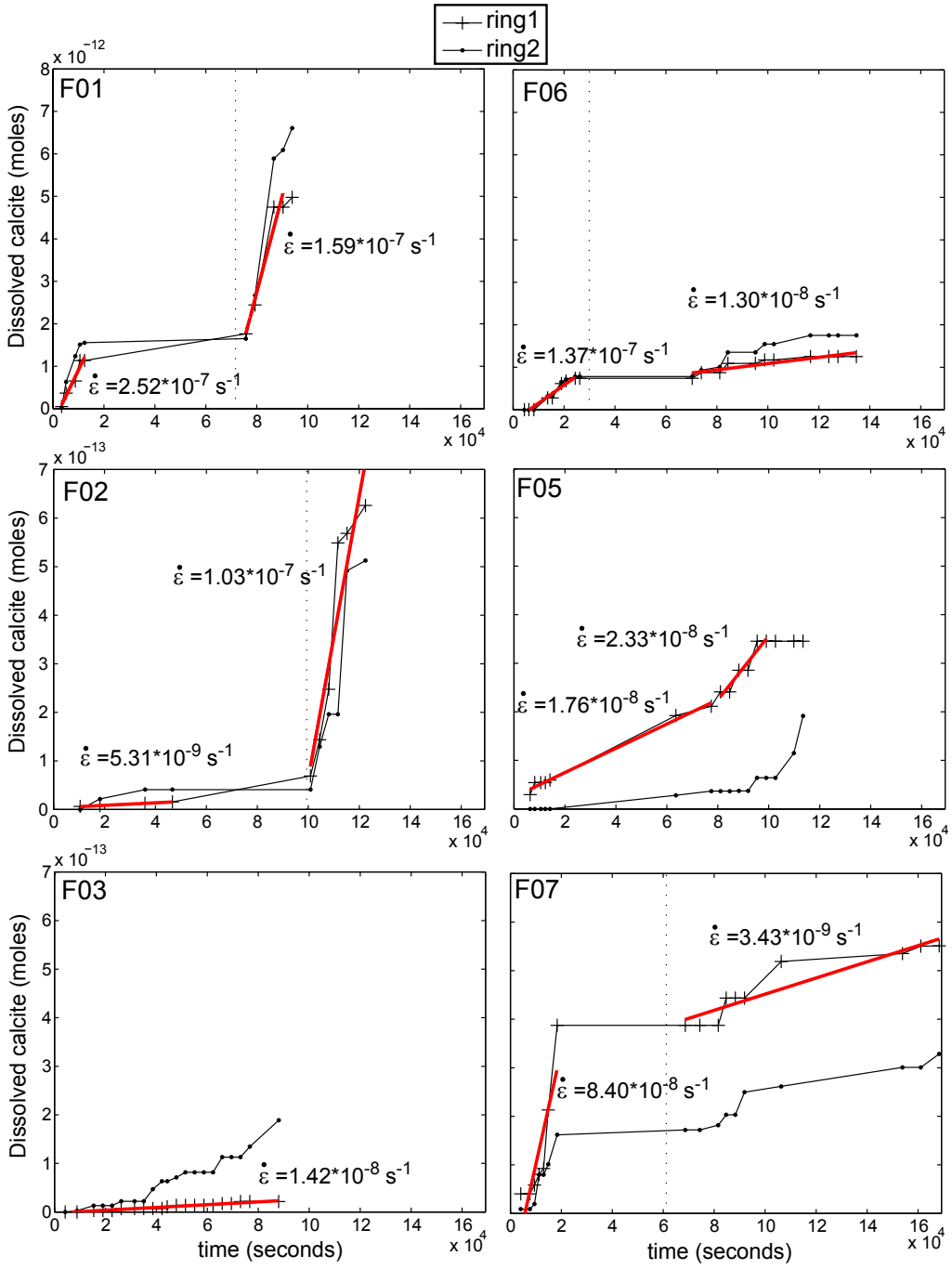

Figure 4.6: Volume of calcite dissolved as a function of time. Vertical dashed lines represent the time at which water was added after the initial water had evaporated in experiments F01, F02, F06 and F07. Strain rates were calculated using data from the first Newton ring (ring 1). Strain rates values are displayed next to each curve, and the grey lines correspond to the data interval taken into account when calculating strain rates.

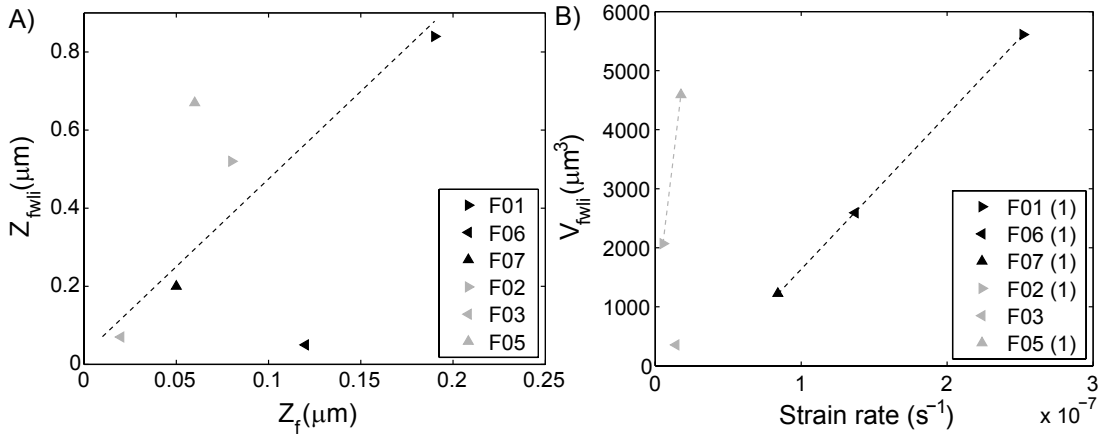

Figure 4.7: Comparison of *in situ* and *ex situ* measurements. A) *Ex situ* penetration of the half–ball lens as a function of the *in situ* measurements. B) *Ex situ* volume of calcite dissolved as a function of the strain rates for the first part of the experiments.

4.4.2 Roughness of the interface and damage

Vertical displacements of the lens into the crystal as measured by white light interferometry are always greater than those obtained from *in situ* measurements, i.e. $Z_{fwli} > Z_f$ (Table 4.1, Figure 4.7). The load was not removed between the two measurements, therefore the discrepancy between the two results is possibly related to the time gap between the end of *in situ* measuring and taking the white light interferometry measurements and also to the fact that dissolution started right after water was added to the system before the first picture was taken. That is to say $Z_{fwli} > Z_f$ may be attributed to the fact that dissolution under stress starts before the first *in situ* measurements and continues in between the two measurements. Overall Z_{fwli} and Z_f follow a similar trend, values for experiments F06 and F05 are, however, rather dissimilar (Figure 4.7). To some extent the discrepancy can be attributed to the different accuracy of the two measurement methods.

Two families of contact structure were differentiated from the vertical profiles of the contact and the half-ball lens fitted on it, depending on the presence or absence of cracks crossing the contact. Comparing the volume of dissolved calcite measured *ex situ*, V_{fwli}, with *in situ* strain rates two trends appear corresponding to the two families of contact (Figure 4.7). Experiments F02, F05 and, to some extent, F03, are examples of the first type of contact obtained during pressure solution in the present study, where roughness develops within the contact and the shape of the holes observed in vertical profiles closely resemble the shape of the half-ball lens indenter (Figure 4.8). Observation by scanning electron microscopy of crystal surfaces after experiments did not reveal any cracks. Therefore, in those experiments, dissolution and associated diffusion of matter outside the stressed surface area of contact most likely occurred along

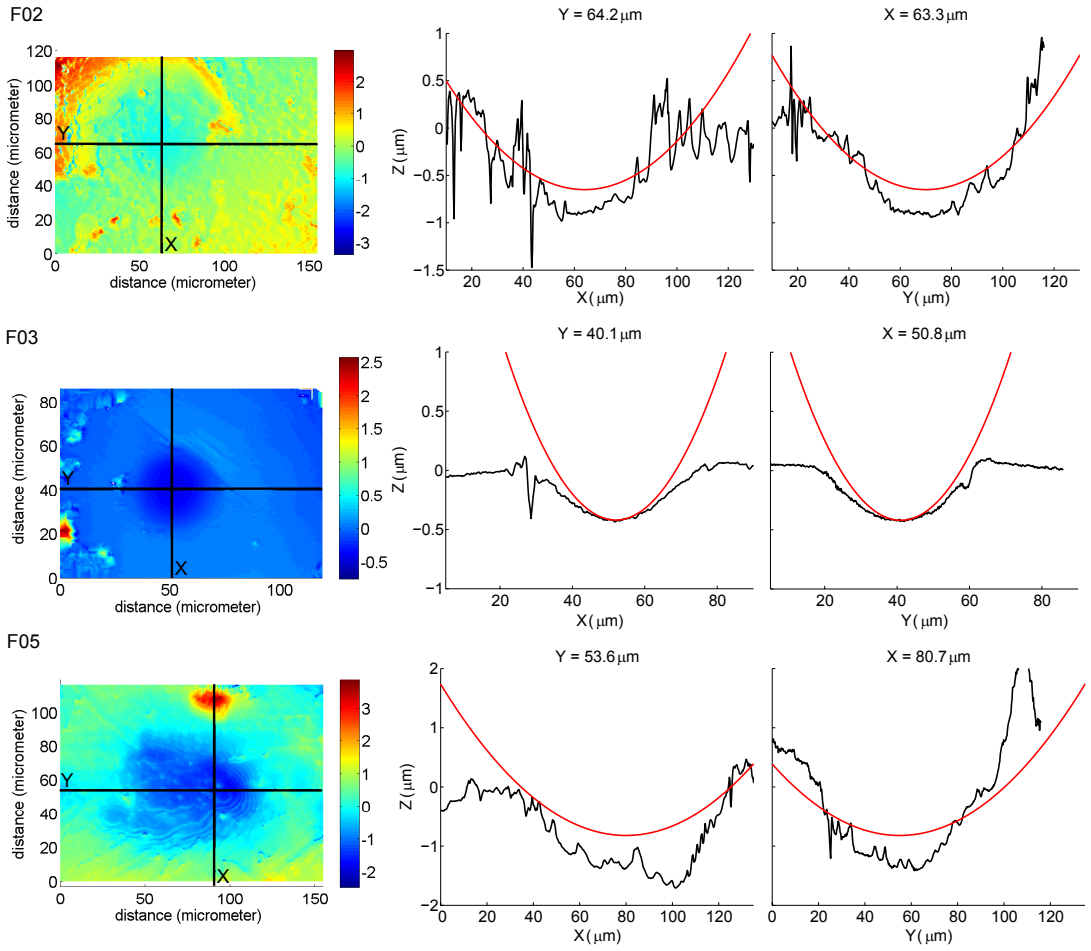

Figure 4.8: Observation by white light interferometry of the contact after experiments F02, F03 and F05. For each experiment the surface topography (colour scale bar in micrometres) and two vertical profiles are shown. The grey line on the vertical profiles corresponds to the shape of the equivalent half-ball lens. Note the difference of scale between the horizontal and vertical axes.

the calcite/indenter interface.

Experiments F01, F06 and F07 are examples of the second type of contact obtained during pressure solution in the present study. In these experiments a hole developed below the indenter (Figure 4.9). Associated with this feature, radial cracks emanating from the contact were observed using scanning electron microscopy (Figure 4.10). The depth, h, of the hole below the indenter tends to increase with time (Table 4.1), leading to the conclusion that the growth of cracks below the indenter is also time dependent. In addition, crack propagation was observed during *in situ* measurements of experiment F01.

The two types of contact geometry possess one common feature: the indenter does not reach the bottom of the hole created by pressure solution during indentation of the crystal. Pressure solution experiments were also conducted on halite. Halite was indented by glass in the presence of water saturated with respect to halite; the diameter of the spherical indenter was about 100 μm (Figure 4.11). Experiments were conducted at various temperatures, and with load applied

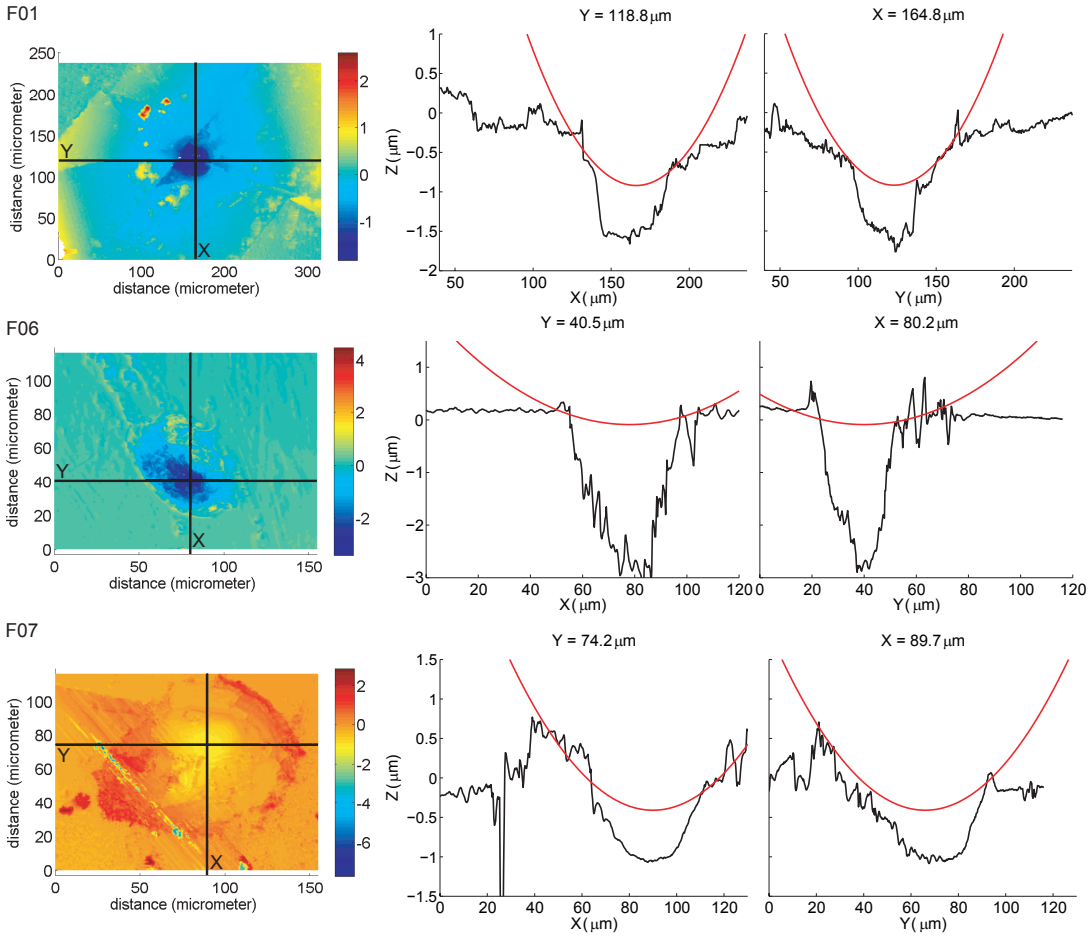

Figure 4.9: Observation by white light interferometry of the contact area after experiments F01, F06 and F07. For each experiment the surface topography (colour scale bar in micrometres) and two vertical profiles are shown. The grey line on the vertical profiles corresponds to the shape of the equivalent half-ball lens. Note the difference of scale between the horizontal and vertical axes.

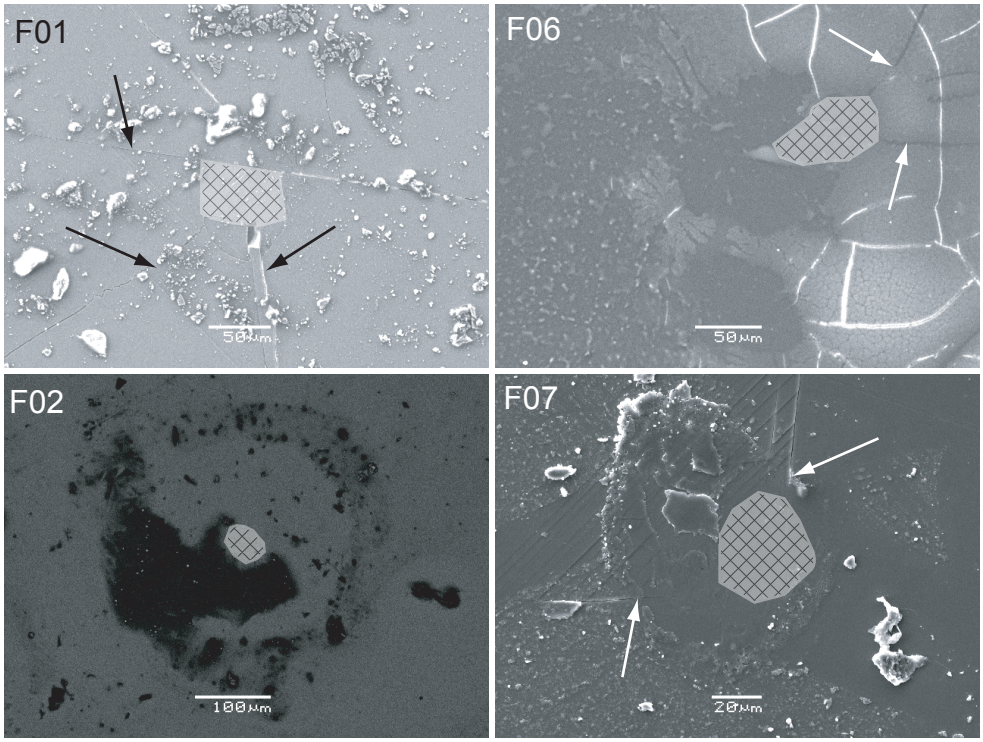

Figure 4.10: Scanning electron micrographs of the crystal surfaces after experiments F01, F02, F06 and F07. Hatched areas represent approximate surface areas of contact during experiments, since the vertical resolution of the scanning electron microscope is low the area were determined by comparing these pictures with the white light interferometry data. The arrows point to cracks which start at the contact and continue beyond the contact area. The white flacks on pictures of F01 and F07 contacts corresponds to calcite precipitation.

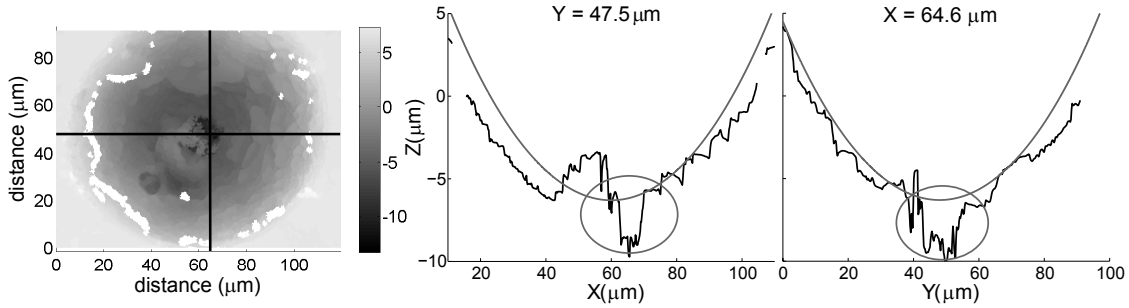

Figure 4.11: White light interferometry surface and topography profiles of a halite crystal indented by glass, approximate shape of the indenter displayed on the profiles. Red circles on both profiles indicate a hole that formed under the indenter. Note the difference of scale between the horizontal and vertical axes.

over several days. In all the experiments on halite a hole was present under the indenter, as observed in Figure 4.11.

Using information from both *in situ* and white light interferometry measurements, it is observed that experiments in which a crack propagate under the indenter are characterized by higher rates of dissolution (Figure 4.12).

4.5 Discussion

Topographic profiles taken using white light interferometry show that two different mechanisms have controlled dissolution and diffusion in the present experiments. During the first phase of the *in situ* measurements strain rates can also be split in the two same groups. Deformation occurs either by dissolution and transport along the contact interface, i.e. pressure solution, or by a combination of pressure solution and subcritical crack growth.

4.5.1 Deformation by pressure solution

Experiment F03 is characterised by very little deformation and a very flat lens/calcite interface. Moreover, the shape of the hole is almost exactly the shape of the indenter, as should be the case for purely plastic deformation. It is therefore questionable whether or not pressure solution was active in this experiment. However, for experiments F02 and F05, the combination of the rate of indentation and the observation of the topography profiles of the contact at the end of experiments strongly indicates that deformation by a pressure solution mechanism was active. Indentation of calcite occurred by dissolution and diffusion along the lens/calcite interface (Figure 4.8).

Even though this is at the limit of the data resolution, it is observed that the lens did not

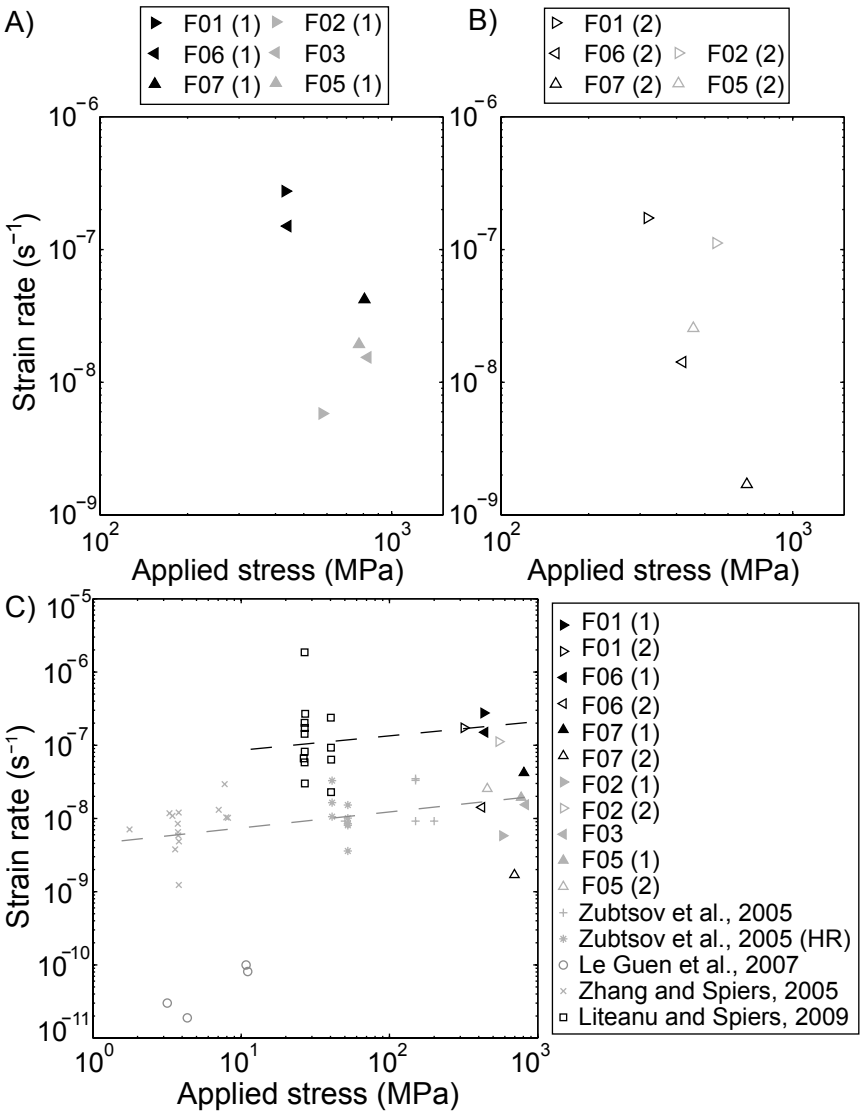

Figure 4.12: Strain rates as a function of the applied stress represented in log-log coordinates. The number 1 and 2 in parenthesis refer to the stages in strain rate measurements. A) First phase and B) second phase of the experiments, as indicated in Figure 6. C) The present data are compared with data found in other published experiments on carbonates. Experiments in which subcritical crack growth was active are displayed in black. The lines present on the graphs are not regression lines but are present to highlight the increase in strain rate when pressure solution is combined with crack propagation. HR in the figure legend refers to the high resolution experiments in the paper of Zubtsov et al., 2005

reach the bottom of the hole created by dissolution of calcite during experiments (Figure 4.8). Two different hypotheses concerning the way the interface develops, may be drawn from this observation. Firstly, the space between the indenter and the crystal may be attributed to the roughness of the interface. Roughness develops at the stressed crystal/fluid interface due to the thermodynamic instability of a flat solid/fluid interface (*Srolovitz*, 1989; *Angheluta et al.*, 2009). In this case the roughness amplitude would be equivalent to the measured value h, 0.20 and 0.45 μm for F02 and F05, respectively. Coarsening of a grain boundary structure is related to the stress concentration in the grooves (*Koehn et al.*, 2004); the same trend is observed in the present experimental study where F05 is characterised by a higher applied stress and a rougher interface. An islands–and–channels structure (*Lehner*, 1990; *Dysthe et al.*, 2002; *den Brok et al.*, 2002) would then be the most appropriate model to explain the present results. However, the amplitude of the observed roughness is quite large, which might be an indication that the islands–and–channels structure roughened toward a grain–boundary structure as described by *Koehn et al.* (2006), for which the amplitude of the roughness might be of the order of one micrometre. The mean profile roughness under the indenter is of 0.11 μm for F02 and of 0.18 μm for F05. The slightly greater roughness correlates with higher strain rate for the first phase in experiments F02 and F05 (Figure 4.6), which is in agreement with similar results on quartz (*Gratier et al.*, 2009).

Secondly, the space between the indenter and the crystal may be attributed to the development of a hole in the crystal below the indenter. In this case dissolution of calcite under the indenter must be attributed to the high strain energy stored in the crystal. Previous experimental studies have shown dissolution of free surfaces driven by strain energy (*den Brok and Morel*, 2001; *Koehn et al.*, 2004; *Bisschop and Dysthe*, 2006). The control experiments with indentations in water, but with no load, shows that it is not the energy stored by defects, but strain energy due to the load applied by the indenter that drives the dissolution. The observed hole would then be a way for the crystal to lower the energy of the system. Similar observations were made on halite crystals that were indented by glass half–ball lenses (Figure 4.11) using a similar experimental set-up as for the calcite crystals.

4.5.2 Deformation by a combination of pressure solution and subcritical crack growth

In experiments F01, F06 and F07, the depth of the hole below the indenter is of the same order or greater than the penetration depth of the indenter into the crystal (Figure 4.9, Table 4.1). This implies that the same amount, or more, of calcite was dissolved under the indenter

than calcite that was replaced by the indenter. Since cracks are observed on both optical and scanning electron microscope images (Figure 4.10), in these cases the hole present under the indenter might be due to a combination of dissolution and crack propagation. In brittle material subjected to high stresses, a zone of inelastic deformation immediately below the contact area may develop, leading to the formation of what are called 'vent cracks' (*Lawn and Wilshaw*, 1975). Dissolution of minerals occurs preferentially at active sites such as edges, dislocations or microfractures (*Lasaga*, 1981; *Schott et al.*, 1989). In the present experiments, the hole below the lens may therefore be a result of the combination of crack development due to high stresses associated with dislocation plasticity, and dissolution of material in the presence of a reactive fluid. While cracks crossing contacts in experiments F06 and F07 remained stable throughout experiments, in F01 crack propagation occurred during the experiment. This observation might explain why strain rate is rather constant in experiment F01 while it diminishes in experiment F06 and F07.

The presence or absence of cracks below the indenter cannot be explained from the present experimental conditions. The two most important parameters controlling crack propagation are the applied tensile stress and the size of the flaw (*Anderson*, 1995). Experiments in which a crack propagates below the indenter are not characterised by higher applied stresses than in the other experiments. Therefore, the propagation or not of a crack, in the present study, is probably due to the presence or absence of a flaw in the crystal below the indenter. This hints to the possibility that density of flaws is as important for strain rate as stress itself. However, it must be taken into consideration that the loads and the contact stresses have been varied by less than a factor 2. A systematic study of the development of contact fractures for a wide range of stresses and flaw densities might be useful.

4.5.3 Rate–controlling step

Although too little data are available to draw any firm conclusion about the relationship between dissolution and applied stress, it does appear that subcritical crack growth and pressure solution are characterised by different strain rates. Strain rates in experiments in which crack propagation occurred are two orders of magnitude higher than for experiments in which diffusion occurs only through the rough lens/calcite interface (Figure 4.7 and 4.12).

Experiments in which evaporation occurred are characterised by two strain rates (Figure 4.6). For F01, F06 and F07 the rate of dissolution was either constant or decreased after evaporation. The fast initial rate of deformation might indicate that at first crack propagation controls the vertical displacement of the indenter, while continued vertical displacement of the lens be-

comes increasingly controlled by the rate of dissolution of calcite at the contact points between the lens and the crystal.

Conversely, the rate of dissolution in experiments F02 and F05 increases during the second phase. In these experiments, no cracks crossed the contact, therefore diffusion must occur through the thin film present at the interface. The thickness of the water film might be related to the deviatoric stress at the grain-to-grain contact (*Renard and Ortoleva*, 1997), while in the case of the islands–and–channel structure the decrease of stress might lead to an increase of the water film thickness, which enables faster diffusion and therefore a greater strain rate. In experiments in which crack propagation occurred, diffusion proceeded through the crack and was not limited by the applied stress.

If the rate of pressure solution is controlled by diffusion, the displacement rate of the half-ball lens, dZ/dt, as a function of the measured diameter, d, may be expressed as, $dZ/dt = \alpha/d_i^2$ in cases where the applied stress is constant (*Weyl*, 1959). In the present study the applied force is constant, but not the stress. Therefore the displacement rate of the half-ball lens as a function of the diameter, d, may here be expressed as,

$$\frac{dZ}{dt} \approx \alpha \frac{1}{d_i^4}, \tag{4.5}$$

in which α, in μm^3/s, is mainly a function of the lens/calcite interface geometry and thickness, Δ, and of the diffusion coefficient, D, i.e. $\alpha \sim D\Delta$. For all experiments, the relationship between diffusion path diameter and rate of deformation was tested. However, it was difficult to firmly conclude on whether the diameter influence on the vertical displacement rate was of the form $1/d^2$ or $1/d^4$. Therefore it is not possible to conclude whether or not diffusion was the rate–limiting step for pressure solution in the present experiments.

4.5.4 Comparison with other studies

Strain rates obtained in this study are in agreement with those obtained in other studies, and three different trends can be observed (Figure 4.12).

Numerous strain rate laws describing deformation of minerals or aggregates by pressure solution have been derived (*Weyl*, 1959; *Rutter*, 1976; *Lehner*, 1990; *Spiers et al.*, 1990), even though they contain various dissimilarities they all describe the strain rate as positively correlated to the applied stress. However, strain rate data in Figure 4.12 do not display a strong dependency on applied stress. Experiments in which pressure solution is assumed to be the main process controlling deformation are characterized by a slight increase in the strain rate as stress is increasing (*Zhang and Spiers*, 2005; *Zubtsov et al.*, 2005). However, at the same

applied stress the effect of grain size or pore fluid might have a much stronger effect than the variations in applied stress on the strain rate.

Fracture development during slow sediment compaction increases the pressure solution strain rate (*Gratier et al.*, 1999). Published experiments on calcite in which crack propagation occurred (*Liteanu and Spiers*, 2009) are characterised by slightly higher strain rates than experiments for which pressure solution was the main mechanism of compaction. This feature was also observed within the present experimental results (Figure 4.12). From the wide range of experimentally measured strain rates, it can be deduced that the variation of strain rates is mostly a function of the processes active during chemical compaction, i.e. pressure solution or subcritical crack growth, rather than of the applied stress.

As mentioned by *Tada and Siever* (1989) (and references therein), early cementation has an inhibiting effect on intergranular pressure solution. This feature is clearly observed in Figure 4.12 where cemented rocks deforming by pressure solution (*Le Guen et al.*, 2007) exhibit strain rates that are 2 to 3 orders of magnitude lower than for aggregates. Faster strain rates observed in aggregates or in the present study might in nature be associated with compaction of loose carbonate sediments or compaction of fault gouges.

4.6 Conclusion

This is the first study that compares results of calcite slow deformation, from nanometer resolution techniques both *in situ* and *ex situ*. From these results it was possible to identify the relative importance of pressure solution driven by normal load, and free surface dissolution driven by strain energy, and how these mechanisms couple to mass transport in fluid films and fractures.

The present experimental study enabled the determination of two different processes occurring during pressure solution of calcite crystals at the grain scale. In half of the experiments, diffusion of the dissolved solid took place in the pore fluid present along a rough interface between calcite and the indenter. In the other half of the experiments, diffusion occurred through cracks that propagated from the contact toward the less stressed part of the crystal. The occurrence of one or the other mechanism does not appear to be ruled by the applied stress but is most likely dependent on the presence or not of a flaw in the crystal.

Strain rates are higher for experiments in which crack propagation occurred. The present calculated strain rates are in agreement with the ones obtained in other studies. Overall it seems strain rates are not really stress dependent but rather dependent on the grain size or whether crack propagation occurs or not. The first main difference in strain rates is to be seen between experiments conducted in rock, for which strain rates are three orders of magnitude lower than

experiments conducted in aggregates. Within experiments conducted on aggregates or single crystals, when crack propagation occurs strain rates increase by one to two orders of magnitude.

Acknowledgements

We would like to thank J. P. Gratier for fruitful discussions. Olav Gundersen is thanked for his help in the laboratory. Reinier van Noort and an anonymous reviewer are thanked for their positive and constructive reviews.

Bibliography

Anderson, T. L. (1995), *Fracture mechanics: fundamentals and applications*, CRC Press, Boca Raton, 2nd ed.

Angevine, C. L., D. L. Turcotte, and M. D. Furnish (1982), Pressure solution lithification as a mechanism for the stick-slip behavior of faults, *Tectonics*, *1*(2), 151–160.

Angheluta, L., E. Jettestuen, and J. Mathiesen (2009), Thermodynamics and roughening of solid-solid interfaces, *Physical Review E (Statistical, Nonlinear, and Soft Matter Physics)*, *79*(3), 031,601–11.

Atkinson, B. K. (1982), Subcritical crack propagation in rocks: theory, experimental results and applications, *Journal of Structural Geology*, *4*(1), 41–56, doi: 10.1016/0191-8141(82)90005-0.

Baker, P. A., M. Kastner, J. D. Byerlee, and D. A. Lockner (1980), Pressure solution and hydrothermal recrystallization of carbonate sediments; an experimental study, *Marine Geology*, *38*(1-3), 185–203.

Bisschop, J., and D. K. Dysthe (2006), Instabilities and coarsening of stressed crystal surfaces in aqueous solution, *Physical review letters*, *96*(14), 146,103.

De Meer, S., and C. J. Spiers (1999), On mechanisms and kinetics of creep by intergranular pressure solution, in *Growth, dissolution and patterns formation in geosystems*, edited by B. Jamtveit and P. Meakin, Kluwer Academic Publishers, Dordrecht, The Netherlands.

den Brok, B., J. Morel, and M. Zahid (2002), In situ experimental study of roughness development at a stressed solid/fluid interface, in *Deformation Mechanisms, Rheology and Tectonics: Current Status and Future Perspectives*, vol. 200, edited by S. DeMeer, M. R. Drury, J. H. P. DeBresser, and G. M. Pennock, pp. 73–83, The Geological Society, London.

den Brok, S. W. J., and J. Morel (2001), The effect of elastic strain on the microstructure of free surfaces of stressed minerals in contact with an aqueous solution, *Geophys. Res. Lett.*, *28*.

Dysthe, D. K., Y. Podladchikov, F. Renard, J. Feder, and B. Jamtveit (2002), Universal scaling in transient creep, *Physical Review Letters*, *89*(24), 246,102.

Fischer-Cripps, A. C. (1999), The hertzian contact surface, *Journal of Materials Science*, *34*(1), 129–137.

Gratier, J. P. (1987), Pressure solution-deposition creep and associated tectonic differentiation in sedimentary rocks, in *Deformation of sediments and sedimentary rocks.*, *Geological Society Special Publications*, vol. 29, edited by M. E. Jones and M. F. Preston, pp. 25–38, London, United Kingdom.

Gratier, J. P., F. Renard, and P. Labaume (1999), How pressure solution creep and fracturing processes interact in the upper crust to make it behave in both a brittle and viscous manner, *Journal of Structural Geology*, *21*(8-9), 1189–1197.

Gratier, J. P., R. Guiguet, F. Renard, L. Jenatton, and D. Bernard (2009), A pressure solution creep law for quartz from indentation experiments, *Journal of Geophysical Research-Solid Earth*, *114*, doi:10.1029/2008jb005652.

Gratz, A. J. (1991), Solution-transfer compaction of quartzites - progress toward a rate law, *Geology*, *19*(9), 901–904.

Griffith, A. A. (1920), The phenomena of rupture and flow in solids, *Philosophical Transactions of the Royal Society of London. Series A, Containing Papers of a Mathematical or Physical Character*, *221*, 163–198.

Hickman, S. H., and B. Evans (1991), Experimental pressure solution in halite - the effect of grain interphase boundary structure, *Journal of the Geological Society*, *148*, 549–560.

Hickman, S. H., and B. Evans (1995), Kinetics of pressure solution at halite-silica interfaces and intergranular clay films, *Journal of Geophysical Research-Solid Earth*, *100*(B7), 13,113–13,132.

Johnson, K. L. (1985), *Contact mechanics*, Cambridge University Press, Cambridge.

Karcz, Z., E. Aharonov, D. Ertas, R. Polizzotti, and C. H. Scholz (2006), Stability of a sodium chloride indenter contact undergoing pressure solution, *Geology*, *34*(1), 61–63, doi:10.1130/G21722.1.

Koehn, D., D. K. Dysthe, and B. Jamtveit (2004), Transient dissolution patterns on stressed crystal surfaces, *Geochimica et Cosmochimica Acta*, *68*(16), 3317–3325.

Koehn, D., A. Malthe-Sorenssen, and C. W. Passchier (2006), The structure of reactive grain-boundaries under stress containing confined fluids, *Chemical Geology*, *230*(3-4), 207–219.

Lasaga, A. C. (1981), Rate laws of chemical reactions, *Reviews in Mineralogy*, *8*, 1–68.

Lawn, B., and R. Wilshaw (1975), Indentation fracture - principles and applications, *Journal of Materials Science*, *10*(6), 1049–1081.

Le Guen, Y., F. Renard, R. Hellmann, E. Brosse, M. Collombet, D. Tisserand, and J. P. Gratier (2007), Enhanced deformation of limestone and sandstone in the presence of high p-co_2 fluids, *Journal of Geophysical Research - Solid Earth*, *112*(B5), doi:10.1029/2006JB004637.

Lehner, F. K. (1990), Thermodynamics of rock deformation by pressure solution, in *Deformation Processes in Minerals, Ceramics and Rocks*, edited by D. J. Barber and P. G. Meredith, p. 423, Unwin Hyman Ltd, London, United Kingdom.

Liteanu, E., and C. J. Spiers (2009), Influence of pore fluid salt content on compaction creep of calcite aggregates in the presence of supercritical co_2, *Chemical Geology*, *265*(1-2), 134–147, doi:10.1016/j.chemgeo.2008.12.010.

Olagnon, C., J. Chevalier, and V. Pauchard (2006), Global description of crack propagation in ceramics, *Journal of the European Ceramic Society*, *26*(15), 3051–3059, doi: 10.1016/j.jeurceramsoc.2005.11.004.

Raj, R. (1982), Creep in polycrystalline aggregates by matter transport through a liquid-phase, *Journal of Geophysical Research*, *87*(NB6), 4731–4739.

Ramsay, J. G. (1980), The crack-seal mechanism of rock deformation, *Nature*, *284*(5752), 135–139, 10.1038/284135a0.

Renard, F., and P. J. Ortoleva (1997), Water films at grain-grain contacts; debye-hueckel, osmotic model of stress, salinity, and mineralogy dependence, *Geochimica et Cosmochimica Acta*, *61*(10), 1963–1970.

Renard, F., J. P. Gratier, and B. Jamtveit (2000), Kinetics of crack-sealing, intergranular pressure solution, and compaction around active faults, *Journal of Structural Geology*, *22*, 1395–1407.

Rutter, E. H. (1976), The kinetics of rock deformation by pressure solution, *Philosophical Transactions of the Royal Society of London, Series A: Mathematical and Physical Sciences*, *283*(1312), 203–219.

Rutter, E. H. (1983), Pressure solution in nature, theory and experiment, *Journal of the Geological Society of London*, *140*(5), 725–740.

Scholz, C. H. (2002), *The mechanics of earthquakes and faulting*, 2nd ed. ed., Cambridge University Press, Cambridge.

Schott, J., S. L. Brantley, D. A. Crerar, C. Guy, M. Borcsik, and C. Willaime (1989), Dissolution kinetics of strained calcite, *Geochimica et Cosmochimica Acta*, *53*(2), 373–382.

Sorby, H. C. (1863), The bakerian lecture: On the direct correlation of mechanical and chemical forces, *Proceedings of the Royal Society of London*, *12*, 538–550.

Spiers, C. J., P. M. T. M. Schutjens, R. H. Brzesowsky, C. J. Peach, J. L. Liezenberg, and H. J. Zwart (1990), Experimental determination of constitutive parameters governing creep of rocksalt by pressure solution, in *Deformation mechanisms, rheology and tectonics.*, *Geological Society Special Publications*, vol. 54, edited by J. Knipe Robert and E. H. Rutter, pp. 215–227, London, United Kingdom.

Srolovitz, D. J. (1989), On the stability of surfaces of stressed solids, *Acta Metallurgica*, *37*(2), 621–625.

Tada, R., and R. Siever (1986), Experimental knife-edge pressure solution of halite, *Geochimica et Cosmochimica Acta*, *50*(1), 29–36, doi:10.1016/0016-7037(86)90045-1.

Tada, R., and R. Siever (1989), Pressure solution during diagenesis, *Annual Review of Earth and Planetary Sciences*, *17*, 89–118.

Tolansky, S. (1973), *An introduction to interferometry*, Longman, London, 2nd ed.

van Noort, R., C. Spiers, and C. Peach (2007), Effects of orientation on the diffusive properties of fluid-filled grain boundaries during pressure solution, *Physics and Chemistry of Minerals*, *34*(2), 95–112, 10.1007/s00269-006-0131-9.

van Noort, R., H. J. M. Visser, and C. J. Spiers (2008), Influence of grain boundary structure on dissolution controlled pressure solution and retarding effects of grain boundary healing, *J. Geophys. Res.*, *113*, doi:10.1029/2007JB005223.

Weyl, P. K. (1959), Pressure solution and the force of crystallization – a phenomenological theory, *Journal of Geophysical Research*, *64*(11), 2001–2025.

Yamasaki, N., and T. Weiping (1993), Hydrothermal hot-pressing of calcium carbonate with sea water, *Journal of Materials Science Letters*, *12*(7), 516–519, 10.1007/BF00452814.

Yasuhara, H., D. Elsworth, and A. Polak (2003), A mechanistic model for compaction of granular aggregates moderated by pressure solution, *Journal of Geophysical Research-Solid Earth*, *108*(B11).

Zhang, X., and C. J. Spiers (2005a), Compaction of granular calcite by pressure solution at room temperature and effects of pore fluid chemistry, *International Journal of Rock Mechanics and Mining Sciences*, *42*, 950–960.

Zhang, X., and C. J. Spiers (2005b), Effects of phosphate ions on intergranular pressure solution in calcite: An experimental study, *Geochimica et Cosmochimica Acta*, *69*(24), 5681–5691.

Zhang, X., J. Salemans, C. J. Peach, and C. J. Spiers (2002), Compaction experiments on wet calcite powder at room temperature; evidence for operation of intergranular pressure solution, in *Deformation mechanisms, rheology and tectonics; current status and future perspectives.*, edited by S. de Meer, R. Drury Martyn, J. H. P. de Bresser, and M. Pennock Gill, Geological Society of London. London, United Kingdom.

Zubtsov, S., F. Renard, J. P. Gratier, R. Guiguet, D. K. Dysthe, and V. Traskine (2004), Experimental pressure solution compaction of synthetic halite/ calcite aggregates, *Tectonophysics*, *385*(1-4), 45–57.

Zubtsov, S., F. Renard, J. P. Gratier, D. K. Dysthe, and V. Traskine (2005), Single-contact pressure solution creep on calcite monocrystals, in *Deformation mechanisms, rheology and tectonics; from minerals to the lithosphere.*, edited by D. Gapais, P. Brun Jean, and R. Cobbold Peter, Geological Society of London. London, United Kingdom.

Paper 3: Experimental mechanical and chemical compaction of carbonate sand

Journal of Geophysical Research – Solid Earth (in press)

Experimental mechanical and chemical compaction of carbonate sand

Delphine Croizé[a,b], Knut Bjørlykke[a], Jens Jahren[a], and François Renard[b,c]

[a] Department of Geosciences, University of Oslo, Norway

[b] Université Joseph Fourier - Grenoble I, LGCA-CNRS-Observatoire de Grenoble, France

[c] Physics of Geological Processes (PGP), University of Oslo, Norway

Abstract

Uniaxial compression tests were conducted on bioclastic sand and crushed calcite crystals. Mechanical and chemical processes were investigated to better quantify carbonates petrophysical properties and their evolution with burial or during fault zone processes. The grain size was in the range 63–500 μm and the samples were saturated with water in equilibrium with carbonate, glycol, decane or air. During loading, effective stress was increased to 32 MPa. Mechanical compaction processes, *i.e.* grain rearrangement, crushing, could be separated from chemical processes, *i.e.* pressure solution, subcritical crack growth. P- and S–waves monitored during the tests showed low velocity in samples saturated with reactive fluids. This suggested that chemical reactions at grain contacts reduced the grain framework stiffness. Creep tests were also carried out on bioclastic sand at effective stress of 10, 20 and 30 MPa. No creep was observed in samples saturated with non–reactive fluids. For all the samples saturated with reactive fluids, strain as a function of time was described by a power law of time with a single exponent close to 0.23. Parameters controlling creep rate were, in order of importance, grain size, effective stress and water saturation. Microstructural observations showed that compaction of bioclastic carbonate sand occurred both mechanically and chemically. Crack propagation probably contributed to mechanical compaction and enhanced chemical compaction during creep. Experimental compaction showed that compaction of carbonates should be modelled as a function of both mechanical and chemical processes, also at relatively shallow depth and low temperature.

5.1 Introduction

Compaction of sediments, *i.e.* porosity loss and density increase, induces changes in petrophysical properties of rocks. These petrophysical properties are crucial to for instance, model the stability of slopes, or for the determination of the elastic properties of the medium to image reservoirs using seismic waves or electromagnetic signals. Processes leading to porosity loss

in sediments may be divided into mechanical compaction which is a function of stress, and chemical compaction which is controlled by the thermodynamics and kinetics of fluid–rock interactions (*Bjørlykke*, 2003). Pressure solution and subcritical crack growth (stress corrosion) are two irreversible deformation processes responsible of sediments compaction that are occurring in presence of reactive fluids (*Weyl*, 1959; *Atkinson*, 1982).Even though these deformation mechanisms are driven by stress, they are here considered as chemical compaction processes since their rate is controlled by chemical reactions such as fluid-rock reactions or diffusion in a fluid phase. In carbonate sediments, unlike siliceous sediments, mechanical and chemical processes occur simultaneously from the surface, affecting each other (*Athy*, 1930; *Weller*, 1959; *Fruth et al.*, 1966; *Schmoker and Halley*, 1982; *Bassinot et al.*, 1993; *Ehrenberg*, 2006). In carbonate sediments the interaction between the different mechanical and chemical compaction processes, and the effect of the various initial conditions and their relation to diagenetic changes make porosity prediction difficult.

The primary porosity of carbonates at the surface ranges from 50 to 70 % (*Hamilton*, 1976; *Schmoker and Halley*, 1982; *Fabricius*, 2003), grain rearrangement may therefore be an important process of compaction during the first hundreds of meters. Then, when sediments reach a locked state, grain crushing becomes the main mechanism of mechanical compaction (*Chuhan et al.*, 2002; *Karner et al.*, 2005). Stress independent dissolution of thermodynamically unstable minerals, e.g. aragonite or magnesian calcite, followed by precipitation of calcite and dolomite may also occur at shallow depth (*Athy*, 1930; *Weller*, 1959). When carbonate sediments contain unstable minerals early diagenesis may produce a strong framework mechanically stable preventing further mechanical compaction (*McLimans and Videtich*, 1989; *Kopaska-Merkel et al.*, 1994; *Croizé et al.*, 2009). In such situation porosity loss will proceed by pressure solution creep (*Weyl*, 1959) or a combination of subcritical crack growth and pressure solution (*Atkinson*, 1982).

Compaction curves, *i.e.* porosity or density versus depth curves, are used as an input for basin modelling and prediction of reservoir properties (*Sclater and Christie*, 1980; *Audet and Fowler*, 1992; *Goldhammer*, 1997; *Giles*, 1997). In these studies, porosity loss is often described as an exponential function of stress. However, chemical processes during burial of carbonate sediments make prediction of the relation between porosity and depth more challenging. Experimental compaction studies provide quantitative data by linking various initial conditions to physical properties as a function of stress and fluid content and may simulate both mechanical and chemical compaction.

To image reservoirs, inversion of seismic data needs to be done having a rather good understanding of the relation between elastic wave propagation velocity and rock properties (*Chris-*

tensen and Szymanski, 1991). However, seismic wave propagation is strongly affected by porosity (*Rafavich et al.*, 1984) and the type of pore in presence (*Anselmetti and Eberli*, 1993). Seismic properties of rocks also depend on microstructures (*Wang*, 1997), fractures and cracks especially affecting S-wave propagation (*Dürrast and Siegesmund*, 1999; *Couvreur et al.*, 2001), pore fluids (*Assefa et al.*, 2003), and grain size, shape and sorting (*Eberli et al.*, 2003). The additional difficulty inherent to carbonate rocks is the influence of fluid–rock interactions on P- and S–waves measurements (*Vanorio et al.*, 2008).

The present study considers two type of carbonates. While calcite has been used in a number of pressure solution studies, bioclastic carbonates sand have been less studied but may be more representative of natural sediments. The purpose of the present study is to quantify both mechanical and chemical compaction of these two materials. To this end, bioclastic carbonates and crushed calcite crystals were uniaxially compacted up to 32 MPa effective stress under drained conditions. In addition creep tests were carried out at constant vertical stresses of 10, 20, and 30 MPa. The influence of pore fluid chemistry, grain size, mineralogy, applied uniaxial stress and temperature was investigated. Ultrasonic P- and S-wave velocities were recorded during experiments. This study made possible to separate the respective influence of mechanical and chemical mechanisms in carbonate compaction, and to link them to the evolution of specific petrophysical properties, as well as with P- and S–waves ultrasonic velocity.

5.2 Materials and methods

5.2.1 Samples and analyses

Two different materials were used. Firstly, Holocene shell fragments from beaches near Tromsø, northern Norway, are primarily composed of magnesian calcite, *i.e.* high-magnesium calcite, with minor siliceous impurities. Secondly, calcite crystals (Wards international) consisting of more than 99 % calcite were used. The samples were crushed, sieved, and separated into three grain–size fractions. The grain–size fractions used were very fine, 0.063 to 0.125 mm, fine, 0.125 to 0.250 mm, and medium, 0.250 to 0.500 mm. The main difference between the two types of samples is that the bioclastic sand contains mostly microporous shells of moluscs, while the calcite samples are constituted of rhomboedra with no microporosity. Magnesian calcite being more reactive than calcite, chemical compaction is therefore easier to observe in bioclastic carbonate sand under laboratory conditions. The samples were saturated with various fluids having different reactivity with respect to calcite. Non–reactive fluids used were air and N-decane. Reactive fluids were water saturated with carbonate, water with 5% NH_4Cl

saturated with carbonate, and mixtures of water and glycol (see Tables 5.1 and 5.2). Pore water composition was analysed before and after some experiments. The cations were analysed using an atomic absorption spectrometer from Varian Inc..

Table 5.1: Experimental conditions for the uniaxial compaction tests. The uniaxial stress was increased from 0 to 32 MPa.

Temperature	Mineralogy	d[a]	Pore fluid	Φ_i[b]	No[c]
Room temperature	Carbonate sand	250-500	5% NH_4Cl solution saturated with respect to carbonate	52.1	T23
			Water saturated with respect to carbonate	50.8	T30
			Dry	61.0	T10
		125-250	5% NH_4Cl solution saturated with respect to carbonate	60.7, 61.7, 61.0, 55.7	T15, T16, T17, T35
			Water saturated with respect to carbonate	61.8, 55.7	T18, T31
			N-Decane	53.9, 54.9	T20, T22
			Dry	61.2, 53.0	T19, T21
		63-125	5% NH_4Cl solution saturated with respect to carbonate	59.6	T34
			Water saturated with respect to carbonate	59.1	T29
			50% water saturated with respect to carbonate - 50% Glycol	59.49	T33
			97% Glycol	51.1	T36
			Dry	58.9, 59.33	T28, T32
	Calcite	250-500	Water saturated with respect to calcite	43.0, 44.9	T24, T26
			Dry	44.5	T25
		125-250	Dry	47.6	T27
50°C	Carbonate sand	250-500	5% NH_4Cl solution saturated with respect to carbonate	61.7, 61.6	T7, T8
			N-Decane	53.1	T12
			Dry	60.6	T11
	Calcite	100-500	5% NH_4Cl solution saturated with respect to carbonate	44.6	T13

[a] d: Grain size in μm
[b] Φ_i: Initial porosity in percent
[c] No: Experiment identification number

Table 5.2: Experimental conditions for the creep compaction tests. All the experiments were conducted at constant stress on bioclastic carbonate sands.

Temperature	σ_1[a]	d[b]	Pore fluid	Φ_0[c]	No[d]
Room temperature	30	250-500	5% NH_4Cl solution saturated with respect to carbonate	27.87	T23
			Anisole	48.23	T6
			Dry	43.57	T10
		125-250	5% NH_4Cl solution saturated with respect to carbonate	29.39	T35
		63-125	5% NH_4Cl solution saturated with respect to carbonate	33.26	T34
			50% water saturated with respect to carbonate - 50% Glycol	32.87	T33
			97% Glycol	29.22	T36
			Dry	39.46	T32
	10	63-125	5% NH_4Cl solution saturated with respect to carbonate	35.22	T37
	20	63-125	5% NH_4Cl solution saturated with respect to carbonate	31.15	T38
50°C	30	250-500	5% NH_4Cl solution saturated with respect to carbonate	37.49, 36.37	T7, T8
			N-Decane	36.17	T12
			Dry	43.41	T11
80°C	30	250-500	5% NH_4Cl solution saturated with respect to carbonate	26.22	T39

[a] σ_1: constant applied stress in MPa
[b] d: grain size in μm
[c] Φ_0: Porosity at the beginning of the creep test in percent
[d] No: Experiment identification number

5.2.2 Uniaxial compression tests

Drained uniaxial compression tests were carried out to study the compaction of carbonate sand. The samples were cylindrical with a radius of 2.5 cm and a height up to 3.1 cm. Two œdometers

were used (Fig. 5.1), one of them was equipped with P- and S–waves receivers and senders, which were glued onto the top and bottom filters.

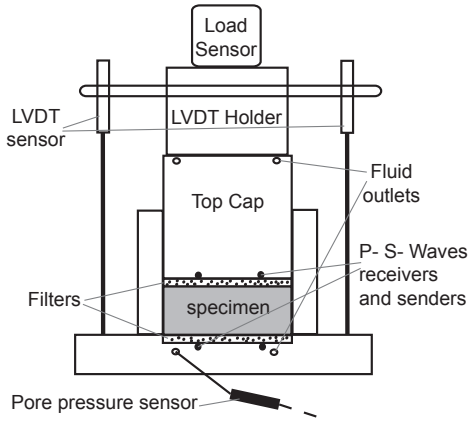

Figure 5.1: Schematic view of an œdometer cell. The top cap is made of titanium grade 5, the rest of the cell is made of stainless steel.

The volume of sand, V_s, poured into the œdometer cell was determined from the known mass of the sample and the assumed grain density, $\rho = 2.7$ g/cm^3. The initial height allowed to determine the initial volume of the samples, V_{ti}. Values of initial porosities, $\Phi_i = (V_{ti} - V_s)/V_{ti}$, are given in Table 5.1.

The load was controlled by a computer so that the vertical stress, σ_1, could be applied automatically at a given loading rate. A pore pressure sensor fixed at the bottom outlet of the œdometer allowed to control the pore pressure, P_p, in the samples. This enabled the determination of the applied effective stress $\sigma_1' = \sigma_1 - P_p$. The pore pressure was always equal to atmospheric pressure, *i.e.* drained conditions. For mechanical compaction tests, the vertical stress was increased from 0 to 32 MPa at a rate of 2 MPa per hour.

In addition, creep tests were carried out at constant vertical stresses of 10, 20 or 30 MPa for about one month. All creep tests were preceded by a mechanical compaction phase where the applied stress was increased to 2 MPa higher than the creep stress. This over–consolidation made the samples mechanically stable. Therefore time dependent deformation observed during creep was mostly due to chemical effects.

Since the samples were confined into a cylindrical steel cell no lateral strain was allowed, therefore the vertical strain, ϵ_1, was equivalent to the volumetric strain, ϵ_v. Strain values were obtained from the vertical displacement values, Def_1 and Def_2, measured by two high resolution displacement sensors (LVDT). Strain values were calculated as follows: $\epsilon_1 = (((Def_1 + Def_2)/2)/(h_i)) * 100$, where h_i was the initial sample's height. For all the measured values, σ_1, Def_1, Def_2 and P_p, one data point per minute was recorded.

Intragranular porosity, Φ_g, was determined from available thin–sections of the compacted

samples, the mean value was found to be Φ_g = 0.27.

The reproducibility of the stress–strain curves obtained was controlled for few experiments. 0.1 % difference in initial porosity for tests T7 and T8 lead to 1 % difference in final strain at 32 MPa stress. The 3 % difference in final strain obtained for T15 and T16 may be related to the 1 % difference in initial porosity. From these observations it was concluded that the results obtained were reproducible and representative of the compaction behaviour of the material used.

5.2.3 Ultrasonic velocity measurements

Compressional and shear wave velocities were measured throughout the tests at regular time intervals using the pulse transmission technique (*Birch*, 1960). P- and S-wave piezoelectric transducers were mounted inside the base and top plates of the triaxial cell to measure P- and S-wave velocities along the plug axis. Resonant frequency of the crystals was 500 kHz. Compressional and shear wave velocities were measured in the range 1000 - 2500 and 500 - 1250 m/s, respectively. Although the resonant frequency of the glued crystals may deviate somewhat from the one of the pure crystal, the wavelength of the ultrasonic pulse is assumed to range from 1 to 5 mm, which is less than the plugs radius. This arrangement is most likely sufficient to avoid diffraction phenomena and unwanted shape mode. The signals were recorded on a computer, and first arrival times were picked manually. Correction for equipment was applied to the P- and S-wave velocities. First arrival times, t_0, were measured when no sample was present in the œdometer. This zero time was then subtracted from the picked traveltime, $t_{p/s}$, measured with a plug present. The plug's compressional or shear wave velocity was then calculated as follows: $V_{p/s} = h_s/(t_{p/s} - t_0)$, where h_s is the height of the sample.

5.2.4 Microstructures observation

After completion of the compaction tests some of the samples were impregnated with epoxy to make thin–sections of the compacted material. The central part of the sample was used for thin–sections, that were then imaged in a JEOL JSM 6460LV scanning electron microscope (SEM). About 30 scanning electron micrographs were taken per samples. Cracks were outlined manually and measured with the help of an image processing software (ImageJ). The median length value and the length distribution of the cracks were then graphically depicted using boxplot display (*Velleman and Hoaglin*, 1981).

5.3 Results

5.3.1 Porosity loss under increasing stress

The effects of pore fluid composition (Figure 5.2A), grain size and mineralogy on the stress–strain relationships were investigated. At effective stress of 32 MPa bioclastic carbonate sand samples were more compressible than crushed calcite samples (Table 5.3). Final strains, ϵ_{32}, obtained in bioclastic carbonate sand ranged from 27.09 to 39.67 %. For crushed calcite samples the range of final strains was narrower with ϵ_{32} between 26.41 and 28.55 %.

Table 5.3: Results of mechanical compaction: values of porosity (Φ in %), strain (ϵ in %) and P- and S–wave velocities (V_p and V_s in m/s) are given for vertical effective stress values of 5, 10 and 32 MPa (subscripts design the effective stress at which the value was taken).

No[a]	Φ_0[b]	Φ_5	Φ_{10}	Φ_{32}	ϵ_5	ϵ_{10}	ϵ_{32}	V_{p5}	V_{p10}	V_{p32}	V_{s5}	V_{s10}	V_{s32}
T23	52.1	43.91	38.45	28.12	14.53	22.02	32.85	1306	1670	2400	713	924	1249
T30	50.8	44.3	39.09	28.63	11.53	19	30.52	1337	1694	2402	699	898	1251
T10	61	55.8	52.14	43.58	11.55	18.22	30.29						
T15	60.7	51.47	46.13	37.05	18.96	27	37.24	1329	1680	2439	670	826	1191
T16	61.7	51.82	46.47	37.2	20.28	28.15	38.42	1267	1598	2356	680	829	1179
T17	61	49.93	44.21	34.85	21.97	29.89	39.67	1282	1620	2309	662	824	1140
T35	55.5	45.34	39.79	29.4	18.4	25.82	36.37	1241	1560	2233	668	840	1174
T18	61.8	51.83	46.48	37.39	20.61	28.45	38.5	1235	1596	2329	682	834	1180
T31	55.7	46.39	41.14	31.4	17.26	24.54	34.92	1232	1555	2250	674	836	1187
T20	53.9	48.48	44.35	34.29	10.39	16.93	29.23	1161	1424	2020	603	759	1068
T22	54.9	48.79	44.54	34.71	11.66	18.33	30.23	1076	1359	1976	593	749	1063
T19	61.2	55.69	51.58	42.25	12.39	19.73	32.35	1229	1531	2126	650	806	1108
T21	53	48.38	44.75	34.97	8.8	14.67	27.09	1208	1506	2125	655	809	1145
T34	59.5	48.48	43.09	33.27	21.38	28.74	38.9	1178	1484	2194	646	799	1142
T29	59	48.29	42.95	33.49	20.86	28.23	38.17	1121	1432	2067	613	773	1085
T33	59.4	47.65	42.27	32.88	22.56	29.69	39.24	1167	1488	2188	632	789	1128
T36	51.1	39.24	35.87	29.21	19.41	23.55	30.36	1080	1396	2065	590	748	1101
T28	58.8	52.93	48.98	39.74	12.51	19.2	31.27	1113	1382	1958	596	747	1046
T32	59.2	52.86	48.83	39.61	13.64	20.37	32.24	1094	1364	1938	606	760	1062
T24	43	35.5	30.21	20.97	11.52	18.12	27.34	1545	1935	2659	835	1026	1403
T26	44.9	37.13	31.91	22.36	12.26	18.9	28.55	1573	1936	2621	809	988	1359
T25	44.5	37.7	33.01	24.03	10.78	16.93	26.41	1579	1937	2609	900	1064	1419
T27	47.5	40.47	35.77	26.71	11.79	18.14	27.88	1498	1861	2530	834	1015	1377
T7	61.5	51.75	46.45	37.52	20.4	28.3	38.6						
T8	60.9	50.9	45.41	36.4	20.98	28.93	39						
T12	54.1	49.63	45.94	36.16	8.8	14.91	27.56	1266	1566	2202		820	1110
T11	60.5	56.31	52.45	43.41	9.74	17	29.99	1297	1614	2209	692	870	1154
T13	44.1	36.25	31.77	23.05	12.29	18.04	27.33						

[a] No: Experiment identification number

[b] Φ_0: Initial porosity

To further investigate the mechanisms leading to porosity loss, the present data were first fitted with the exponential law proposed by *Athy* (1930). This law, often used to describe porosity loss in sedimentary basins, can be expressed as follows,

$$\Phi(\sigma') = \Phi_0 \cdot exp(F\sigma'), \tag{5.1}$$

with Φ the porosity, Φ_0 the initial porosity, and F a compaction factor which value depends upon the sediments compositions (*Royden and Keen*, 1980) and acts as a fitting parameter. Granular media compaction can alternatively be viewed as a progress of the grains from an initial perturbed configuration toward an equilibrium state involving a number of different relaxation phenomena (*Knight et al.*, 1995). Therefore the present data were also fitted by a stretched exponential law, which best describes relaxation in disordered systems (*Philippe and Bideau*, 2002),

$$\frac{\Phi(\sigma')}{\Phi_0} = exp\left(-\left(\frac{\sigma'}{\tau}\right)^{\beta}\right), \tag{5.2}$$

with τ and β two free parameters related to the relaxation phenomena involved. These two existing compaction models were fitted to the present set of data. The root mean square errors, i.e. measurement of the differences between values predicted by the models and the actual values, are displayed in Figure 5.2B. The fits of the data are about twenty times better when using the stretched exponential law.

All the experimental data were collapsed onto a single stretched exponential curve using the relation described in equation 5.2 (Figure 5.2C, D, E). The model fits well the bioclastic sand saturated with non-reactive fluids data. For bioclastic carbonate sand saturated with reactive fluids and crushed calcite the model initially deviates from the observed data, indicating that several mechanisms may be responsible for porosity loss at short time scale. However, the model fits well all the data after this initial stage. Different values of τ and β were attributed to each experiment in order to obtain the best fit possible. Values of τ range between 61–96 MPa for experiments in which the samples were saturated with reactive fluids, between 87–147 MPa for samples saturated with non reactive fluids, and between 47–68 MPa for calcite samples. Values of β range between 0.58–0.74 for samples saturated with reactive fluids, between 0.68–0.80 for samples saturated with non-reactive fluids, and between 0.64–0.72 for calcite.

Effect of the pore fluid chemistry

For all the grain sizes tested, bioclastic sand was more compressible when saturated with reactive fluids (e.g. fine bioclastic carbonate sand in Figure 5.2A). The difference between strain, ϵ, obtained in samples saturated with reactive fluids and strain in samples saturated with non–reactive fluids increased up to a vertical stress of 2 to 3 MPa. At effective stress greater than 2–3

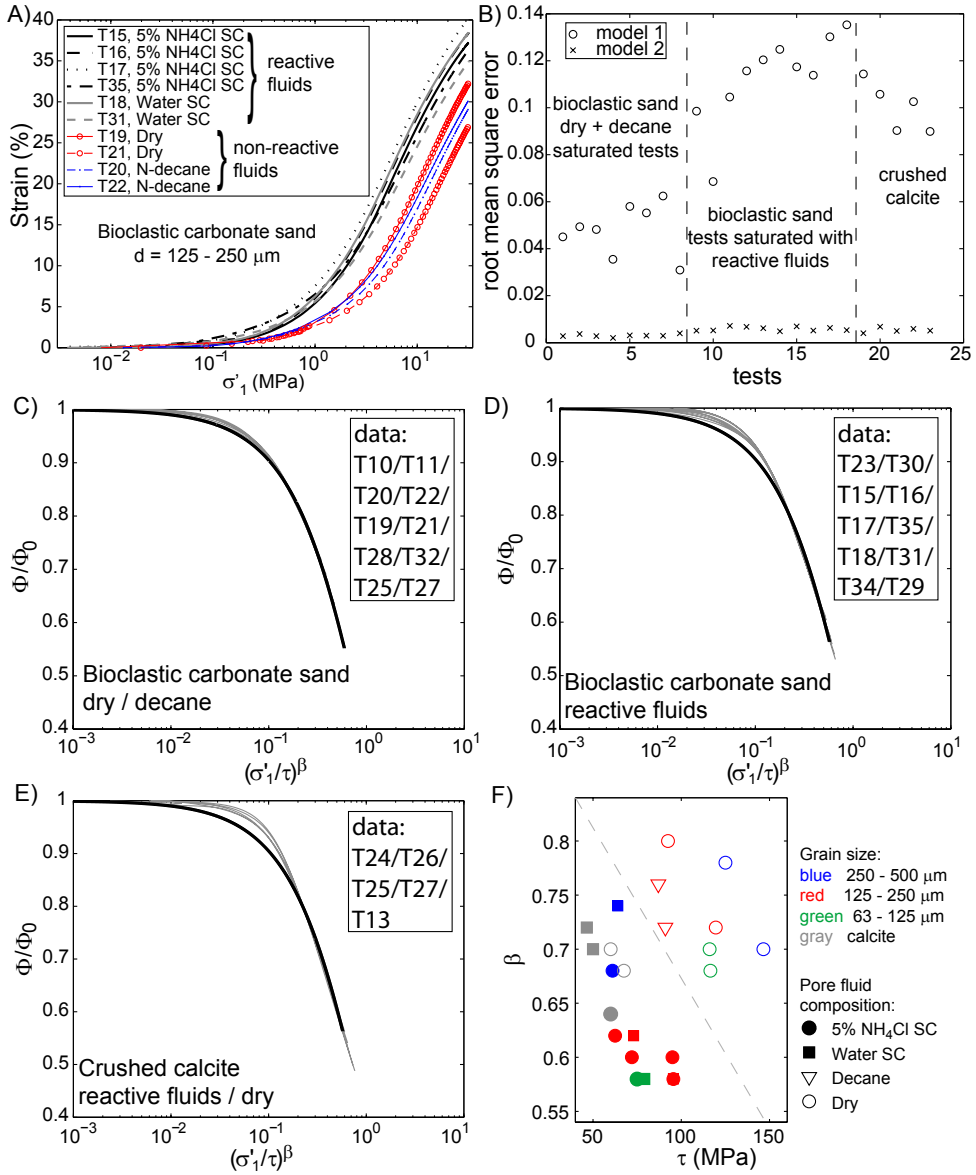

Figure 5.2: A) Example of stress–strain relationship obtained during mechanical compaction (SC = saturated with respect to carbonate). B) Comparison of the root mean square errors obtained when fitting equations 5.1 (model 1) and 5.2 (model 2) to the present experimental data. Data (gray lines) collapsed using the exponential stretched model (black line) for C) bioclastic sand saturated with non–reactive fluids, D) bioclastic sand saturated with reactive fluids, E) crushed calcite samples. F) τ and β fitting parameters used to collapsed the data onto a single curve.

MPa $\epsilon_{reactive fluid} - \epsilon_{non-reactive fluid}$ is rather constant. Bioclastic carbonate samples tested saturated with reactive or non–reactive fluids could be discriminated from each other using values of β and τ obtained by fitting the data with equation 5.2 (grey dashed line in Figure 5.2F).

In crushed calcite samples, unlike bioclastic carbonate sand, very little increase of compaction was observed in tests carried out with water saturated with respect to calcite compared to those conducted dry. 2 % more strain at 32 MPa occured in T26 (water saturated with respect to calcite) compared to T25 (dry) (Table 5.3). No definite difference between reactive and non-reactive fluids was found for the β and τ values (Figure 5.2F).

Another feature was that samples saturated with glycol compacted more than samples saturated with decane (Table 5.3).

Effect of grain size

In dry tests, grain size does not have a significant effect on the stress–strain relationship (Figure 5.3A). In bioclastic carbonate sand saturated with reactive fluids, compressibility is greater in finer samples (Figure 5.3A, B). The effect of grain size on crushed calcite samples was not tested.

The initial grain rearrangement process in samples having an initial porosity greater than 60% is most likely greater than in samples starting with lower porosity. This influenced their overall compaction curve. Samples with initial porosity Φ_0 <60% show a good correlation between strain and grain size (Figure 5.3B). This correlation could be expressed as:

$$\epsilon = C\frac{1}{d^n}, \tag{5.3}$$

with ϵ the strain in percent, d the mean grain size in micrometer, and C a constant. The grain size exponent, n, slightly decreased with increasing stress, n = 0.35, 0.24, 0.14, at effective stresses of 5, 10 and 32 MPa respectively (Figure 5.3B).

While no correlation was found between grain size and β (eq. 5.2) for samples saturated with non–reactive fluids, β increased with grain size in samples saturated with reactive fluids (Figure 5.3C).

Microstructures in the bioclastic carbonate sand

Grain crushing or collapse of the internal grain structure on the edge of bioclastic carbonate grains was observed in thin–sections (Figure 5.4C, D). The internal porosity remained unchanged in the centre of each grain, while at the grain–to–grain contact internal porosity was drastically reduced. This edge deformation mechanism seems to be mainly mechanical since

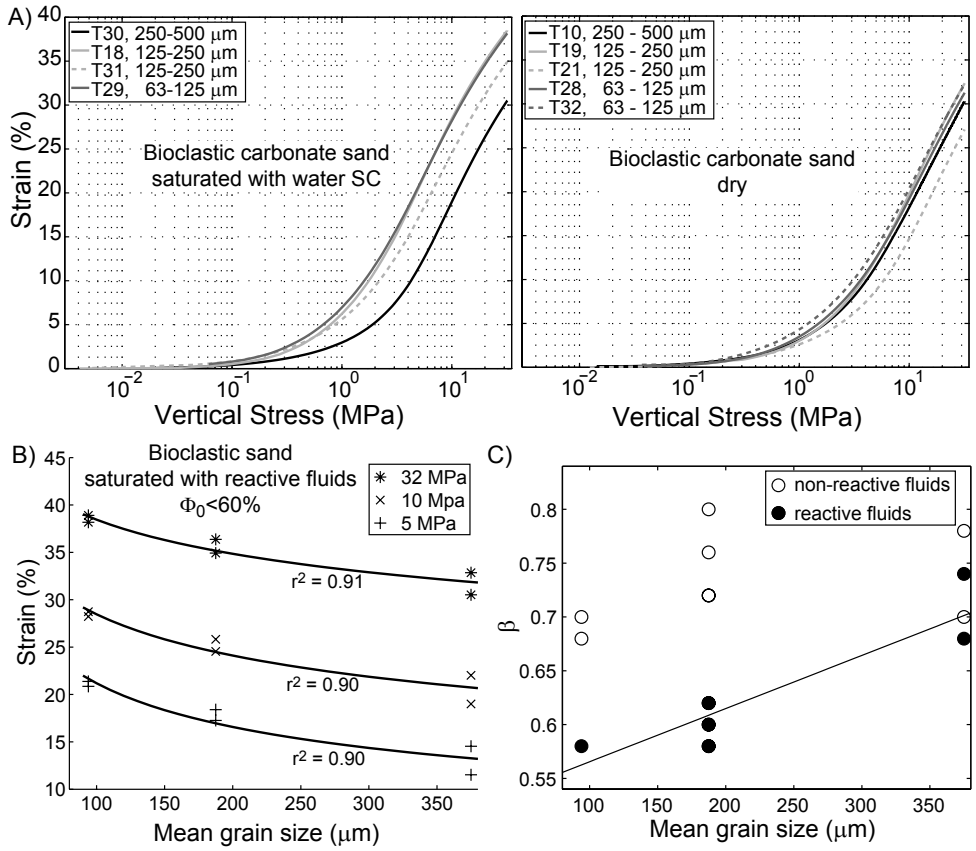

Figure 5.3: A) Effect of the grain size on stress–strain curves for bioclastic sand either saturated with water saturated with respect to carbonate (SC) or dry. B) Strain–grain size relationship (eq. 5.3) for samples with an initial porosity lower than 60%. C) β (eq. 5.2) as a function of grain size for both samples saturated with reactive and non-reactive fluids.

samples compacted dry and samples saturated with reactive fluids show about the same deformation pattern. The crushed rims appear, however, slightly thicker in samples saturated with reactive fluids (Figure 5.4C, D). In crushed calcite samples the crack density is higher compared to the bioclastic carbonate samples (Figure 5.4B).

Thin–sections also showed that crack propagation occurred during experiments (Figure 5.4E). Crack length correlated positively with carbonate solubility in the different fluids used (Figure 5.4F), which might be an indication that subcritical crack growth was active (*Anderson and Grew*, 1977).

Ultrasonic velocity measurements under increasing stress

P- and S-wave velocities increased with increasing stress and decreasing porosity, for all grain sizes and pore fluid compositions tested (Table 5.3). The incerase of P- and S–waves with decreasing porosity was linear. V_p ranged from 705 to 2440 m/s and V_s from 535 to 1250 m/s. In Figure 5.5 (A, B, C), V_p, V_s and bulk moduli are displayed as a function of porosity for ten samples. The samples can be split in two groups characterised by different initial porosities. Even though the initial sample porosities were different, the initial velocity measurements are similar indicating a strong effect of the applied vertical effective stress on the ultrasonic velocity measurements.

At a given vertical effective stress, bulk moduli of samples saturated with reactive fluids are greater than bulk moduli of samples saturated with non–reactive fluids (Figure 5.5C). The two different initial porosity groups show the same bulk modulus–porosity relationship.

To investigate further the effect of effective stress, pore fluid composition, and porosity on the propagation of ultrasonic waves in the present bioclastic carbonate sand, data were compared to a rock–physics porous–grain soft–sand model (PGSO) similar to the model described by *Ruiz and Dvorkin* (2009) (Figure 5.5D). This model considers the samples as a pack of elastic porous grains. The effective bulk and shear moduli of the dry granular frame, K_{dry} and μ_{dry}, were obtained from equations 3–5 in *Ruiz and Dvorkin* (2009). The Hertz-Mindlin moduli at the critical porosity, Φ_c = 0.4, were calculated using a coordination number of 5 (see eq. 4 in *Ruiz and Dvorkin* (2009)). Effective bulk and shear moduli of the porous grains, K_g and μ_g, were determined using the differential effective medium model (*Norris*, 1985; *Mavko et al.*, 2009). In the present study, the inclusion were considered as spherical and the coupled system of differential equations was solved using spheres inclusion shape coefficients (*Berryman*, 1995; *Mavko et al.*, 2009). The inclusions volumetric concentration was set equal to the internal porosity of the grain, Φ_g, and were filled with water. Saturated bulk moduli, K_{sat}, were

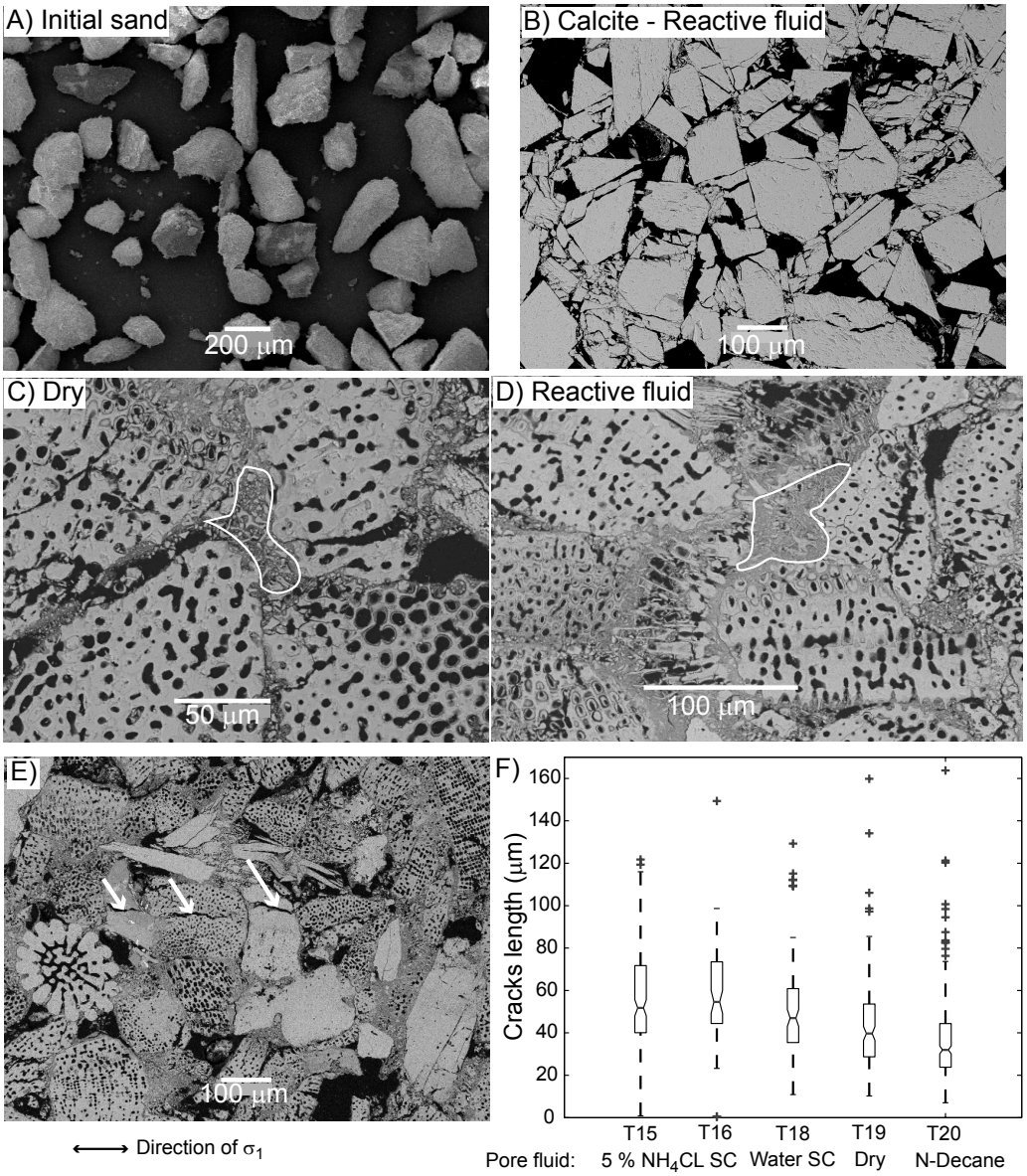

Figure 5.4: Microstructures observations. A) bioclastic carbonate sand of grain size 125–250 μm before exeriments. Grain crushing at the grain–to–grain contacts after mechanical compaction in B) calcite sample, C) dry bioclastic carbonate sample, D) bioclastic carbonate sample saturated with reactive fluid. E) Scanning electron micrograph of sample T18. The arrows point out the cracks parallel to the main stress axis. F) Box plots showing the mean crack length for samples T15, T16, T18, T20 and T19, i.e. bioclastic carbonate sand samples with grain size 125–250 μm.

calculated following *Gassmann* (1951) fluid substitution theory.

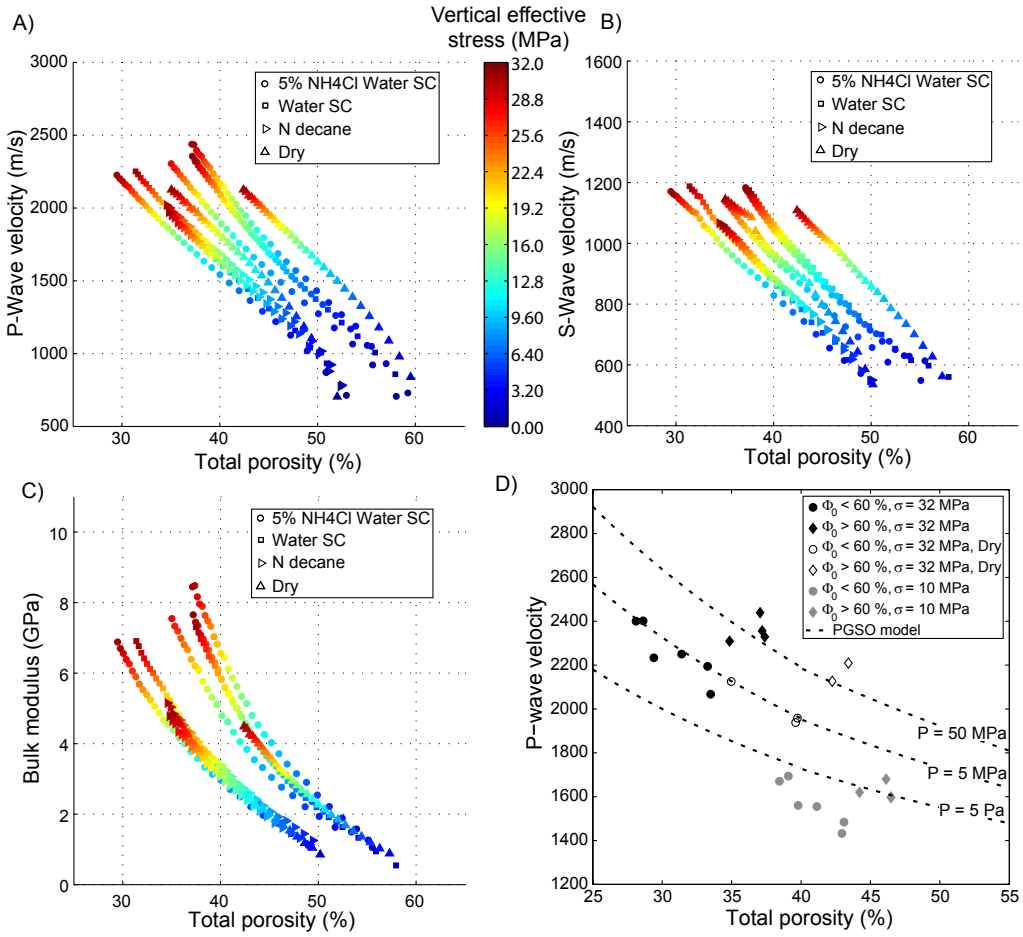

Figure 5.5: From A to C, P–wave velocities, S–wave velocities and bulk moduli as a function of porosity for bioclastic carbonate sand (d = 125–250 μm) saturated with various fluids. The colour fill represents the applied vertical effective stress. D) P–wave velocity for all the samples tested as a function of total porosity. Samples saturated with reactive fluids are filled in black (σ_1 = 32 MPa) or in gray (σ_1 = 10 MPa), dry samples are unfilled. Dashed lines correspond to results obtained with the PGSO model (*Ruiz and Dvorkin*, 2009).

At effective stress greater than 10 MPa, it was possible to compare the present data to the PGSO model (Figure 5.5D). P–wave velocities at 32 MPa effective stress were plotted against porosities for samples saturated with reactive fluids and dry samples (Figure 5.5D). The plot shown in Figure 5.5D separates data into two groups. The first group (tests T19, T15, T16 and T18) have initial porosities greater than 60%, while the second group (tests T20, T21, T22, T31 and T35) have porosities lower than 60% (Table 5.1). The PGSO model was used to fit the data varying values of differential pressures, P, acting on the grains from 5 Pa to 50 MPa. Samples with greater initial porosities display higher P-wave velocities and could be fitted by a PGSO model with $P = 50$ MPa, while a P equal to 5 Mpa fitted the samples having initial porosities lower than 60%. The dry samples had less porosity and lower P-wave velocity but

could be fitted the same way than the saturated samples having velocity lower than expected by the theory.

P- and S–wave velocities increased with increasing grain size in both bioclastic carbonate sand and crushed calcite samples (Figure 5.6 A, B, C, D). A positive correlation exists between the P–wave acoustic impedance, $I_p = V_p \cdot \rho$, and grain size,

$$I_p(\sigma) = A + BLog(d); \tag{5.4}$$

where $I_p(\sigma)$ is the P–wave acoustic impedance at a given stress and d the mean grain size. Good correlation was obtained for samples saturated with reactive fluids (Figure 5.6E). No satisfactory relation between acoustic impedance and grain size was found for the dry samples.

5.3.2 Creep

Table 5.4: Creep results: values of strain and P- and S-wave velocity after 40, 100 and 250 hours of creep. Values of the fitting parameters α and p

No	ϵ_{40h}	ϵ_{100h}	ϵ_{250h}	α[a]	p[b]	V_{p40h}	V_{p100h}	V_{p150h}	V_{s40h}	V_{s100h}	V_{s150h}
T23	0.19	0.28	0.40	0.11	0.65	2521	2545	2575	1304	1317	1330
T6	0.09	0.15		0.05							
T35	0.46	0.59	0.72	0.21	0.90	2347	2395	2423	1323	1244	1256
T34	0.62	0.80	0.98	0.27	0.92	2307	2343	2395	1197	1228	1244
T33	0.47	0.59	0.73	0.20	0.89	2301	2338	2372	1170	1197	1223
T36	0.34	0.42	0.50	0.14	0.95	2162	2174	2222	1136	1163	1175
T37	0.12	0.16	0.21	0.06	0.83	1693	1707	1713	867	875	888
T38	0.27	0.35	0.47	0.12	0.87	2084	2109	2156	1094	1100	1116
T7	0.43	0.65	0.91	0.25	0.75						
T8	0.47	0.68	0.92	0.25	0.75						
T39	0.31	0.42	0.52	0.14	0.87	2493	2552	2617	1276	1296	1309

[a] α_j in equation 5
[b] p in equation 7

Effect of pore fluid composition, grain size, temperature, and stress

No deformation was observed during creep of samples saturated with non–reactive fluids, i.e. air or decane. Significant deformation was, however, observed in samples saturated with a solution of 5% NH_4Cl water in equilibrium with carbonates or in samples saturated with glycol or anisole. The amount of strain found in samples saturated with reactive fluids increased with water saturation (Figure 5.7A, B), applied stress (Figure 5.7C), and decreasing grain size (Figure 5.7D). Only a minor temperature effect was observed on samples saturated with reactive

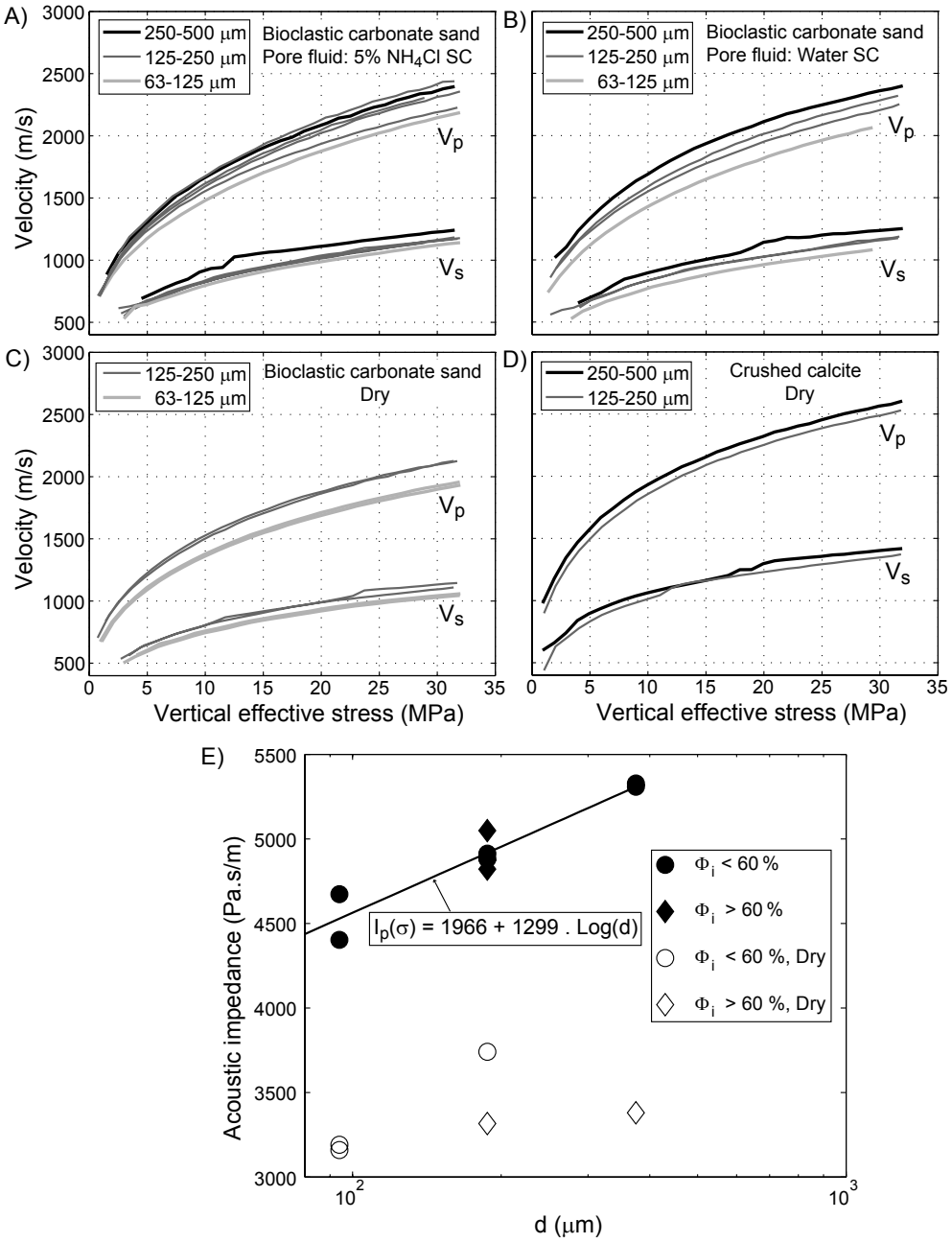

Figure 5.6: Effect of grain size on V_p and V_s as a function of stress for A–B) bioclastic carbonate sand saturated with reactive fluids; C) dry bioclastic carbonate sand and; D) dry crushed calcite. E) Acoustic impedance at 32 MPa vertical effective stress as a function of grain size for dry samples and samples saturated with reactive fluids.

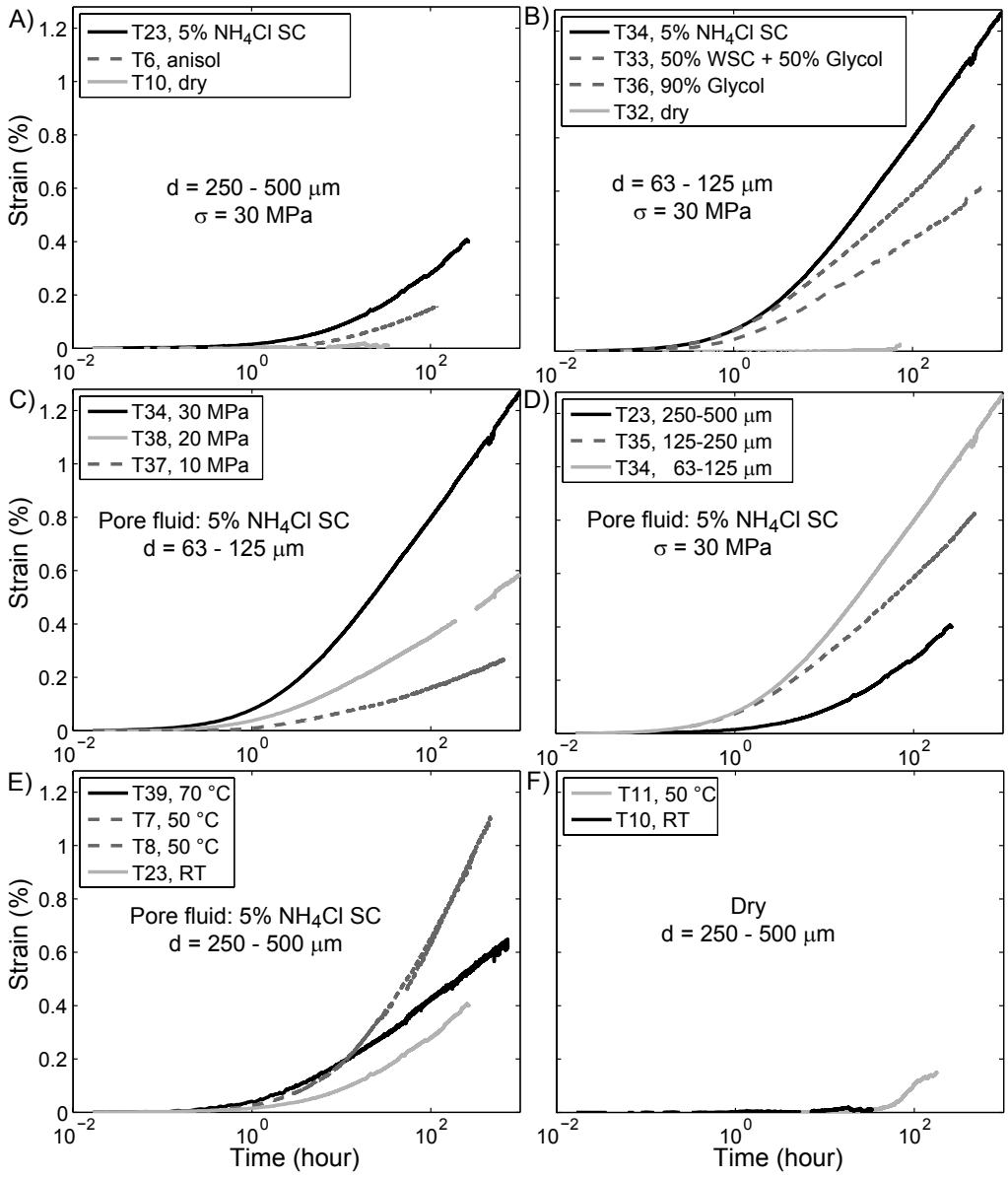

Figure 5.7: Strain versus time (logarithm scale for the time) for creep of bioclastic carbonate sand. If not specified, the tests were run at room temperature. A– B) Effect of the pore fluid composition for two different grain sizes; C) Effect of applied vertical effective stress; D) Effect of the grain size; E–F) Effect of the temperature.

fluids (Figure 5.7E), and no effect was observed on the dry samples (Figure 5.7F), the range of temperatures used in the various experiments was small, however.

Both magnesium and calcium concentration increased in the pore water during the water saturated tests (Table 5.5). The $[Mg^{2+}]/[Ca^{2+}]$ ratio in the pore water also increased resulting in a relative build–up of magnesium concentration in the pore water.

Table 5.5: Water Analyses. Concentration are given in ppm.

No	Mg^{2+}	Ca^{2+}	Na^{+}	K^{+}	Alk.[c]
T7 before tests	60	161	35	3.3	14.40
T7 after tests	244	243	250	15	
T8 before tests	28	150	8	0.73	15.16
T8 after tests	208	208	197	11.6	
T35 before tests	81	213	280	12.7	
T35 after tests	211	165	1300	63	
T38 before tests	67	353	132	9	
T38 after tests	261	540	790	57	

[c] Alkalinity in meq/L

In glycol or anisole saturated samples, the measured strain values were intermediate between dry samples and samples saturated with a solution of 5% NH_4Cl water in equilibrium with carbonate (Figure 5.7, Table 5.4). Increasing the water/glycol ratio also enhanced compaction.

To better understand the parameters controlling creep in the present study the entire dataset was fitted with a power law of time, t, (Figure 5.8A),

$$\epsilon_j(t) = \alpha_j t^{\theta}, \tag{5.5}$$

with j comprised between 1 and 11, the number of creep experiments taken into consideration. In the present study the time exponent θ is close to 0.23 for all experiments. The compaction parameter, α_j, was used as a scaling parameter to collapse all the data on the theoretical curve (black line Figure 5.8A) for which α = 1. Since α is a time independent factor, it is possible to quantify the respective influence of the tested parameters alone (*Renard et al.*, 2001).

Grain size, d, vertical effective stress, σ, and water saturation, w, affected creep of bioclastic carbonate sand in various ways (Figure 5.8, Table 5.4). The compaction parameter, α, could be expressed as a function of the above mentioned parameters as follows,

$$\alpha = c_1 \cdot exp(c_2 \cdot d + c_3 \cdot \sigma) + c_4 w + c_5, \tag{5.6}$$

with c_1, c_2, c_3, c_4, and c_5 material dependant constants. Creep deformation was mostly affected by grain size, then by the applied vertical effective stress and to a lesser extent by the water

concentration resulting in the following ranking of equation 5.6 parameters: $c_2 >> c_3 >> c_4$ (Figure 5.8B, C, D).

The samples compacted at 50 and 70 °C both showed more creep than the sample compacted at room temperature (Figure 5.7E and Table 5.4). More deformation was observed in samples at 50 °C than the one at 70 °C probably related to higher initial porosities in tests T7 and T8. Tests T23 and T39 with similar starting porosity also showed a similar creep development. However, the temperature effect was rather small, with α increasing from 0.11 to 0.14 for T increasing from 22 °C to 70 °C.

For power law creep, with a low value of the exponent, there is for some materials a possibility that the creep does not behave as a power law, but rather like a logarithm in time. To test this hypothesis, the strain rates (with a slope of -1 in the case of logarithmic creep) rather than the strain should be fitted. This hypothesis was tested. The strain rates, $\partial\epsilon/\partial t = \dot{\epsilon}$, decreased from 1.26 10^{-3} - 1.97 10^{-4} to 1.71 10^{-4} - 1.69 10^{-6} min^{-1}.

In the present study, a linear strain rate decrease in the log-log space as a function of time was observed after 200 minutes of creep (Figure 5.8E), and could be expressed as a power law,

$$\dot{\epsilon} = Et^{-p}, \tag{5.7}$$

with p the strain rate decay exponent and E a constant. The strain rate decay exponent p was somewhat affected by the different parameters tested (Figure 5.8F), but was always significantly smaller than 1 (Table 5.4), indicating that the power law in time best represent the best fit.

Ultrasonic velocity measurements during creep

During creep tests, P- and S-wave velocities increased linearly with strain, $V_{p/s} = a\epsilon + b$. The V_p to V_s ratio stayed constant during creep tests and was comprised between 1.9 and 2.0 for all the tests. The effects of pore fluid, grain size, and applied uniaxial stress on velocity is shown in Figure 5.9. S–wave velocity was not affected by the pore fluid composition, and was influenced in a similar way as P–wave velocity by grain size and applied stress. Samples saturated with water or with a mixture of 50% water and 50% glycol had the same P–wave velocity while the samples saturated with 97% glycol showed lower velocities (Figure 5.9A). V_p increased of 8% in water saturated samples (T34, T33) from the end of the loading phase until 250 hours of creep. For the same period of time, a smaller velocity increase was observed when the sample was saturated with 97% glycol, *i.e.* 7% increase in test T36 (Table 5.4).

As observed during the initial mechanical phase of the tests, P- and S-wave velocities increased with increasing grain size and stress (Figure 5.9B, C). However, compaction being

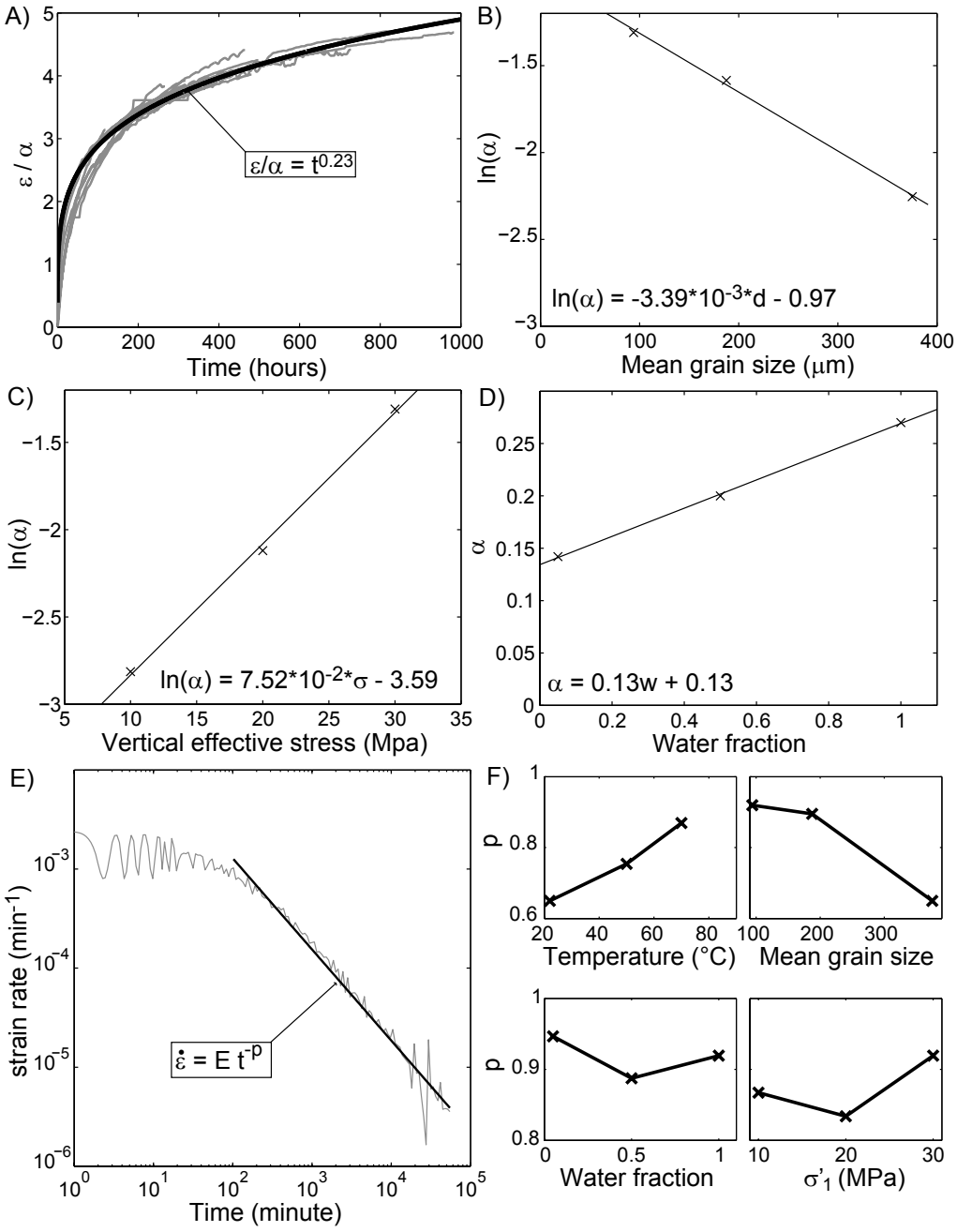

Figure 5.8: A) Data collapsed onto a single curve and fitted by equation 5.5. B) α as a function of effective uniaxial stress; C) α as a function of mean grain size; D) α as a function of water fraction. E) Strain rate versus time (log–log plot) for creep test T34. F) p exponents as a function of parameters tested.

faster in finer grained samples, velocity also increased faster, *i.e.* 8.4% increase from the end of the loading phase to 250 hours of creep in T34 against 6.8% in T23 (Table 5.4).

5.4 Discussion

5.4.1 Porosity loss with increasing stress

Effect of carbonate dissolution

The amount of chemical compaction is given by the difference between the strain in samples saturated with reactive fluids and the lower strain in samples saturated with non–reactive fluids. Chemical compaction rate being controlled by diffusion or reaction kinetics, its observed amount is therefore related to the loading rate used (2 MPa/h), *i.e.* slower loading rate would produce greater difference between compressibility of samples saturated with reactive and non–reactive fluids. More chemical compaction was observed in bioclastic samples than in crushed calcite samples. This is probably related to the fact that calcite is both thermodynamically more stable and less soluble than magnesian calcite (*Morse and Mackenzie*, 1990; *Stumm and Morgan*, 1996), and that the surface area available for chemical reaction was higher in the bioclastic carbonate sand. This suggests that at least part of the chemical compaction observed in bioclastic carbonate samples is related to carbonate dissolution. An other indication for active dissolution in the present study is that in samples saturated with reactive fluids the compressibility increased with decreasing grain size (Figure 5.3B, C). In finer grain–sized samples the mean coordination number is higher than in coarser samples (*Lange*, 1984), resulting in the observed increased dissolution in fine-grained samples saturated with a reactive fluid, *i.e.* pressure solution.

Effect of stress corrosion

Cracks propagated parallel to the main stress axis and the length of the cracks correlated positively with grain solubility and was therefore depending on the nature of the fluid (Figure 5.4C, D). Crack propagation occurred faster in water saturated samples. In addition, compressibility of bioclastic sand was higher in the presence of glycol than decane (Table 5.3). Subcritical crack growth occurs in brittle material at stresses lower than the critical fracture stress, and is sensitive to the fluid present (*Atkinson*, 1982). The material resistance to crack, G, is a function of the surface energy, γ such that $G = 2\gamma$. Therefore, lowering the surface energy facilitates crack propagation (*Olagnon et al.*, 2006). The surface energy of carbonates is lowered by adsorption

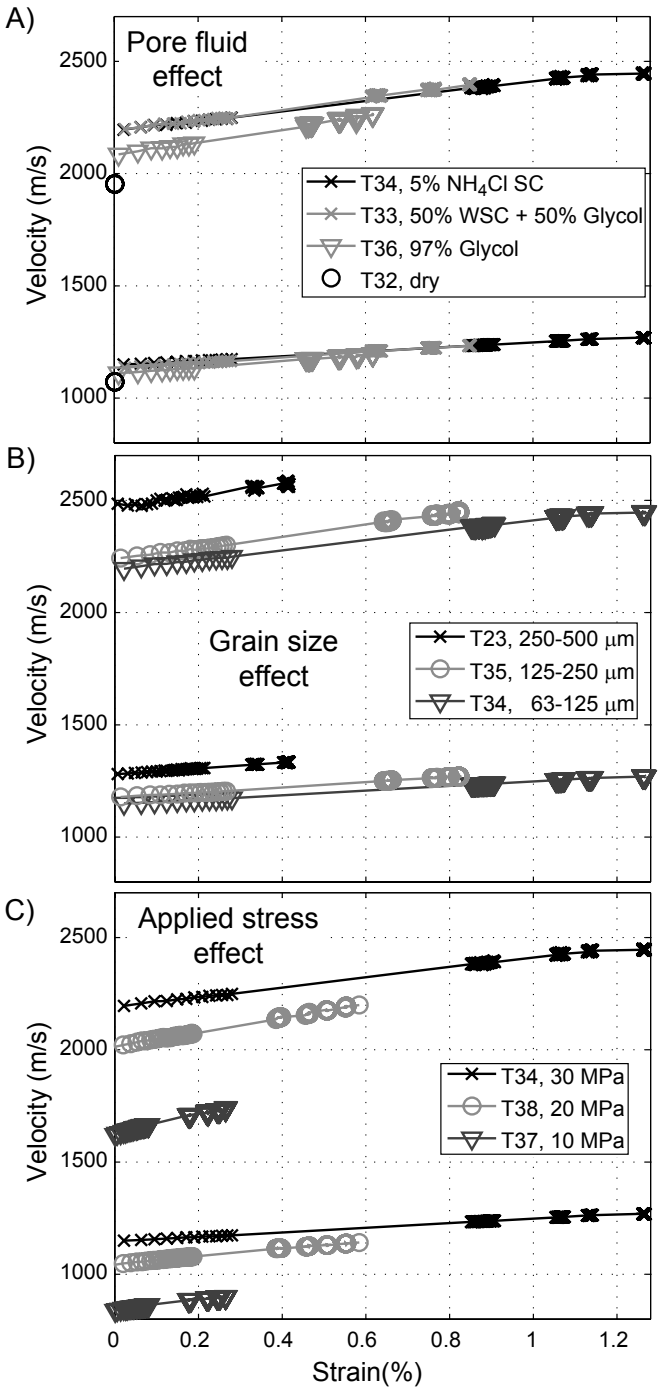

Figure 5.9: V_p and V_s as a function of strain at constant stress. Effect of the pore fluid, grain size and applied stress.

of water onto the mineral surface and creation of chemical bounds between Ca in carbonate and O in water (*Cygan et al.*, 2002). Glycol contains two hydroxyls groups probably resulting in formation of a similar $Ca - O$ bound as in water, which lower the surface energy. Formation of similar bounds is not possible between decane or air and calcite surfaces and explains why the cracks length was smaller in these fluids.

Effects at the grain contacts

For the bioclastic sand material, the internal grain porosity collapsed at the rim of the grain–to–grain contacts (Figure 5.4). This mechanism was active in all bioclastic carbonate sand experiments and independent of the pore fluid composition. The amount of grain crushing related to this mechanism seems, however, to be greater in samples saturated with reactive fluids (Figure 5.4A, B). Note that collapse of porous shell structures was described as a compaction mechanism in naturally occurring limestones (*Meyers*, 1980).

Compaction laws

All the compaction curves were fitted by a stretched exponential law (eq. 5.2), also named the Kohlraush–Williams–Watts (KWW) law. Even though this law has been widely used to describe compaction in material science, it has traditionally not been used in rock physics. The KWW law fitted well the tests carried out on bioclastic carbonate samples saturated with non–reactive fluids (Figure 5.2C), *i.e.* the purely mechanical part of the compaction. This is in agreement with the fact that the KWW law is also used to describe relaxation in non–cohesive granular media (*Richard et al.*, 2005). Relaxation can be described as a set of processes driving the grains from an initial low density state toward a more stable higher density packing (*Philippe and Bideau*, 2002). During compaction of sand, relaxation occurs mainly by collective particle motion and grain sliding, *i.e.* grain rearrangement (*Ben-Naim et al.*, 1998; *Philippe and Bideau*, 2002), those are therefore most likely dominant mechanisms of deformation during mechanical compaction of the present bioclastic carbonate sand.

The onset of grain crushing is assumed to start at the intersection between the two linear parts of the $\epsilon = f(log(\sigma))$ curve (Figure 5.2A), that is around 2 to 3 MPa effective stress. Early initiation of grain crushing during compaction of carbonate sand was also observed by *Chuhan et al.* (2003). Grain crushing was most likely the process explaining deviation of the present experimental compaction curves from the KWW law.

An important result is that initial porosity is an important parameter controlling further compaction (Figures 5.2C, D, E and 5.3B). The initial geometrical configuration of the grains

determines the amplitude of the large scale grain rearrangements (*Caglioti et al.*, 1997) and thus the amount of final relaxation. This result supports suggestion from earlier studies that initial porosity needs to be taken into account to predict subsequent compaction (*Royden and Keen*, 1980; *Sclater and Christie*, 1980).

Since both calcite and bioclastic carbonate sand could be fitted by the same law, this suggests that compaction of other type of sediments could also be fitted by the KWW law. Also to be mentioned, the range of values for the β parameter is rather narrow, 0.6-0.7, for bioclastic sand saturated with reactive fluids. To fit larger carbonate compaction datasets with the KWW law, a mean value of β could be used. As a result, only one free parameter, τ, would be necessary to describe carbonate compaction using the KWW law.

5.4.2 Creep

Chemical effects

The absence of observable creep in samples saturated with non–reactive fluids, while strain was observed in samples saturated with reactive fluids, indicate that creep was due to chemical reactions (Figure 5.7). The significant increase in both Mg^{2+} and Ca^{2+} concentrations in the fluid after tests also shows that dissolution of magnesian calcite occurred during experiments (Table 5.5). In addition the Mg^{2+} concentration increased about 2 times more than the Ca^{2+} concentration during the tests (Table 5.5). Taking into account the stoichiometric dissolution of the bioclastic carbonates, about 5 times more Ca^{2+} than measured should be present in the pore fluid. This significant build–up of Mg^{2+} relative to Ca^{2+} indicates active calcite precipitation/cementation in the bioclastic system during creep.

Chemical compaction rheology: interplay between pressure solution creep and stress corrosion

All the data could be fitted by a power law (eq. 5.5) with a single exponent (Figure 5.8A), in a similar way as done by *Renard et al.* (2001) for salt aggregates compacting by pressure solution. The time exponent $\theta = 0.23$ is different than the traditional exponent of 1/3 expected for Andrade creep. However, this Andrade exponent may depend on the active deformation process (*Vishnevskii et al.*, 1989). Several studies in material science, where sample were deformed under compression in a creep regime showed similar power-law, with an exponent varying between 0.18 and 0.5 (*Chari*, 1967; *Greener et al.*, 1980; *Vishnevskii et al.*, 1989).

The time independent compaction parameter (α_j in eq. 5.5) increased with decreasing grain

size (Figure 5.8B). The increase of strain rate as a function of decreasing grain size is characteristic of various creep processes, among them pressure solution (*Weyl*, 1959). The strong influence of the grain size on α is in agreement with pressure solution models in which the relaxation time constant is strongly dependent on the mean grain diameter (*Revil*, 1999; *Revil et al.*, 2006). As opposed to pressure solution, the rate of aggregate compaction resulting from subcritical crack growth should be proportional to the grain size (*Cruden*, 1970; *Chantikul et al.*, 1990). The compaction parameter, α, was found to increase with both stress and water concentration (Figure 5.8C, D). Pressure solution and subcritical crack growth are sensitive to stress in a similar way (*Charles*, 1958; *Lehner*, 1990). Both processes were most likely active in the present study since significant creep was observed not only in samples saturated with fluids where calcite is soluble, like water, but also in samples saturated with glycol or anisole in which calcite is hardly soluble. The comparison between the 50/50 mixed water/glycol T33 test and the 3/97 mixed water/glycol T36 test (Figure 5.7B) indicates that pressure solution is a more effective deformation process than subcritical crack growth in water based systems. While subcritical crack growth will dominate when samples are saturated with either anisole or glycol.

In the present study final strain rates range from $2.82 \cdot 10^{-8}$ to $2.85 \cdot 10^{-6}$ sec^{-1}. Earlier experimental studies of carbonate creep found strain rates comprised between $1.24 \cdot 10^{-9}$ and $3.49 \cdot 10^{-8}$ sec^{-1} when pressure solution is responsible for the compaction (*Zhang and Spiers*, 2005; *Zubtsov et al.*, 2005) and between $2.29 \cdot 10^{-8}$ and $1.86 \cdot 10^{-6}$ sec^{-1} when compaction is due to interactions between pressure solution and subcritical crack growth (*Liteanu and Spiers*, 2009; *Croizé et al.*, 2010). Based on these previous studies, the rates found in the present study indicate that both pressure solution and subcritical crack growth were active during creep.

Comparison with relaxation processes in fault zones

Strain rate decay as a function of time during primary creep can be described by different power laws, *e.g.* Omori's law for earthquakes (*Omori*, 1894) or Andrade's law for metals (*Andrade*, 1910) and many industrial materials (*Chari*, 1967; *Greener et al.*, 1980; *Vishnevskii et al.*, 1989). The value of the time exponent p is usually lower than one. In the present experiments, the strain rate decay can be expressed as a power law (eq. 5.7, Figure 5.8E), with p ranging from 0.65 to 0.95, having a mean value of p = 0.85. This value is comparable to the one found in models of primary creep in brittle rocks (*Amitrano and Helmstetter*, 2006). Similar variations of the p exponent are also observed when fitting afterslip and aftershock data with the Omori law (*Schaff et al.*, 1998; *Helmstetter and Shaw*, 2009). These studies showed that post-seismic relaxation, i.e. fault afterslip, can be described with a p exponent similar to the one describing relaxation of

bioclastic carbonate sand or various granular material during creep in compression. However, it is difficult to conclude if the mechanisms are the same in such various and different systems.

5.4.3 Ultrasonic velocities

At low stresses, V_p measurements lower than 1500 m/s may be partly explained by a small under–saturation (*Knight et al.*, 1998), in the present case the skeletal grains internal porosity may not have been completely filled with water. However, this is not sufficient to explain the low velocity obtained. It is also difficult to understand the fact that velocities of samples saturated with reactive fluids are lower than velocity of dry samples. A possible explanation can be related to the dissolution at grain contacts of carbonates saturated with reactive fluids. At the same effective stress, samples saturated with reactive fluids were more compressible than samples saturated with non-reactive fluids. The link between compressibility and chemical processes made in the previous section must therefore be taken into account while interpreting the present ultrasonic velocity measurements. Crack propagation may also lower elastic wave velocity (*Couvreur et al.*, 2001), and reactive surface areas lower grain contact stiffness (*Vanorio et al.*, 2010), which might also explain lower velocity measurements in samples saturated with reactive fluids (Figure 5.5A, B).

The measured ultrasonic velocities were dependent on the actual effective stress values (Figure 5.5A, B). This known effect (*Hughes and Kelly*, 1953) is outlined by the fact that several samples of the present study having different porosities show similar velocities when subjected to the same effective stress (Figure 5.5A, B). This effect is even more clear when looking at the bulk modulus (Figure 5.5 C). P-wave velocities at specific stresses where plotted against porosity (Figure 5.5D) to better investigate the velocity-porosity relation. Fitting the experimental data to the existing PGSO rock–physics model shows that the initial porosity should also be taken into account to predict the P-wave velocity–porosity relation (Figure 5.5D).

The velocity increase observed in coarser grained samples (Figure 5.6) can be explained by the presence of larger contact areas in coarser samples (*Sutton et al.*, 1957). In samples saturated with reactive fluids, the positive correlation found between P–wave acoustic impedance and grain size (Figure 5.6D) might be linked to the positive correlation between β and grain size (Figure 5.3C). No such correlation was found in dry samples (Figures 5.6D and 5.3C).

During creep tests the V_p to V_s ratio remained constant, in the range between 1.9 and 2.0. This is in agreement with other studies and allows differentiation between limestones and sandstones having lower velocity ratio (*Assefa et al.*, 2003). Both during loading and creep phases velocity increased linearly with decreasing porosity, a feature in agreement with other studies

of carbonate (*Nolen-Hoeksema et al.*, 1995; *Wang*, 1997).

5.4.4 Implications for porosity prediction in sedimentary basins

In the present study, chemical compaction was active during the loading phase enabling the separation between mechanical and chemical compaction. Since chemical compaction is strongly time dependent, its amount depends upon the loading rate resulting in more chemical compaction with lower loading rate. This agrees with field observations where mechanical compaction patterns correlate positively with the sedimentation rate (*Scholle and Halley*, 1985).

The compressibility of bioclastic carbonate sand was significantly higher when saturated with reactive fluids than when saturated with non-reactive fluids. This difference was not as marked for the crushed calcite samples. This illustrates that initial compaction of carbonates is highly dependent on the primary mineralogy. If the sediments are initially composed of unstable minerals, aragonite dissolution and precipitation of calcite will occur independently of stress (*Morse and Mackenzie*, 1990). This is also true for magnesian calcite if Mg^{2+} is removed or precipitated as dolomite. If such cementation occurs a mechanically stable framework may be produced preventing further mechanical compaction (*Kopaska-Merkel et al.*, 1994; *Croizé et al.*, 2009). However, in the case of thermodynamically stable low–magnesium calcite sediments like planktonic forams or coccolithophores, compaction will be driven by stress and the subsequent compaction can most likely be explained by processes described in this study.

Magnesium is a known inhibitor of both calcite dissolution (*Arvidson et al.*, 2006) and calcite precipitation (*Berner*, 1975). If the sediments are composed of magnesian calcite, as in this study, the potential build–up of Mg^{2+} in the pore space might either reduce or prevent the porosity loss by slowing down the rate of pressure solution (*Zhang and Spiers*, 2005), precipitation of dolomite in the pore space might also occur. The inhibiting effect of Mg^{2+} on pressure solution was also observed in shallow-water carbonates of South-Florida (*Schmoker and Halley*, 1982).

The present experimental data show that only minor amounts of water is sufficient for chemical compaction to occur. This explains why field observations show that cementation can occur even if oil migrates through a reservoir (*McLimans and Videtich*, 1989). Based on these observations oil emplacement in carbonate reservoirs may not stop compaction but rather result in a different compaction mechanism than in carbonate sediments saturated with water. This was observed in bioclastic carbonate samples saturated with glycol. Glycol was shown to have the same effect than oil on chalk compaction (*Risnes et al.*, 2003). The results from the present study suggest that subcritical crack growth will be the main mechanism responsible for com-

paction in oil filled carbonate sediments.

5.5 Conclusion

Uniaxial compression tests were carried out on bioclastic carbonate sands and crushed calcite samples with grain size in the range 63–500 μm. In samples saturated with reactive fluids, *e.g.* glycol/water mixture or water in equilibrium with carbonate, significant chemical compaction was documented during the loading phase. Samples saturated with non–reactive fluids, *e.g.* air or decane, showed less strain at the same effective stress since the compaction was only mechanical. When saturated with reactive fluids, finer grained samples were more compressible than coarser grained samples due to chemical compaction. Chemical compaction occurred by pressure solution which was enhanced by the presence of cracks at the grain–to–grain contacts. Compaction related microstructures identified in thin–sections support these findings.

During creep tests carried out on bioclastic carbonate sand the deformation was mostly due to chemical reactions. Furthermore pore water analysis, and especially the evolution of the Mg^{2+}/Ca^{2+} ratio, showed that magnesian calcite dissolved during experiments. In all the creep experiments, the strain versus time relation followed a power law in time, with a single exponent equal to 0.23. From this observation, it was inferred that the same deformation mechanisms were active in all the creep experiments. Overall it was found that a combination of pressure solution creep and subcritical crack growth (stress corrosion) was responsible for strain, and strain rates were in the range $2.88{\cdot}10^{-8}$–$2.82{\cdot}10^{-6}$ s^{-1}.

The compressibility of the samples was controlled by, in order of importance, grain size, stress, and water saturation. Pressure solution was most likely the dominant mechanism of compaction in samples saturated with water. Conversely, in samples saturated with glycol or anisole, subcritical crack growth was most likely the main mechanism of deformation.

Ultrasonic velocity measurements showed that P- and S–waves velocities were in the range of 705 to 2440 m/s and 535 to 1250 m/s, respectively. Low velocities were especially observed in samples saturated with reactive fluids. Dissolution and transport affecting the grain–to–grain contacts geometry and crack propagation are likely to be the reason for such velocity alteration.

All these observations indicate that relaxation processes at work in a granular material can have universal behaviours in systems as different as sedimentary layers during burial or fault zones during the interseismic period. In all cases, the nature of the fluid, the initial grain packing, and the grain size represent important control parameters of the final strain and the strain rates for a given stress.

Acknowledgements

The experiments were conducted at the Norwegian Geotechnical Institute (NGI). Gudmund Havstad is thanked for his help in the laboratory. Nils Martin Hanken is gratefully acknowledged for providing the bioclastic carbonate sand. Lars Grande, Paul Meakin and Agnès Helmstetter are acknowledged for sharing helpful discussions and analysis.

Bibliography

Amitrano, D., and A. Helmstetter (2006), Brittle creep, damage, and time to failure in rocks, *J. Geophys. Res.*, *111*(B11), B11,201, 0148-0227.

Anderson, O. L., and P. C. Grew (1977), Stress-corrosion theory of crack-propagation with applications to geophysics, *Reviews of Geophysics*, *15*(1), 77–104.

Andrade, E. N. d. C. (1910), On the viscous flow in metals, and allied phenomena, *Proceedings of the Royal Society of London. Series A, Containing Papers of a Mathematical and Physical Character*, *84*(567), 1–12.

Anselmetti, F. S., and G. P. Eberli (1993), Controls on sonic velocity in carbonates, *Pure and Applied Geophysics*, *141*(2-4), 287–323.

Arvidson, R. S., M. Collier, K. J. Davis, M. D. Vinson, J. E. Amonette, and A. Luettge (2006), Magnesium inhibition of calcite dissolution kinetics, *Geochimica et Cosmochimica Acta*, *70*(3), 583–594.

Assefa, S., C. McCann, and J. Sothcott (2003), Velocities of compressional and shear waves in limestones, *Geophysical Prospecting*, *51*(1), 1–13.

Athy, L. F. (1930), Density, porosity, and compaction of sedimentary rocks, *AAPG Bulletin*, *14*(1), 1–24.

Atkinson, B. K. (1982), Subcritical crack propagation in rocks: theory, experimental results and applications, *Journal of Structural Geology*, *4*(1), 41–56, doi: 10.1016/0191-8141(82)90005-0.

Audet, D., and A. C. Fowler (1992), A mathematical model for compaction in sedimentary basins, *Geophysical journal international*, *110*(3), 577–590.

Bassinot, F., J. Marsters, L. Mayer, and R. Wilkens (1993), Variations of porosity in calcareous sediments from the ontong java plateau, in *Proc. ODP, Sci. Results*, vol. 130, edited by L. W.

Kroenke, W. H. Berger, T. R. Janecek, et al., pp. 653 – 661, College Station, TX (Ocean Drilling Program), doi:10.2973/odp.proc.sr.130.058.1993.

Ben-Naim, E., J. B. Knight, E. R. Nowak, H. M. Jaeger, and S. R. Nagel (1998), Slow relaxation in granular compaction, *Physica D: Nonlinear Phenomena*, *123*(1-4), 380–385, doi: 10.1016/S0167-2789(98)00136-5.

Berner, R. (1975), The role of magnesium in the crystal growth of calcite and aragonite from sea water, *Geochimica et Cosmochimica Acta*, *39*(4), 489–504.

Berryman, J. G. (1995), Mixture theories for rock properties, in *Rock Physics and Phase Relations: a Handbook of Physical constants*, edited by T. Ahrens, pp. 205–228, American Geophysical Union, Washington DC.

Birch, F. (1960), The velocity of compressional waves in rocks to 10 kilobars, part 1, *Journal of Geophysical Research*, *65*(4), 1083–1102.

Bjørlykke, K. (2003), Compaction (consolidation) of sediments, in *Encyclopedia of sediments and sedimentary rocks*, edited by G. V. Middleton and M. J. Church, pp. 161 – 167, Kluwer Academic Publishers, Boston.

Caglioti, E., V. Loreto, H. J. Herrmann, and M. Nicodemi (1997), A "tetris-like" model for the compaction of dry granular media, *Physical Review Letters*, *79*(8), 1575.

Chantikul, P., S. J. Bennison, and B. R. Lawn (1990), Role of grain size in the strength and r-curve properties of alumina, *Journal of the American Ceramic society*, *73*(8), 2419–2427, doi: 10.1111/j.1151-2916.1990.tb07607.x.

Chari, S. S. (1967), Creep of carbon mixes at the temperature of extrusion, *Carbon*, *5*(1), 61–63, doi: 10.1016/0008-6223(67)90107-8.

Charles, R. J. (1958), Dynamic fatigue of glass, *Journal of Applied Physics*, *29*(12), 1657–1662.

Christensen, N. I., and D. L. Szymanski (1991), Seismic properties and the origin of reflectivity from a classic paleozoic sedimentary sequence, valley and ridge province, southern appalachians, *Geological Society of America Bulletin*, *103*(2), 277–289.

Chuhan, F. A., A. Kjeldstad, K. Bjørlykke, and K. Høeg (2002), Porosity loss in sand by grain crushing; experimental evidence and relevance to reservoir quality, *Marine and Petroleum Geology*, *19*(1), 39–53.

Chuhan, F. A., A. Kjeldstad, K. Bjørlykke, and K. Høeg (2003), Experimental compression of loose sands; relevance to porosity reduction during burial in sedimentary basins, *Canadian Geotechnical Journal = Revue Canadienne de Geotechnique*, *40*(5), 995–1011.

Couvreur, J. F., A. Vervoort, M. S. King, E. Lousberg, and J. F. Thimus (2001), Successive cracking steps of a limestone highlighted by ultrasonic wave propagation, *Geophysical Prospecting*, *49*(1), 71–78.

Croizé, D., S. N. Ehrenberg, K. Bjørlykke, F. Renard, and J. Jahren (2009), Petrophysical properties of bioclastic platform carbonates: implications for porosity controls during burial, *Marine and Petroleum Geology*, *In Press, Corrected Proof*, doi: 10.1016/j.marpetgeo.2009.11.008.

Croizé, D., F. Renard, K. Bjørlykke, and D. K. Dysthe (2010), Experimental calcite dissolution under stress: Evolution of grain contact microstructure during pressure solution creep, *J. Geophys. Res.*, *in press*, doi:10.1029/2010JB000869.

Cruden, D. (1970), A theory of brittle creep in rock under uniaxial compression, *J. Geophys. Res.*, *75*(17), 3431–3442.

Cygan, R. T., K. Wright, D. K. Fisler, J. D. Gale, and B. Slater (2002), Atomistic models of carbonate minerals: Bulk and surface structures, defects, and diffusion, *Molecular Simulation*, *28*(6-7), 475–495, doi:10.1080/08927020290030099.

Dürrast, H., and S. Siegesmund (1999), Correlation between rock fabrics and physical properties of carbonate reservoir rocks, *International Journal of Earth Sciences*, *88*(3), 392–408.

Eberli, G. P., G. T. Baechle, F. S. Anselmetti, and M. L. Incze (2003), Factors controlling elastic properties in carbonate sediments and rocks, *The Leading Edge*, *22*(7), 654–660.

Ehrenberg, S. N. (2006), Porosity destruction in carbonates platforms, *Journal of Petroleum Geology*, *29*(1), 41–52, doi:10.1111/j.1747–5457.2006.00041.x.

Fabricius, I. L. (2003), How burial diagenesis of chalk sediments control sonic velocity and porosity, *AAPG Bulletin*, *87*(11), 1755–1778.

Fruth, J., L S, G. R. Orme, and F. A. Donath (1966), Experimental compaction effects in carbonate sediments, *Journal of Sedimentary Petrology*, *36*(3), 747–754.

Gassmann, F. (1951), Elasticity of high-porosity sandstone: Uber die elastizitat poroser medien, *Vierteljahrsschr. Nat. Ges. Zurich*, *96*, 1 – 23.

Giles, M. R. (1997), *Diagenesis: a quantitative perspective – Implications for basin modelling and rock property prediction*, Kluwer Academic Publishers, Dordrecht, The Netherlands.

Goldhammer, R. K. (1997), Compaction and decompaction algorithms for sedimentary carbonates, *Journal of Sedimentary Research*, *67*(1), 26–35.

Greener, E. H., K. Szurgot, and E. P. Lautenschlager (1980), Time-temperature behavior for creep of dental amalgam, *Journal of Biomedical Materials Research*, *14*(2), 161–171, doi: 10.1002/jbm.820140207.

Hamilton, E. L. (1976), Variations of density and porosity with depth in deep-sea sediments, *Journal of Sedimentary Petrology*, *46*(2), 280–300.

Helmstetter, A., and B. E. Shaw (2009), Afterslip and aftershocks in the rate-and-state friction law, *J. Geophys. Res.*, *114*(B1), B01,308, 0148-0227.

Hughes, D. S., and J. L. Kelly (1953), Second-order elastic deformation of solids, *Physical Review*, *92*(5), 1145.

Karner, S. L., J. S. Chester, F. M. Chester, A. K. Kronenberg, and A. Hajash (2005), Laboratory deformation of granular quartz sand: Implications for the burial of clastic rocks, *AAPG Bulletin*, *89*(5), 603–625.

Knight, J. B., C. G. Fandrich, C. N. Lau, H. M. Jaeger, and S. R. Nagel (1995), Density relaxation in a vibrated granular material, *Physical Review E*, *51*(5), 3957.

Knight, R., J. Dvorkin, and A. Nur (1998), Acoustic signatures of partial saturation, *Geophysics*, *63*(1), 132–138.

Kopaska-Merkel, D. C., S. D. Mann, and J. W. Schmoker (1994), Controls on reservoir development in a shelf carbonate; upper jurassic smackover formation of alabama, *AAPG Bulletin*, *78*(6), 938–959.

Lange, F. F. (1984), Sinterability of agglomerated powders, *Journal of the American Ceramic Society*, *67*(2), 83–89, doi: 10.1111/j.1151-2916.1984.tb09620.x.

Lehner, F. K. (1990), Thermodynamics of rock deformation by pressure solution, in *Deformation Processes in Minerals, Ceramics and Rocks*, edited by D. J. Barber and P. G. Meredith, p. 423, Unwin Hyman Ltd, London, United Kingdom.

Liteanu, E., and C. J. Spiers (2009), Influence of pore fluid salt content on compaction creep of calcite aggregates in the presence of supercritical CO_2, *Chemical Geology*, *265*(1-2), 134–147, doi:10.1016/j.chemgeo.2008.12.010.

Mavko, G., T. Mukerji, and J. Dvorkin (2009), *The Rock Physics Handbook: Tools for Seismic Analysis of Porous Media*, 2nd ed., Cambridge University Press, Cambridge.

McLimans, R. K., and P. E. Videtich (1989), Diagenesis and burial history of great oolite limestone, southern england, *AAPG Bulletin*, *73*(10), 1195–1205.

Meyers, W. J. (1980), Compaction in mississippian skeletal limestones, southwestern new mexico, *Journal of Sedimentary Research*, *50*(2), 457–474.

Morse, J. W., and F. T. Mackenzie (1990), *Geochemistry of sedimentary carbonates*, Elsevier, Amsterdam.

Nolen-Hoeksema, R. C., Z. Wang, J. M. Harris, and R. T. Langan (1995), High-resolution crosswell imaging of a west texas carbonate reservoir: Part 5—core analysis, *Geophysics*, *60*(3), 712–726.

Norris, A. N. (1985), A differential scheme for the effective moduli of composites, *Mechanics of Materials*, *4*(1), 1–16.

Olagnon, C., J. Chevalier, and V. Pauchard (2006), Global description of crack propagation in ceramics, *Journal of the European Ceramic Society*, *26*(15), 3051–3059, doi:10.1016/j.jeurceramsoc.2005.11.004.

Omori, F. (1894), On the aftershocks of earthquakes, *J. Coll. Sci. Imp. univ. Tokyo*, *7*, 111–120.

Philippe, P., and D. Bideau (2002), Compaction dynamics of a granular medium under vertical tapping, *EPL (Europhysics Letters)*, *60*(5), 677, 0295-5075.

Rafavich, F., C. H. S. C. Kendall, and T. P. Todd (1984), The relationship between acoustic properties and the petrographic character of carbonate rocks, *Geophysics*, *49*(10), 1622–1636.

Renard, F., D. Dysthe, J. Feder, K. Bjørlykke, and B. Jamtveit (2001), Enhanced pressure solution creep rates induced by clay particles; experimental evidence in salt aggregates, *Geophysical Research Letters*, *28*(7), 1295–1298.

Revil, A. (1999), Pervasive pressure-solution transfer: a poro-visco-plastic model, *Geophysical Research Letters*, *26*(2), 255–258.

Revil, A., P. Leroy, A. Ghorbani, N. Florsch, and A. R. Niemeijer (2006), Compaction of quartz sands by pressure solution using a cole-cole distribution of relaxation times, *J. Geophys. Res.*, *111*(B9), B09,205.

Richard, P., M. Nicodemi, R. Delannay, P. Ribiere, and D. Bideau (2005), Slow relaxation and compaction of granular systems, *Nature Materials*, *4*(2), 121–128.

Risnes, R., H. Haghighi, R. I. Korsnes, and O. Natvik (2003), Chalk-fluid interactions with glycol and brines, *Tectonophysics*, *370*(1-4), 213–226.

Royden, L., and C. E. Keen (1980), Rifting process and thermal evolution of the continental margin of eastern canada determined from subsidence curves, *Earth and Planetary Science Letters*, *51*(2), 343–361.

Ruiz, F., and J. Dvorkin (2009), Sediment with porous grains: Rock-physics model and application to marine carbonate and opal, *Geophysics*, *74*(1), E1–E15.

Schaff, D. P., G. C. Beroza, and B. E. Shaw (1998), Postseismic response of repeating aftershocks, *Geophys. Res. Lett.*, *25*(24), 4549–4552, doi: org/10.1029/1998GL900192.

Schmoker, J. W., and R. B. Halley (1982), Carbonate porosity versus depth; a predictable relation for south florida, *AAPG Bulletin*, *66*(12), 2561–2570.

Scholle, P. A., and R. B. Halley (1985), Burial diagenesis; out of sight, out of mind!, in *Carbonate cements.*, *Special Publication - Society of Economic Paleontologists and Mineralogists*, vol. 36, edited by N. Schneidermann and M. Harris Paul, pp. 309–334, SEPM (Society for Sedimentary Geology), Tulsa, OK, United States.

Sclater, J. G., and P. A. F. Christie (1980), Continental stretching; an explanation of the post-mid-cretaceous subsidence of the central north sea basin, *Journal of Geophysical Research*, *85*(B7), 3711–3739.

Stumm, W., and J. J. Morgan (1996), *Aquatic chemistry: chemical equilibria and rates in natural waters*, 3rd ed., Wiley, New York.

Sutton, G. H., H. Berckhemer, and J. E. Nafe (1957), Physical analysis of deep sea sediments, *Geophysics*, *22*(4), 779–812.

Vanorio, T., C. Scotellaro, and G. Mavko (2008), The effect of chemical and physical processes on the acoustic properties of carbonate rocks, *The Leading Edge*, *27*(8), 1040–1048.

Vanorio, T., G. Mavko, S. Vialle, and K. Spratt (2010), The rock physics basis for 4D seismic monitoring of CO_2 fate: Are we there yet?, *The Leading Edge*, *29*(2), 156–162.

Velleman, P., and D. Hoaglin (1981), *Applications, Basics, and Computing of Exploratory Data Analysis*, Duxbury Press, Pacific Grove.

Vishnevskii, I. I., L. D. Smirnova, and Y. N. Yarovoi (1989), Unsteady creep equation in refractory materials during monoaxial compression, *Refractories and Industrial Ceramics*, *30*(1–2), 22–27, doi: 10.1007/BF01292534.

Wang, Z. (1997), Seismic properties of carbonate rocks, in *Carbonate seismology*, vol. 6, edited by I. Palaz and K. J. Marfurt, pp. 29–52, SEG.

Weller, J. M. (1959), Compaction of sediments, *AAPG Bulletin*, *43*(2), 273 – 310.

Weyl, P. K. (1959), Pressure solution and the force of crystallization – a phenomenological theory, *Journal of Geophysical Research*, *64*(11), 2001–2025.

Zhang, X., and C. J. Spiers (2005), Compaction of granular calcite by pressure solution at room temperature and effects of pore fluid chemistry, *International Journal of Rock Mechanics and Mining Sciences*, *42*, 950–960.

Zubtsov, S., F. Renard, J. P. Gratier, D. K. Dysthe, and V. Traskine (2005), Single-contact pressure solution creep on calcite monocrystals, in *Deformation mechanisms, rheology and tectonics; from minerals to the lithosphere*, *Geological Society Special Publications*, vol. 243, edited by D. Gapais, P. Brun Jean, and R. Cobbold Peter, pp. 81–95, Geological Society of London, London, United Kingdom.